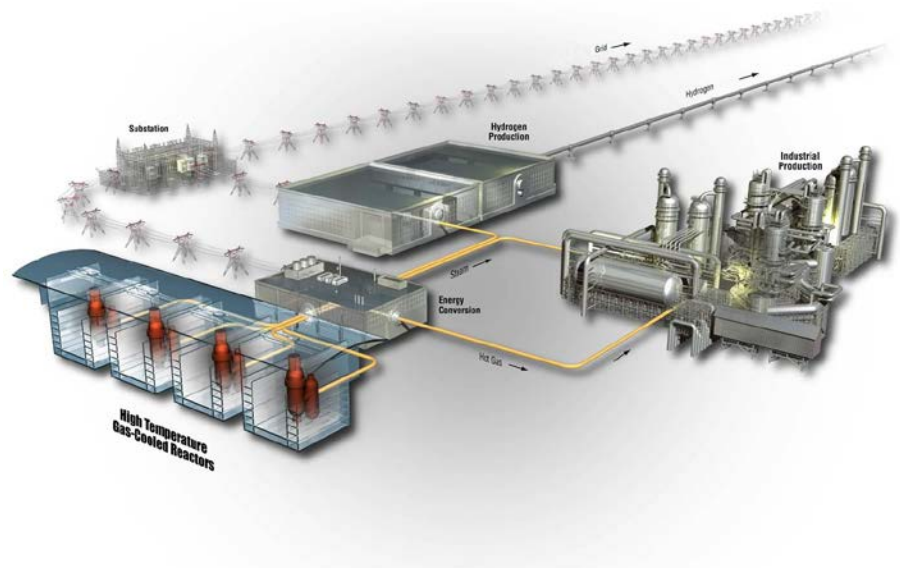


Uncertainty Quantification of Calculated Temperatures for AGR-3/4 Experiment

Binh T. Pham
Jeffrey J. Einerson
Grant L. Hawkes

September 2015

The INL is a
U.S. Department of Energy
National Laboratory
operated by
Battelle Energy Alliance



DISCLAIMER

This information was prepared as an account of work sponsored by an agency of the U.S. Government. Neither the U.S. Government nor any agency thereof, nor any of their employees, makes any warranty, expressed or implied, or assumes any legal liability or responsibility for the accuracy, completeness, or usefulness, of any information, apparatus, product, or process disclosed, or represents that its use would not infringe privately owned rights. References herein to any specific commercial product, process, or service by trade name, trade mark, manufacturer, or otherwise, does not necessarily constitute or imply its endorsement, recommendation, or favoring by the U.S. Government or any agency thereof. The views and opinions of authors expressed herein do not necessarily state or reflect those of the U.S. Government or any agency thereof.

Uncertainty Quantification of Calculated Temperatures for AGR-3/4 Experiment

**Binh T. Pham
Jeffrey J. Einerson
Grant L. Hawkes**

September 2015

**Idaho National Laboratory
INL ART Program
Idaho Falls, Idaho 83415**

<http://www.inl.gov>

**Prepared for the
U.S. Department of Energy
Office of Nuclear Energy
Under DOE Idaho Operations Office
Contract DE-AC07-05ID14517**

INL ART Program

Uncertainty Quantification of Calculated
Temperatures for AGR-3/4 Experiment

INL/EXT-15-36431
Revision 0

September 2015

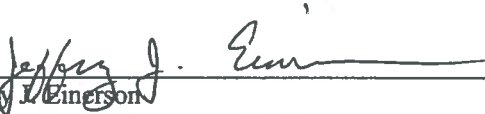
Approved by:



Binh T. Pham
INL Advanced Reactor Technologies TDO

9 / 11 / 2015

Date



Jeffrey J. Emerson
INL Advanced Reactor Technologies TDO

9 - 14 - 2015

Date



Grant L. Hawkes
INL Advanced Reactor Technologies TDO

9/11/2015

Date



Daren K. Jensen
INL Advanced Reactor Technologies TDO Quality
Assurance

9/14/15

Date



David A. Petti
Advanced Reactor Technologies Co-National Technical
Director

9/11/2015

Date

ABSTRACT

This report documents the quantification of uncertainty of the calculated temperature data for the third and fourth Advanced Gas Reactor (AGR)-3/4 fuel irradiation experiments conducted in the Advanced Test Reactor at Idaho National Laboratory in support of the Advanced Reactor Technology Research and Development program. Recognizing uncertainties inherent in physics and thermal simulations of the AGR-3/4 test, the results of the numerical simulations are used in combination with statistical analysis methods to improve qualification of measured data. The temperature simulation data for AGR tests are also used for validation of the fission product transport and fuel performance simulation models. These crucial roles of the calculated fuel temperatures in ensuring achievement of the AGR experimental program objectives require accurate determination of the model temperature uncertainties. In this version of the report only temperature uncertainty results for Capsule 5, 7, 11, and 12 are included. Results for the remaining capsules will be presented in a later report.

To quantify the uncertainty of AGR-3/4 calculated temperatures performed by the ABAQUS finite element heat transfer code, this study identifies and analyzes model parameters of potential importance to the AGR-3/4 predicted thermocouple and fuel temperatures. The selection of input parameters for uncertainty quantification is based on the ranking of their influences upon variation of temperature predictions. Thus, selected input parameters include those with high sensitivity and those with the largest uncertainty. Propagation of model parameter uncertainty and sensitivity is then used to quantify the overall uncertainty of AGR-3/4 calculated temperatures. Expert judgment is used as the basis to specify the uncertainty range for selected input parameters. The input uncertainties are dynamic, accounting for the effect of unplanned events and changes in thermal properties of capsule components over extended exposure to high temperatures and fast neutron irradiation.

The sensitivity analysis performed in this work went beyond the traditional local sensitivity. Using experimental design, analysis of pairwise interactions of model parameters was performed to establish sufficiency of the first-order (linear) expansion terms in constructing the response surface. To achieve completeness, uncertainty propagation made use of pairwise noise correlations of model parameters. Furthermore, using an interpolation scheme over the input parameter domain, the analysis obtains time-dependent sensitivity over the test campaign duration. This allows computation of uncertainty for the predicted fuel temperatures and the predicted graphite temperatures at thermocouple locations during the entire AGR-3/4 irradiation period.

SUMMARY

S-1 Introduction

This report documents the quantification of uncertainty in the calculated temperatures for the third and fourth Advanced Gas Reactor (AGR)-3/4 fuel irradiation experiment. These experiments, conducted in the northeast flux trap (NEFT) location of the Advanced Test Reactor at Idaho National Laboratory (INL), are in support of the Advanced Reactor Technologies (ART) research and development (R&D) program. While not possible to obtain by direct measurements in the tests, essential fuel irradiation conditions (e.g., temperature, neutron fast fluence, and burnup) are calculated using core physics (JMOCUP) and thermal modeling (ABAQUS) codes. Calculated fuel temperatures serve crucial roles in achieving AGR experimental program objectives and require accurate determination of the model temperature uncertainties. One such role is the validation of the fission product transport and fuel performance simulation models.

S-2 Approach

In general, uncertainty in the prediction of a simulation model arises from two main sources: input uncertainty and model uncertainty. This is assuming that the numerical errors can be eliminated by the use of adequate spatial resolution in computing code. Subsequently, the overall uncertainty of simulation model predictions in terms of variance can be expressed as:

$$\sigma_T^2 = \sigma_p^2 + \sigma_B^2 \quad (\text{S-1})$$

where

σ_T^2 = overall uncertainty of predicted temperature in terms of variance

σ_p^2 = parameter uncertainty in terms of variance

σ_B^2 = model bias in terms of variance.

Model Bias

Early analysis of thermocouple data indicated that the thermocouples performed reliably, especially during the beginning cycles of irradiation. Therefore, the thermal models for each capsule were calibrated by varying the emissivity of surfaces of the graphite rings and stainless-steel retainer to best match temperatures at thermocouple (TC) locations with actual TC measurements during this portion of the irradiation. The TC residuals are the differences between measured and calculated temperatures for operational TCs. Continued monitoring and analysis of residuals beyond the calibration period show a pattern of non-zero horizontal lines as a function of effective full power days (EFPDs) of irradiation for TCs in most of the capsules. This suggests existence of model bias. Here, the model bias in percentage is assumed to be the ratio between the average of TC residuals and the average of TC temperatures for TC1 and TC2, which are presented in Table S-1 for Capsules 5, 7, 11, and 12.

Table S-1. Thermal model biases for -3/4 capsules.

Capsule	5	7	11	12
Model Bias, %	4.3	3.2	2.8	0

Parameter Uncertainty

The parameter uncertainty of a calculated temperature is caused by the uncertainties of inputs to the simulation model. To quantify the parameter uncertainty of AGR calculated temperatures, ABAQUS code's finite element-based thermal model input parameters of potential importance are identified. Identification has two parts: (1) using expert judgment, determine parameters with the largest uncertainties and estimate these uncertainties, and (2) using sensitivity analysis, determine parameters that the modeling is most sensitive to. A set of parameters is selected for predicted temperature uncertainty quantification, including those with high sensitivity and/or those with large uncertainty. The parameter uncertainties and sensitivity coefficients are combined and propagated to quantify the temperature parameter uncertainty using *Equation (S-2)*, because the predicted temperature can be assumed to be the weighted summation of input parameters. This assumption is confirmed during sensitivity analysis.

$$\sigma_p^2 = \sum_i^n a_i^2 \sigma_i^2 + \sum_i^n \sum_{j \neq i}^n \rho_{ij} a_i \sigma_i a_j \sigma_j \quad (\text{S-2})$$

where

σ_p^2 = overall temperature uncertainty in terms of variance due to parameter uncertainties

a_i^2 = square of the sensitivity coefficient for parameter i

σ_i^2 = uncertainty of input parameter i in terms of variance

ρ_{ij} = correlation coefficient for input parameters i and j

n = number of input parameters.

The model parameters identified as most influential on uncertainty are: four gas gap sizes (Gaps 1 to 4), fuel compact heat rate, graphite rings' heat rate, neon fraction, fuel thermal conductivity, and graphite thermal conductivity. These are shown in Figure S-1.

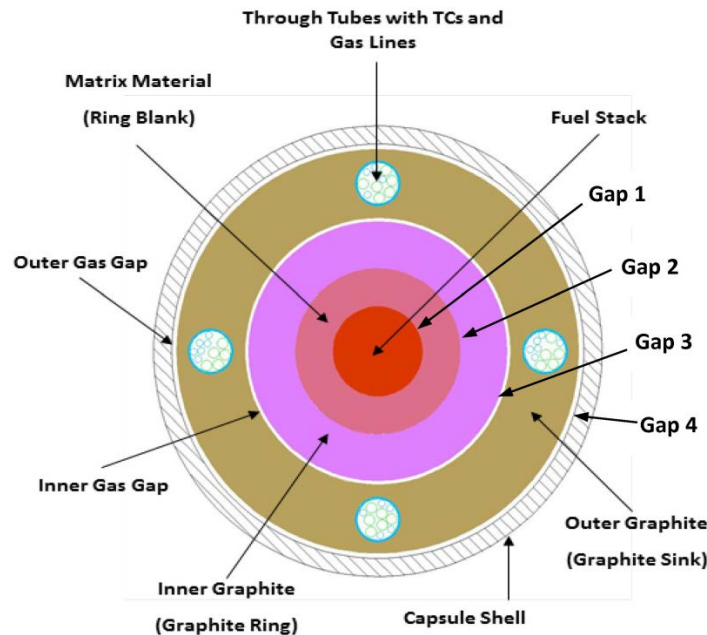


Figure S-1. Cross-section view of AGR-3/4 capsules.

All four gaps were modeled as changing with fast neutron fluence. The as-built dimensions for the gas gaps were adjusted to be the hot gas gap dimensions, which are almost the same as room temperature gas gap dimensions (Hawkes 2015). Experimental data obtained from the AGR-1 experiment (Demkowicz et al. 2011) were used for the compact dimensional change, while data from the AGC-1 experiment (Windes 2012) were used for the graphite shrinkage. Matrix dimensional change data were taken from Gontard and Nabielek (1990) and Hrovat et al. (2008) documents. The complex physics impacting the gaps lead to high uncertainty in estimation of gap sizes during irradiation. However, the excellent consistency in TC residual trend over the entire range of capsule thermal conditions throughout the AGR-3/4 irradiation offers confidence that the thermal model has appropriately incorporated all important physical phenomena occurring in the capsule.

S-3 Input Uncertainty

The uncertainties of the input parameters of interest in the thermal model for the AGR-3/4 capsules were estimated by ART R&D program experts, and are presented in Table S-2 along with the basis for the estimates. The input uncertainties of the gas gap sizes and neon fraction are dynamic, accounting for the effect of changes in thermal properties of capsule components over extended exposure to high temperatures and fast neutron irradiation (e.g., assumed gap size changes add uncertainty in the gap size), as shown in Figure S-2 for Capsule 5. Gap 1 in all capsules has a high relative uncertainty due to its small gap size of less than 3 mil. Gap 2 is also small (about 3 mil) for all capsules except in Capsule 11, where the gap is 39 mil; thus, the relative uncertainty associated with Gap 2 is also high for all capsules except Capsule 11. Gaps 3 and 4 are bigger, leading to smaller relative uncertainty.

Table S-2. Uncertainties of identified significant inputs to thermal model of the AGR-3/4 capsule.

Parameter	Uncertainty	Rationale
Gap 1 about 3 mil Gap 2 [3 to 39 mil] Gap 3 [8 to 150 mil] Gap 4 [12 to 85 mil]	[1 to 1.3 mil] [1 to 1.9 mil] [1 to 2.7 mil] [1 to 4.4 mil]	Uncertainty at start of irradiation is 1 mil based on fabrication tolerance. Uncertainty over course of irradiation is time dependent because of graphite holder shrinkage, which is proportional to the neutron fluence in the graphite. This leads to a physics-based gas gap models. Thus, the absolute gap uncertainty is assumed to be a linear function of fluence. By the end of irradiation, the gap uncertainty is estimated using uncertainty of the AGR-1 and AGC-1 PIE compact and graphite dimensional change data (Subsection 3.3.2.1).
Neon fraction	Function of neon fraction	Uncertainty is based on 1-sccm flow rate tolerance and estimated from neon fraction prediction equation (Subsection 3.3.2.2).
Fuel compacts' heat rate	5%	Based on AGR-1 comparison done by J. Harp with additional input from J. Sterbentz (Subsection 3.3.2.3).
Graphite rings' (matrix, sleeve, and sink) heat rate	3%	
Graphite conductivity	15%	Additional conductivity data for the test graphite allows a lower uncertainty estimate for graphite than for fuel.
Fuel conductivity	20%	Uncertainty is based on work done on surrogate compacts by C. Folsom at Utah State University.

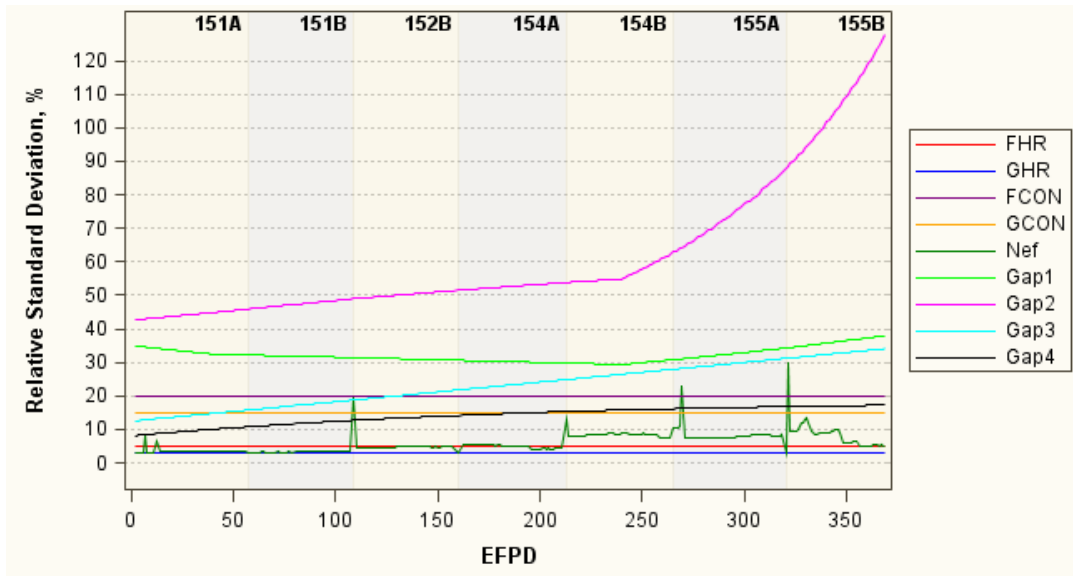


Figure S-2. Capsule 5 input parameter uncertainties in terms of relative standard deviation.

S-4 Input Parameter Sensitivity

The parameter sensitivity analysis of the thermal model is performed to determine the sensitivity coefficients of the most influential variables. A sensitivity coefficient describes how the model predicted temperature would be influenced by changes in an input parameter. The overall uncertainty of the model output increases as the absolute sensitivity coefficient of an input parameter increases.

The sensitivity analysis performed here went beyond the traditional local sensitivity. Using experimental design, analysis of pairwise interactions of model parameters was also performed to establish sufficiency of the first-order (linear) expansion terms in the uncertainty propagation formula *Equation (S-2)*. For each capsule, the sensitivity analysis was performed for three days throughout irradiation and an interpolation scheme over the input parameter domain was then used to obtain time-dependent sensitivity. This allows uncertainty quantification for the instantaneous temperatures of fuel compacts, matrix ring, sleeve ring, and TCs over the whole irradiation period. The parameter sensitivity coefficients for all temperatures of interest in Capsule 5 for one day are presented in Figure S-3. These sensitivities are varying from capsule to capsule and from day to day during the irradiation. The following conclusions could be drawn:

- For heat rates and neon fraction (Panel 1 in Figure S-3), the sensitivity coefficients of fuel heat rate are highest for VA and peak fuel temperatures. The graphite heat rate is more sensitive to graphite rings' and TC temperatures. The neon fraction is sensitive to all temperatures of interest.
- For four gap sizes (Panel 2 in Figure S-3), the sensitivity coefficients range from about 0 to 0.4. Gap 1 is most sensitive to VA and peak fuel temperatures, but has very little impact on other temperatures. Gap 2 has small sensitivity on both fuel and matrix temperatures, but negligible impact on sleeve and TC1/2 temperatures. Gap 3 has relatively high sensitivity to all temperatures, with the highest value for sleeve ring temperature. Gap 4 had highest sensitivities to all temperatures of interest, especially for TC1/2 temperatures, which are adjacent to this gap.
- The sensitivity coefficients of fuel compact thermal conductivity and graphite thermal conductivity (Panel 3 in Figure S-3) are negative and less than 0.1 in absolute value for all temperatures of interest. The sensitivity coefficient of fuel thermal conductivity is near zero for sleeve and TC1/2 temperatures leading to negligible impact on these temperatures, but graphite conductivity impacts all temperatures of interest.

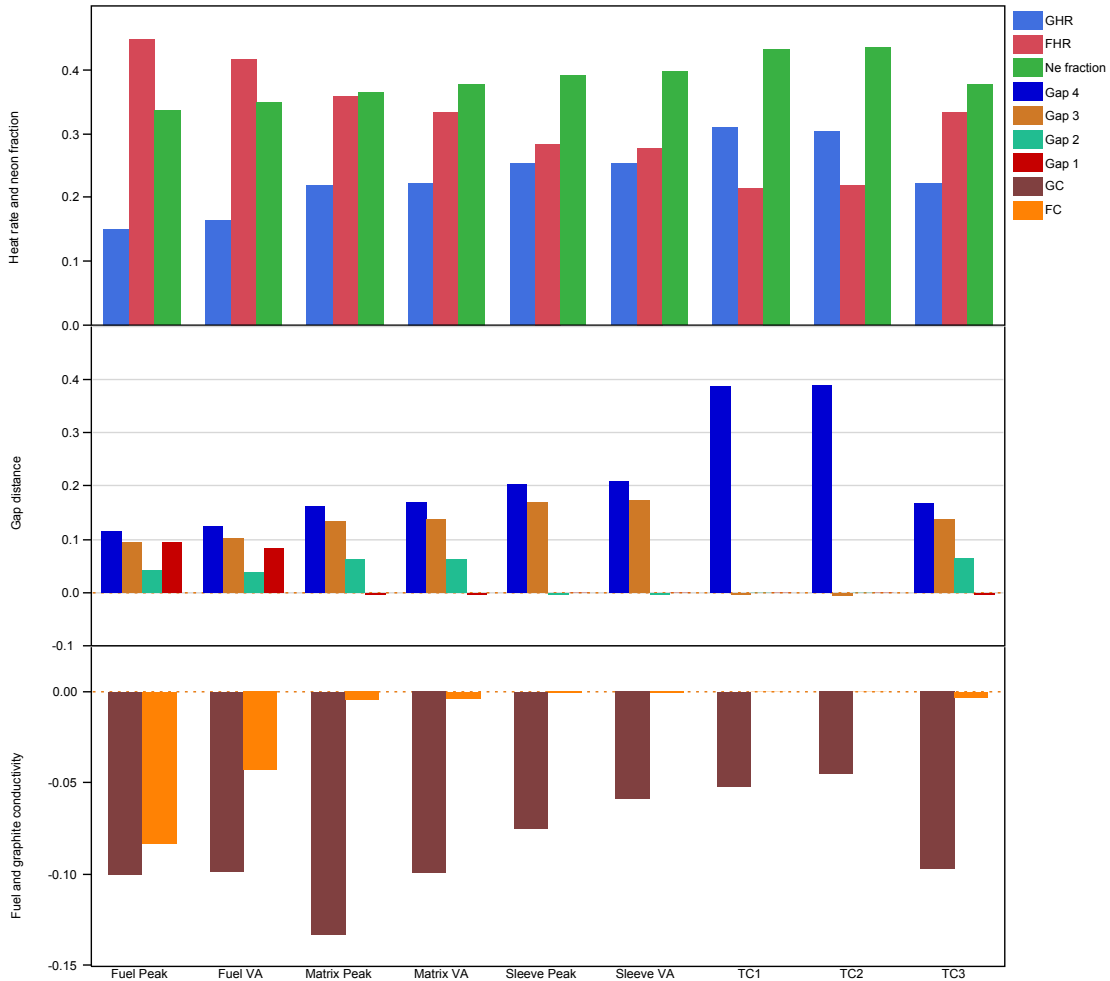


Figure S-3. Parameter sensitivity coefficients for fuel and thermocouple temperatures in Capsule 5.

S-5 Combining Parameter Sensitivity and Uncertainty

The parameter uncertainty of a calculated temperature in terms of variance is obtained through propagation of model parameter uncertainty as the summation of the parameter variances weighted by the squares of their sensitivity coefficients *Equation (S-2)*. Thus, the effect of a parameter on the model prediction variation is a product of input uncertainty and the sensitivity coefficient. As an example, the daily uncertainty results due to input uncertainties for Capsule 5 peak fuel temperature are presented in Figure S-4. The following conclusions are drawn:

- The fuel heat is most sensitive to temperature prediction; but its small input uncertainty (5%) makes it only the third most influential factor on fuel temperature uncertainty. However, it is the most influential factor for matrix and graphite sleeve temperatures. The graphite heat rate and neon fraction are also sensitive to temperature, but their contribution to temperature uncertainty is very insignificant due to their relatively low input uncertainties (about 3%).
- Among the four gap sizes, Gaps 1 and 2 (about 3 mil width) have highest relative input uncertainty (up to 128% by the end of irradiation as shown in Panel 1 in Figure S-4). Even though these gap sensitivities are generally small (less than 0.1 as shown in Panel 2 in Figure S-4), they are the most significant factor contributing to uncertainty of the fuel temperature predictions (Panel 3 in

Figure S-4). On the other hand, Gaps 3 and 4, having significantly lower relative uncertainty, have a minor impact on uncertainty of fuel and graphite temperatures. Gap 4 has the most impact on temperature uncertainty of TC1 and TC2 located near this gap.

- Finally, the fuel and graphite thermal conductivities have similar impact on fuel temperatures as the fuel heat rate. The fuel conductivity has a slight impact on matrix, sleeve, and TC temperatures.

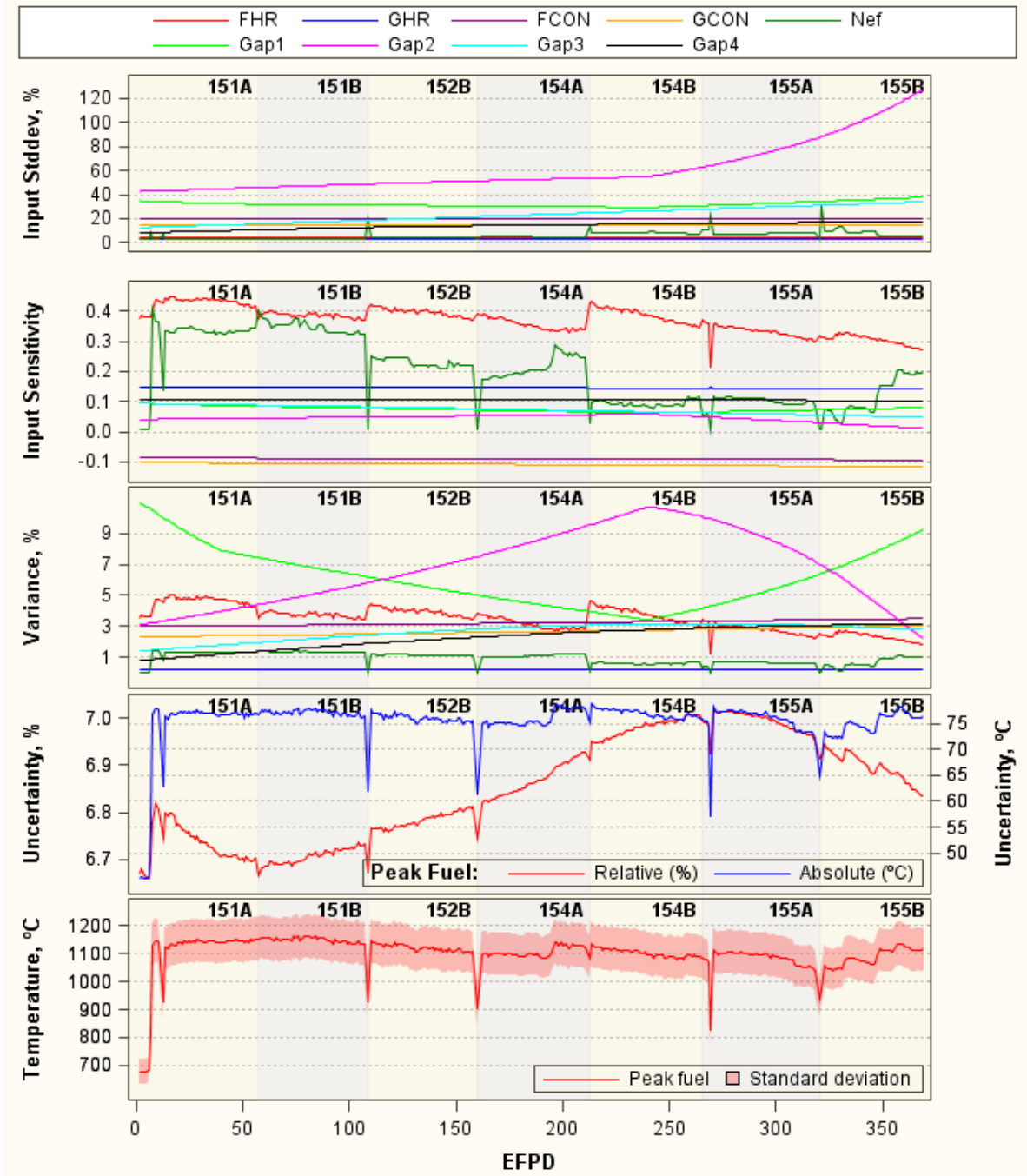


Figure S-4. Daily uncertainty results for Capsule 5 peak fuel temperature.

S-6 Overall Uncertainty

Presently, temperature uncertainty results for Capsules 5, 7, 11, and 12 are included here. Results for the remaining capsules will be presented in a later report. The overall uncertainty in all calculated temperatures of interest ranged from 1.5% to 8.3%, depending on irradiation time (thermal conditions), capsule, and the temperature parameter being predicted. The daily overall uncertainties in terms of relative and absolute standard deviations for instantaneous VA and peak fuel, mid-50%-VA matrix ring and sleeve ring, and TCs temperatures in Capsules 5, 7, 11, and 12, as a function of EFPD, are presented in Figure S-5 and Figure S-6, respectively. Figure S-7 through Figure S-9 show daily calculated temperatures together with one standard deviation for all temperatures of interest in the four capsules.

Table S-3 summarizes the uncertainty range (minimum value / maximum value) for instantaneous temperatures and uncertainty at the end of irradiation for time-averaged temperatures of fuel compacts, matrix ring, and sleeve ring. Result highlights are:

- Capsule 12 has the lowest temperature uncertainty because it has negligible model bias and lower input uncertainties of Gap 1 (about 32%) and Gap 2 (up to 48%).
- Capsule 11 has about 1% higher uncertainty than Capsule 12 because of 2.8% model bias.
- Capsule 7 has high uncertainty (up to 8.1% or 65°C) for TC1/2 due to Gap 4 uncertainty.
- Capsule 5 has the highest temperature uncertainty with a maximum of 8.3% relative standard deviation for mid-50%-VA matrix ring temperature and maximum of 7.0% for peak fuel temperature. This is caused by highest model bias of 4.3% and high input uncertainties of Gap 1 (up to 38%) and Gap 2 (up to 128%).
- For AGR-1 and AGR-2, assuming negligible model bias, the relative uncertainty ranged from 3 to 4% for VA and 3 to 5% for peak fuel temperature. In addition, AGR-1 Capsule 6 had 10% bias in fuel heat rate, causing an overall uncertainty increase up to 5.8% for instantaneous and 5.0% for time-averaged fuel temperature at the end of irradiation. Comparing to these experiments, the overall uncertainties of AGR-3/4 Capsule 12 temperatures are lower, when the model bias is negligible. Capsules 7 and 11 uncertainties, including model bias (3.2% and 2.8% respectively), are comparable to those seen by AGR-1 and AGR-2 capsules. Conversely, Capsule 5 uncertainty, including 4.3% model bias, is clearly higher than uncertainty in AGR-1 and AGR-2 capsules.

Table S-3. Uncertainty range for instantaneous temperature and uncertainty for time-averaged temperatures at the end of irradiation.

Capsule	Peak Fuel	Volume-Averaged Fuel	Volume-Averaged Matrix	Volume-Averaged Sleeve	Peak Fuel	Volume-Averaged Fuel	Volume-Averaged Matrix	Volume-Averaged Sleeve
	Relative Standard Deviation, %				Standard Deviation, °C			
	Instantaneous Temperature – Minimum/Maximum							
12	2.6/3.1	2.4/2.8	1.8/2.5	1.5/2.2	16/28	13/24	10/19	8/14
11	3.5/3.8	3.4/3.7	3.1/3.4	3.1/3.3	34/48	31/45	26/38	22/32
7	4.2/4.7	4.2/4.5	4.2/5.3	3.6/4.6	41/67	37/60	31/63	24/51
5	6.7/7.0	6.3/6.8	6.0/8.3	5.5/7.4	45/79	39/72	30/69	24/62
Time-Averaged Temperature – at End of Irradiation								
12	2.9	2.6	2.2	1.8	25	22	17	13
11	3.6	3.5	3.2	3.1	45	41	35	30
7	4.5	4.4	4.6	4.1	61	56	52	41
5	6.8	6.6	7.5	6.7	75	68	62	49

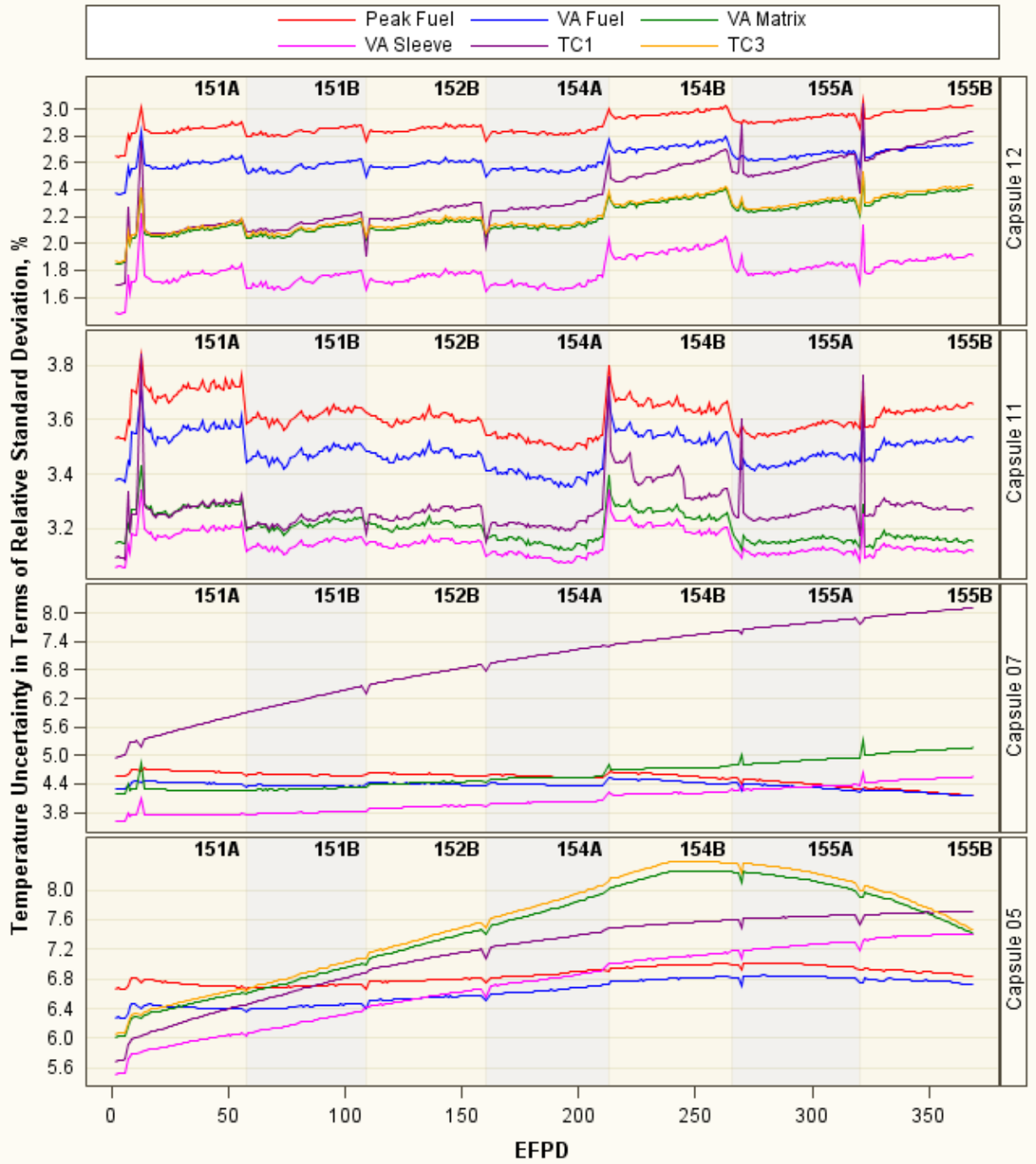


Figure S-5. Daily uncertainty in terms of relative standard deviation for instantaneous temperatures of interest in Capsules 5, 7, 11, and 12.

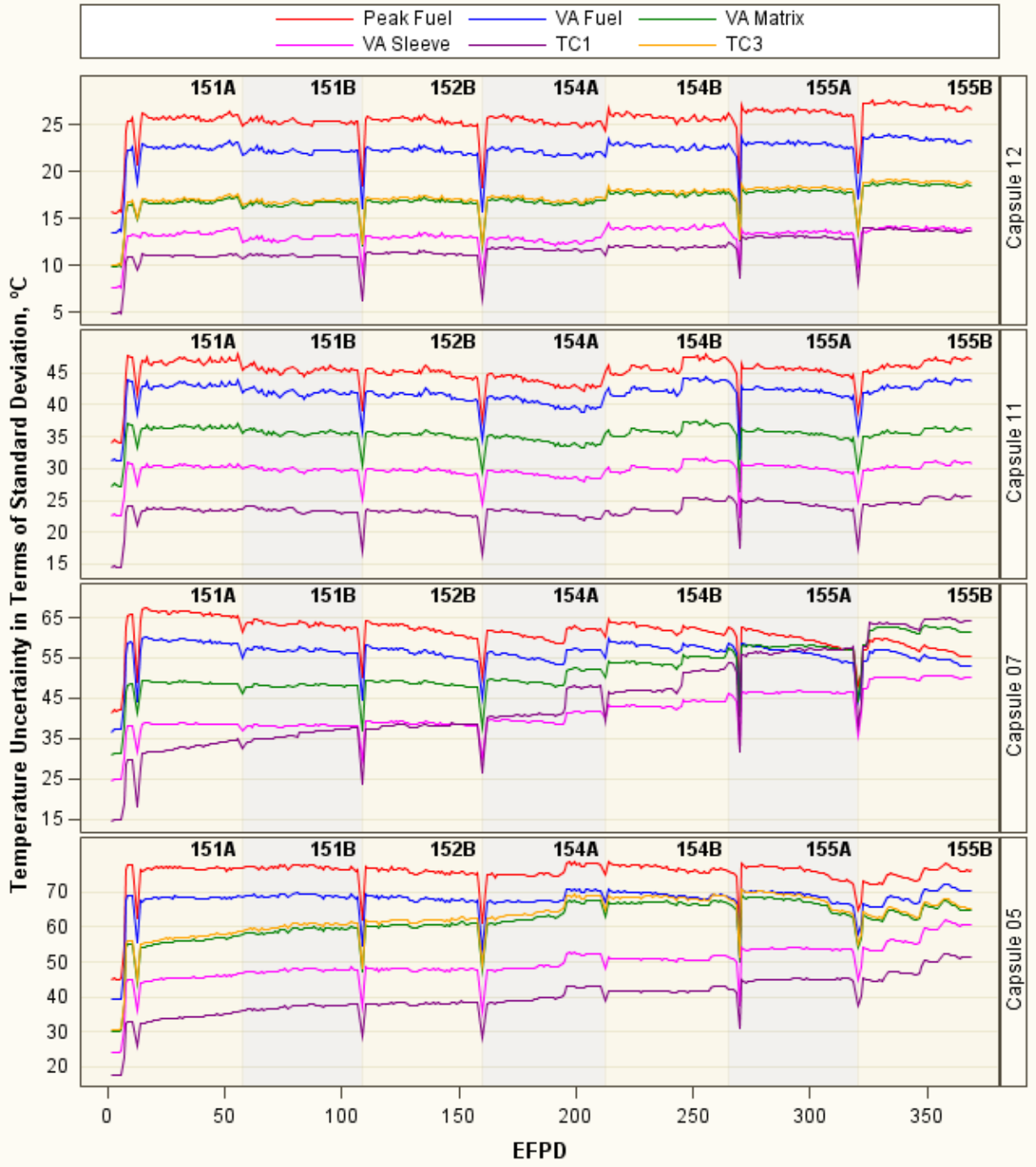


Figure S-6. Daily uncertainty in terms of standard deviation for instantaneous temperatures of interest in Capsules 5, 7, 11, and 12.

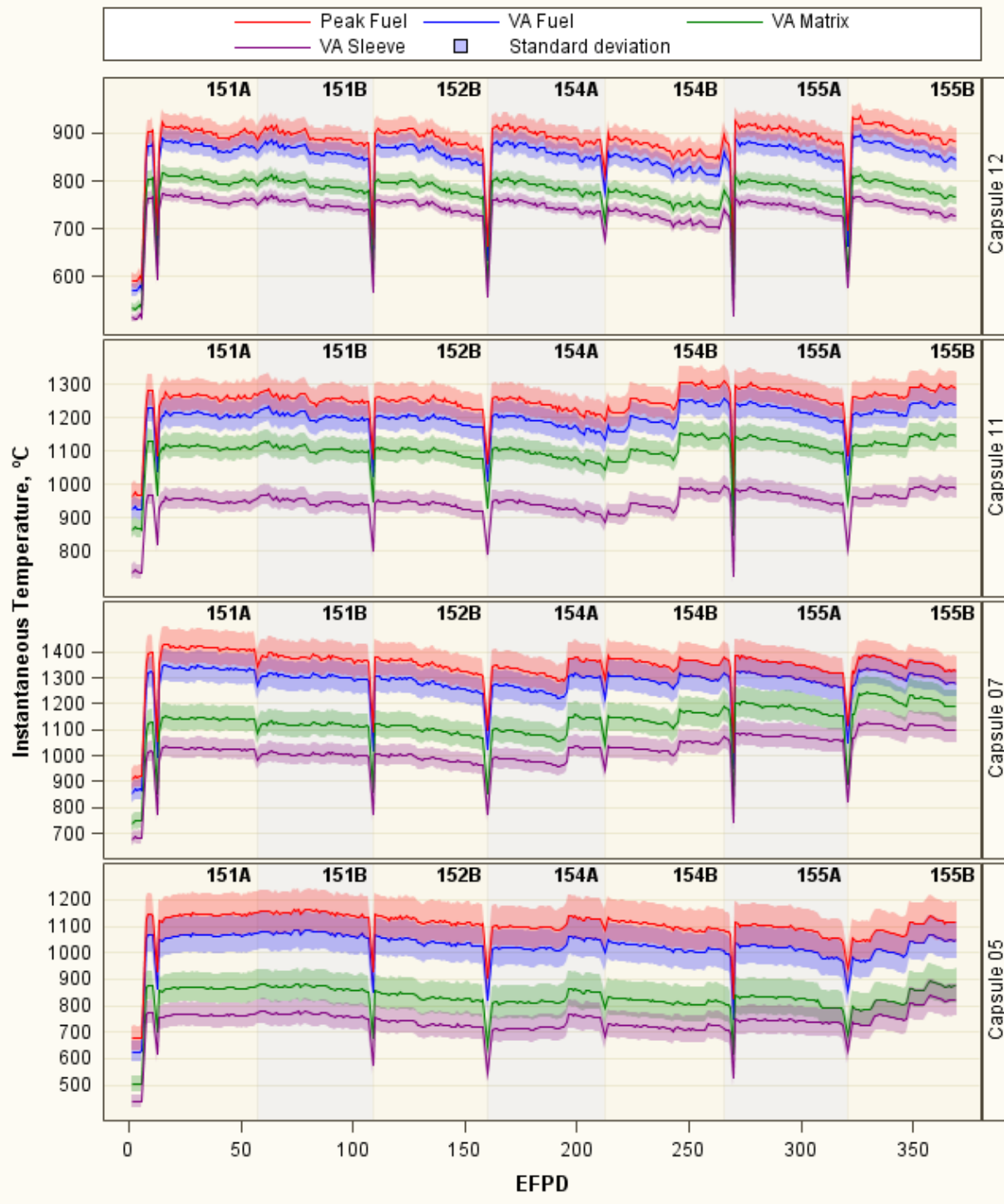


Figure S-7. Instantaneous VA fuel, peak fuel, VA matrix, and VA sleeve temperatures with uncertainty bars in Capsules 5, 7, 11, and 12.

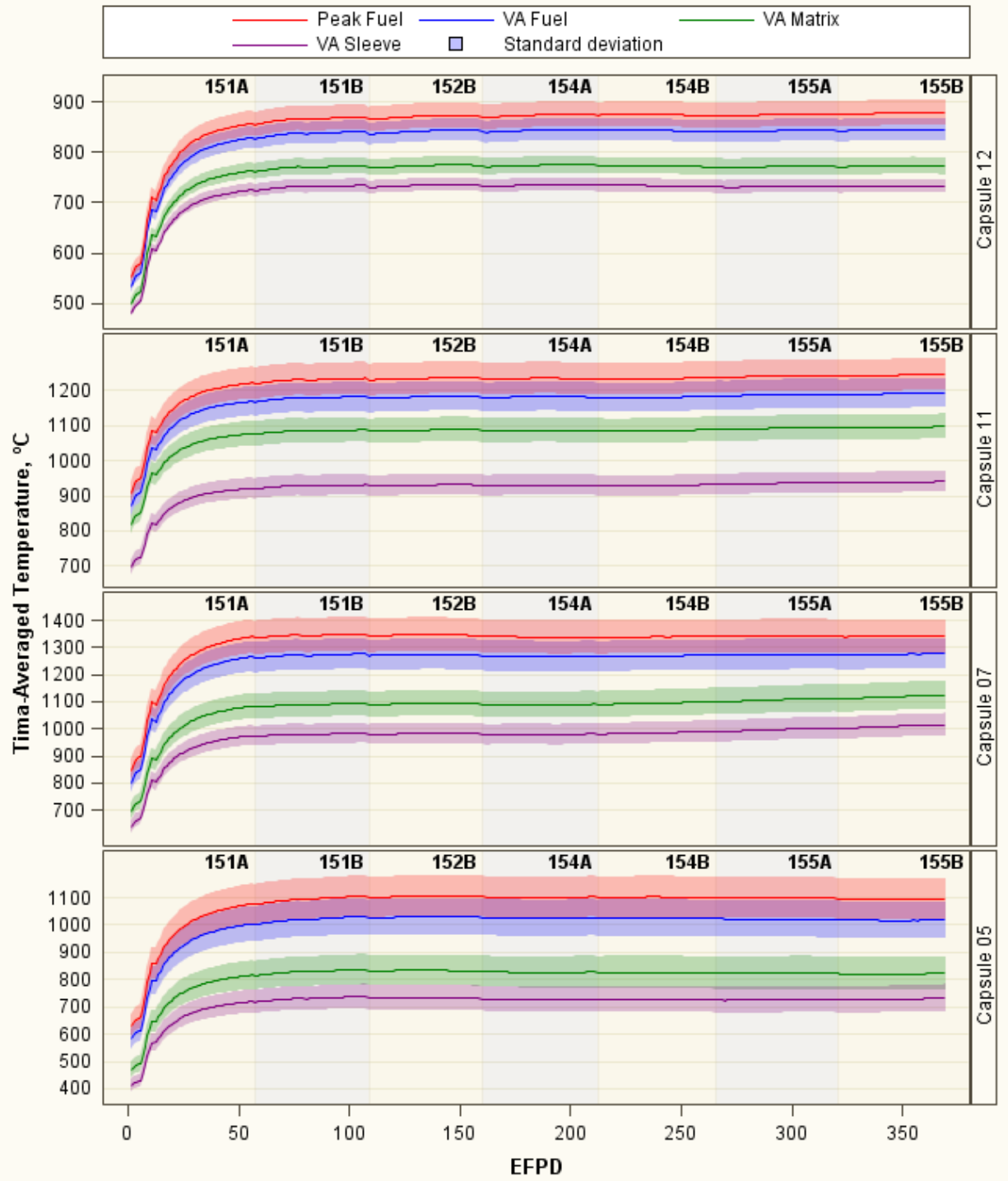


Figure S-8. Time-averaged VA fuel, peak fuel, VA matrix, and VA sleeve temperatures with uncertainty bars in Capsules 5, 7, 11, and 12.

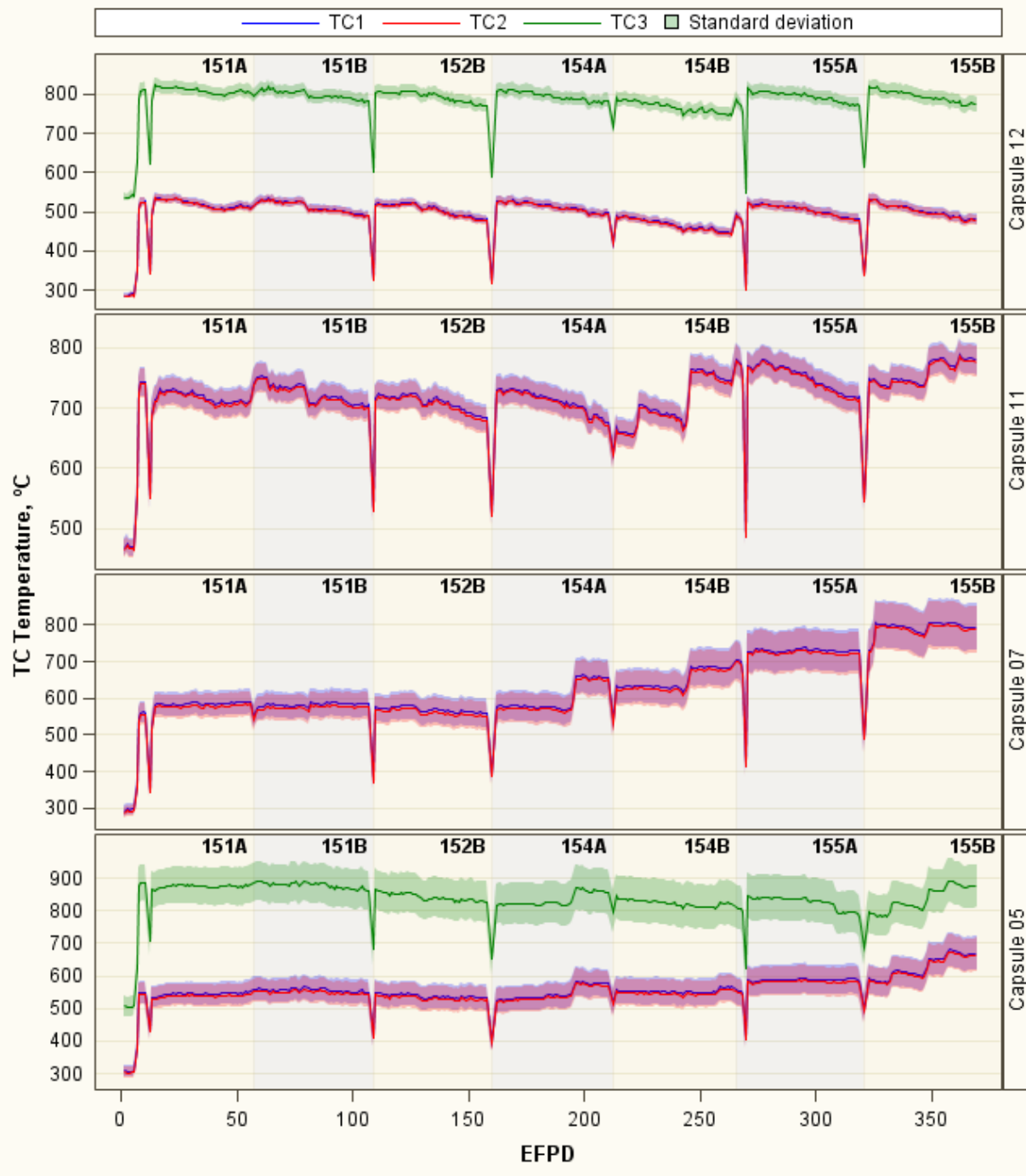


Figure S-9. Instantaneous TC temperatures with uncertainty bars in Capsules 5, 7, 11, and 12.

S-7 Report Structure

The report is organized into four sections and a conclusion:

- Section 1 introduces the AGR Fuel Development and Qualification Program and summarizes AGR-3/4 measured data, test configuration and test procedure, and thermal simulation.
- Section 2 describes the estimation of uncertainties and sensitivities for the thermal model input parameters. This includes parameter uncertainties based on expert judgment, sensitivity analysis of input parameters, and the estimation of correlation coefficients for pairs of input parameters.
- Section 3 describes the propagation of uncertainties and sensitivities for estimation of the overall uncertainty for the daily VA and peak fuel temperatures, daily average temperatures at TC locations, and time-averaged VA and time-averaged peak fuel temperatures.
- Section 4 presents the results of the uncertainty analysis for each of the four AGR-3/4 capsules and discusses the parameters driving the uncertainty.
- The conclusion summarizes important findings of the uncertainty quantification and identifies possible areas of improvement.

CONTENTS

ABSTRACT.....	vii
SUMMARY.....	ix
S-1 Introduction.....	ix
S-2 Approach.....	ix
S-3 Input Uncertainty.....	xi
S-4 Input Parameter Sensitivity.....	xii
S-5 Combining Parameter Sensitivity and Uncertainty.....	xiii
S-6 Overall Uncertainty.....	xv
S-7 Report Structure.....	xxi
ACRONYMS.....	xxvii
1. INTRODUCTION.....	1
2. ADVANCED GAS REACTOR-3/4 EXPERIMENT.....	2
2.1 Irradiation Data.....	3
2.2 Thermal Model for AGR-3/4 Capsules.....	5
2.2.1 Capsule Configuration.....	5
2.2.2 Thermal Model.....	6
3. UNCERTAINTY QUANTIFICATION OF MODEL PREDICTED TEMPERATURE.....	11
3.1 Technical Approach.....	11
3.2 Thermal Model Uncertainty.....	12
3.3 Parameter Uncertainty.....	15
3.3.1 Influential Input Selection.....	15
3.3.2 Input Uncertainties.....	18
3.3.3 Input Parameter Sensitivity.....	33
3.3.4 Correlation Coefficients of Thermal Model Input Parameters.....	42
3.3.5 Propagation of Parameter Uncertainties and Sensitivities.....	45
3.4 Overall Uncertainty Quantification.....	47
3.4.1 Uncertainty for Daily temperature.....	47
3.4.2 Uncertainty for Time Average (TA) Temperature.....	47
4. RESULTS.....	47
4.1 Temperature Uncertainty Results for Capsule 12.....	48
4.2 Temperature Uncertainty Results for Capsule 11.....	53
4.3 Temperature Uncertainty Results for Capsule 7.....	58
4.4 Temperature Uncertainty Results for Capsule 5.....	63
5. CONCLUSIONS.....	68
6. REFERENCES.....	70

FIGURES

Figure S-1. Cross-section view of AGR-3/4 capsules.	x
Figure S-2. Capsule 5 input parameter uncertainties in terms of relative standard deviation.....	xii
Figure S-3. Parameter sensitivity coefficients for fuel and thermocouple temperatures in Capsule 5.	xiii
Figure S-4. Daily uncertainty results for Capsule 5 peak fuel temperature.	xiv
Figure S-5. Daily uncertainty in terms of relative standard deviation for instantaneous temperatures of interest in Capsules 5, 7, 11, and 12.	xvi
Figure S-6. Daily uncertainty in terms of standard deviation for instantaneous temperatures of interest in Capsules 5, 7, 11, and 12.	xvii
Figure S-7. Instantaneous VA fuel, peak fuel, VA matrix, and VA sleeve temperatures with uncertainty bars in Capsules 5, 7, 11, and 12.	xviii
Figure S-8. Time-averaged VA fuel, peak fuel, VA matrix, and VA sleeve temperatures with uncertainty bars in Capsules 5, 7, 11, and 12.	xix
Figure S-9. Instantaneous TC temperatures with uncertainty bars in Capsules 5, 7, 11, and 12.	xx
Figure 1. AGR-3/4 northeast flux trap location in the ATR core cross section.	2
Figure 2. Axial (left) and radial (right) cross-section view of Advanced Gas Reactor-3/4 capsule.	3
Figure 3. Graphical summary of thermal parameters in Advanced Gas Reactor-3/4, Capsule 12.	4
Figure 4. Schematic of radial cut of Advanced Gas Reactor-3/4 capsule.	5
Figure 5. Cutaway view of finite element of Advanced Gas Reactor-3/4 capsule (Hawkes et al. 2015).	6
Figure 6. Temperature distribution in cutaway view of Capsule 5.	7
Figure 7. Calculated history of daily minimum, maximum, and volume-averaged temperatures for Capsules 7 through 12.	9
Figure 8. Calculated history of daily minimum, maximum, and volume-averaged temperatures for Capsules 1 through 6.	10
Figure 9. Difference between measured and predicted thermocouple temperatures for Capsules 7 through 12.	13
Figure 10. Difference between measured and predicted thermocouple temperatures for Capsules 1 through 6. Itinerary.....	14
Figure 11. Parameter sensitivities for Capsule 5 peak fuel temperatures.	16
Figure 12. Parameter sensitivities for Capsule 5 volume-averaged fuel temperatures.	17
Figure 13. Parameter sensitivities for Capsule 5 calculated TC1 temperatures.	17
Figure 14. Initial gap sizes for all 12 AGR-3/4 capsules.	20
Figure 15. ABAQUS gap size as function of effective full-power days for Capsules 5, 7, 11, and 12.	22
Figure 16. Radius changes of Advanced Gas Reactor-1 fuel compacts (Hawkes 2015).	23

Figure 17. Daily uncertainty of distances of Gaps 1 through 4 in Capsules 5, 7, 11, and 12.	25
Figure 18. Neon fraction uncertainty and trend line.	26
Figure 19. Burnup derived from Cs-134/Cs-137 activity ratio for each measured precision gamma scanner slice for all AGR-1 capsules compared to simulations from ECAR-958. Each vertical tick mark represents a separate level in each capsule (Harp 2014).	28
Figure 20. Capsule average fuel compact heat rate versus irradiation time in effective full-power days.	29
Figure 21. Capsule average graphite ring heat rate versus irradiation time in effective full-power days.	30
Figure 22. Uranium oxycarbide compact thermal conductivity varying with fluence and temperature (ECAR-2807).	31
Figure 23. Ratio of irradiated over unirradiated graphite thermal conductivity (k_{irr}/k_0) varying with temperature and displacements per atom.	32
Figure 24. Actual by predicted plot for VA FT for Case 1 (Capsule 5).	34
Figure 25. Parameter estimates (<i>Equation [17]</i>) sorted from largest to smallest for volume-averaged fuel temperature of Scenario 1.	35
Figure 26. Leverage plots for nine main effects and square term of neon fraction for volume-averaged fuel temperatures (parameters are relative ratios to their nominal values and in order of sensitivity from largest to smallest indicated by the slope of the plots).	36
Figure 27. Prediction profiles of functions for volume-averaged fuel, peak fuel, volume-averaged matrix, peak matrix, volume-averaged sleeve, peak sleeve, and thermocouple temperatures.	37
Figure 28. Sensitivity coefficients for fuel, matrix, sleeve (both peak and volume-averaged), and thermocouple temperatures for Case 1.	38
Figure 29. Sensitivity coefficients of fuel heat rate, graphite heat rate, and neon fraction for Capsules 5, 7, 11, and 12.	39
Figure 30. Sensitivity coefficients of four gap sizes for Capsules 5, 7, 11, and 12.	40
Figure 31. Sensitivity coefficients of fuel and graphite conductivities for Capsules 5, 7, 11, and 12.	41
Figure 32. Scatter plot matrix showing correlation between fuel and graphite thermal conductivities at one fuel temperature and two displacements per atom levels (0.5 and 2.0).	44
Figure 33. Correlation coefficients between fuel and graphite thermal conductivities varying with fast neutron fluence.	45
Figure 34. Daily relative standard deviations for nine inputs in Capsule 12.	49
Figure 35. Daily uncertainty results for instantaneous and time-averaged peak and VA fuel temperatures in Capsule 12.	50
Figure 36. Daily uncertainty results for instantaneous and time-averaged mid-50%-VA matrix and sleeve temperatures in Capsule 12.	51
Figure 37. Daily uncertainty results for instantaneous TC temperatures in Capsule 12.	52
Figure 38. Daily relative standard deviations for nine inputs in Capsule 11.	54

Figure 39. Daily uncertainty results for instantaneous and time-averaged peak and VA fuel temperatures in Capsule 11.....	55
Figure 40. Daily uncertainty results for instantaneous and time-averaged mid-50%-VA matrix and sleeve temperatures in Capsule 11.....	56
Figure 41. Daily uncertainty results for instantaneous TC temperatures in Capsule 11.....	57
Figure 42. Daily relative standard deviations for nine inputs in Capsule 7.....	59
Figure 43. Daily uncertainty results for instantaneous and time-averaged peak and VA fuel temperatures in Capsule 7.....	60
Figure 44. Daily uncertainty results for instantaneous and time-averaged mid-50%-VA matrix and sleeve temperatures in Capsule 7.....	61
Figure 45. Daily uncertainty results for instantaneous TC temperatures in Capsule 7.....	62
Figure 46. Daily relative standard deviations for nine inputs in Capsule 5.....	64
Figure 47. Daily uncertainty results for instantaneous and time-averaged peak and VA fuel temperatures in Capsule 5.....	65
Figure 48. Daily uncertainty results for instantaneous and time-averaged mid-50%-VA matrix and sleeve temperatures in Capsule 5.....	66
Figure 49. Daily uncertainty results for instantaneous TC temperatures in Capsule 5.....	67

TABLES

Table S-1. Thermal model biases for -3/4 capsules.....	ix
Table S-2. Uncertainties of identified significant inputs to thermal model of the AGR-3/4 capsule.....	xi
Table S-3. Uncertainty range for instantaneous temperature and uncertainty for time-averaged temperatures at the end of irradiation.....	xv
Table 1. Averaged and standard deviation values of thermocouple residuals for Advanced Gas Reactor-3/4 capsules.....	15
Table 2. Uncertainties of identified significant inputs to thermal model for AGR-3/4 capsules.....	18
Table 3. Initial gap sizes and uncertainties for AGR-3/4 capsules.....	19
Table 4. Compact, matrix, and graphite rate of change varying with fast fluence and temperature.....	20
Table 5. Experimental design matrix for AGR-3/4 thermal model sensitivity analysis.....	33
Table 6. Thermal conditions for 12 selected cases.....	33
Table 7. Correlation coefficients between fuel and graphite thermal conductivities.....	44
Table 8. Summary of temperature uncertainty results for Capsule 12.....	49
Table 9. Summary of temperature uncertainty results for Capsule 11.....	54
Table 10. Summary of temperature uncertainty results for Capsule 7.....	59
Table 11. Summary of temperature uncertainty results for Capsule 5.....	64

ACRONYMS

AGR	Advanced Gas Reactor
ART	Advanced Reactor Technologies
ATR	Advanced Test Reactor
DTF	designed-to-fail
ECAR	engineering calculations and analysis report
EFPD	effective full-power day
FT	fuel temperature
INL	Idaho National Laboratory
N/A	not applicable
NDMAS	Nuclear Data Management and Analysis System
NEFT	northeast flux trap
PIE	post-irradiation examination
TC	thermocouple
TRISO	tristructural isotropic
VA	volume average

Uncertainty Quantification of Calculated Temperatures for AGR-3/4 Experiment

1. INTRODUCTION

A series of Advanced Gas Reactor (AGR) irradiation experiments are being conducted within the Advanced Reactor Technologies (ART) Fuel Development and Qualification Program. The main objectives of the fuel experimental campaign are to provide the necessary data on fuel performance to support fuel process development, qualify a fuel design and fabrication process for normal operation and potential accident conditions, and support development and validation of fuel performance and fission product transport models and codes (INL 2015). The AGR-3/4 experiment was inserted in the northeast flux trap (NEFT) position in the Advanced Test Reactor (ATR) core at Idaho National Laboratory (INL) in December 2011 and successfully completed irradiation in mid-April 2014, resulting in irradiation of the tristructural isotropic (TRISO) fuel for 369.1 effective full-power days (EFPDs) over approximately 2.4 calendar years. The AGR-3/4 experiment data, including the irradiation data and calculated results, were qualified and stored in the Nuclear Data Management and Analysis System (NDMAS) (Pham 2015).

To support United States TRISO fuel performance assessment and provide data for validation of fuel performance and fission product transport models and codes, the daily as-run thermal analysis has been performed separately on each of the 12 AGR-3/4 capsules for the entire irradiation as discussed in Hawkes (2015). The ABAQUS code's finite element-based thermal model predicts the daily average volume-averaged (VA) fuel temperature (FT); peak FT; and graphite matrix, sleeve, and sink temperatures in each capsule. The JMOCUP simulation codes were also created to perform depletion calculations for the AGR-3/4 experiment (Sterbentz 2015). This depletion analysis provides fast fluence and fission heat rate data for all components (e.g., fuel compacts, graphite rings, and stainless-steel retainer), which are used as inputs for the thermal analysis codes. The graphite temperatures from thermocouples (TCs) in each capsule were used to calibrate these thermal analysis codes. However, given the high rate of TC failure under the harsh irradiation and thermal conditions in the AGR-3/4 capsules, the thermal analysis results are very useful in aiding TC data qualification, increasing the confidence in delineating failures of the measuring instruments (TCs) from physical mechanisms that may have shifted the system thermal response (Pham and Einerson 2011).

The thermal model involves complex physical mechanisms (e.g., graphite ring and fuel compact shrinkage) and properties (e.g., conductivity and density). Therefore, the thermal model predictions are affected by uncertainty in input parameters and by incomplete knowledge of the underlying physics leading to modeling assumptions. Therefore, along with the deterministic predictions from a set of input thermal conditions, information about prediction uncertainty is instrumental for the ART program decision-making. Well-defined and reduced uncertainty in model predictions helps increase the quality of and confidence in the AGR technical findings (Pham et al. 2013, 2014).

This report focuses on the uncertainty quantification of TC temperature, FT, and graphite temperature predicted by the ABAQUS-based thermal models for four capsules in the AGR-3/4 experiment, Capsules 5, 7, 11, and 12. Results for the remaining capsules will be presented in a later report. To quantify the uncertainty of AGR calculated temperatures, ABAQUS thermal model input parameters of potential importance are identified. The identification process consists of two parts: (1) using expert judgment to determine parameters with the largest uncertainties and estimate these uncertainties, and (2) using sensitivity analysis to determine parameters that the modeling is most sensitive to. A set of parameters is selected for predicted temperature uncertainty quantification, including those with high sensitivity and those with large uncertainty. The parameter uncertainties and sensitivity coefficients are combined and propagated to quantify the overall uncertainty of temperature outputs. This work is performed to the INL QA program that meets NQA-1-2008/1a-2009 requirements.

2. ADVANCED GAS REACTOR-3/4 EXPERIMENT

AGR-3/4 is the combined third and fourth in a series of planned irradiation experiments conducted in the ATR at INL for the AGR Fuel Development and Qualification Program, which supports development of advanced reactor technologies under the INL ART Technology Development Office (TDO). The primary experimental objectives are to: (1) irradiate TRISO uranium oxycarbide fuel particles, including designed-to-fail (DTF) fuel particles, that will provide a known source of fission products for subsequent transport through compact matrix and structural graphite materials; and (2) assess the effects of sweep gas impurities typically found in the primary circuit of high-temperature gas-cooled reactors, such as CO, H₂O, and H₂ on fuel performance and subsequent fission product transport (INL 2015; INL 2011; INL 2015a). AGR-3/4 test train was inserted into the large (NEFT) location of the ATR core (Figure 1) in December 2011.

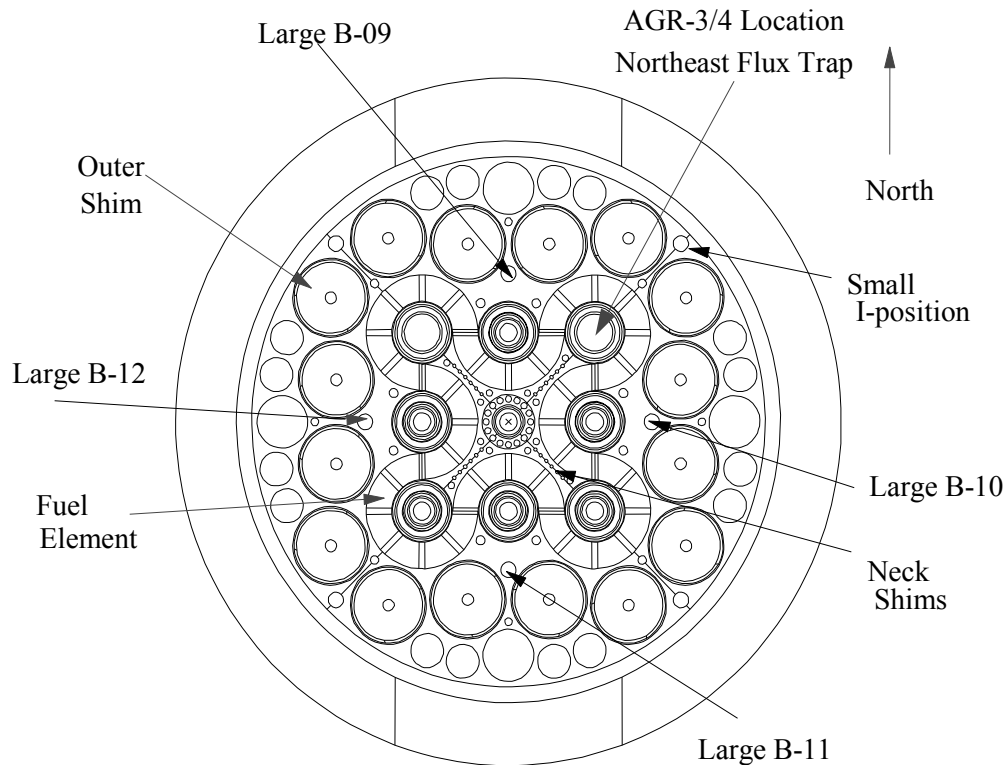


Figure 1. AGR-3/4 northeast flux trap location in the ATR core cross section.

The AGR-3/4 test train is comprised of 12 independently-controlled and -monitored capsules stacked on top of each other to form a test train using the full 1.22-m active core height as shown in the left side of Figure 2. In contrast to AGR-1 and AGR-2, each AGR-3/4 capsule contains only one fuel stack of four 1.27-cm-long compacts (0.5 in.) in the center surrounded by three graphite rings: matrix, graphite, and sink. A stainless-steel leadout tube holds the experiment in position and contains and protects the gas lines and TC wiring extending from the test train to the reactor penetration. The target quantity in each capsule (e.g., peak fuel, or matrix ring, or graphite ring temperature) is supposed to stay within a control band as specified in the test specification (INL 2011). Therefore, the experiment was instrumented with TCs terminated in graphite rings: Three TCs are in each of Capsules 5, 10, and 12; and two TCs are in each remaining capsule, as shown in the right side of Figure 2. The TCs have an installed accuracy of $\pm 2\%$ of readings as required by the test specification (INL 2011). Additionally, each capsule has an independent gas line to route a helium/neon gas mixture to transport any fission products released from the capsule. The mixture of helium-neon gas flowing through the four gas gaps between the fuel stack and

graphite rings is regulated to maintain readings of designated control TC. Periodically, the control TC temperature is redefined, so that the target fuel or graphite temperature stays within a control band.

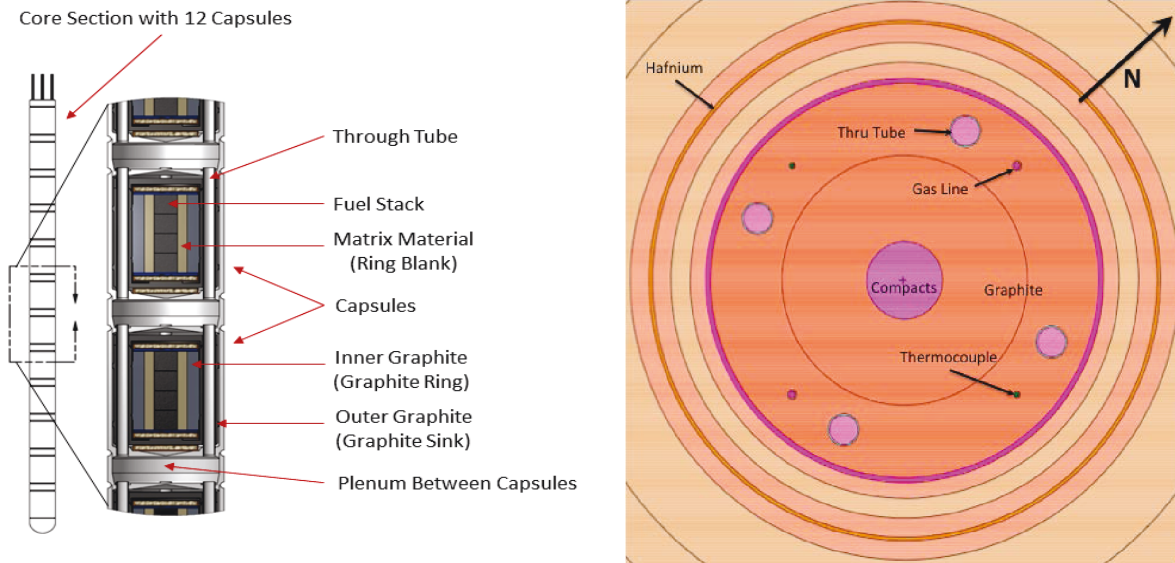


Figure 2. Axial (left) and radial (right) cross-section view of Advanced Gas Reactor-3/4 capsule.

2.1 Irradiation Data

The AGR-3/4 irradiation started in December 2011 (ATR Cycle 151A) and completed in April 2014 (end of ATR Cycle 155B) resulting in 369.1 EFPDs. The AGR-3/4 experimental data, consisting of fabrication data; irradiation data, including fission product monitoring; and post-irradiation examination (PIE) data were collected, scrutinized, and stored in NDMAS. The graphical plots in Figure 3 summarize measured and calculated thermal data in Capsule 12 as a function of EFPDs of irradiation. The data plotted here are daily averaged values: Neon fraction and fission power are in Panel 1 showing the main factors impacting capsule temperature; TC measurements and TC residuals (measured minus calculated) are in Panels 2 and 3, respectively, indicating prediction performance of the thermal model; and fuel compact, matrix ring, and inner graphite ring (or sleeve) temperatures (averaged, minimum, and maximum) are in Panels 4, 5, and 6 showing the variation of the target temperatures.

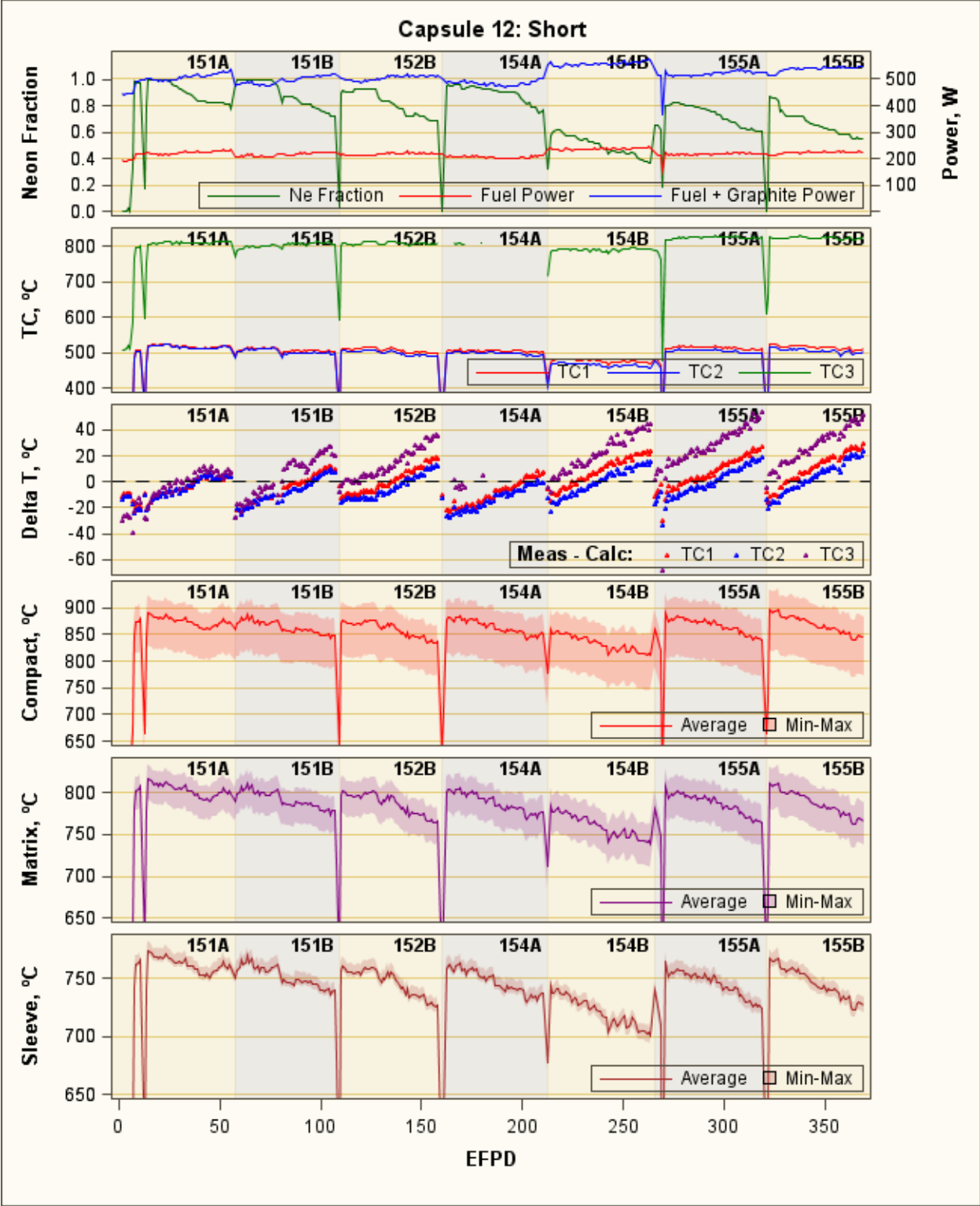


Figure 3. Graphical summary of thermal parameters in Advanced Gas Reactor-3/4, Capsule 12.

The TCs used in the AGR capsules were selected based on the greatest survival probability and least amount of drift in accelerated furnace tests; however, TC failures are still expected because the high temperatures and high neutron fluence exposure during extended irradiation far exceed vendor specifications. By the end of irradiation, five out of 27 TCs in the AGR-3/4 test train failed due to instrument failures. Capsule 3 lost both TCs by the end of ATR Cycle 154B; therefore, neon fraction in Capsule 3 was maintained at a constant level for the last two cycles, Cycles 155A and 155B. The accuracy of TC readings can be assessed by comparison with the readings from other TCs in similar positions or with calculated values (Pham and Einerson 2011). The TC data are rigorously analyzed and qualified in NDMAS (Pham 2015).

The measurements from the designated control TC support temperature control in each capsule of the experiment. The target temperature (fuel or graphite) is independently regulated by variation of the helium-neon gas mixture that fills the four gap volumes. TC measurements provide feedback to the automated sweep gas mass flow controller system for each capsule, which then adjusts gas blend to maintain the reference temperature in response to variation of the components' heat rates as shown by the plots in Panel 1 of Figure 3.

2.2 Thermal Model for AGR-3/4 Capsules

2.2.1 Capsule Configuration

Each AGR-3/4 capsule has a stack of four fuel compacts in the center surrounded by three graphitic annuli: proceeding from the compact out are the matrix ring (inside), graphite sleeve, and graphite sink (outside), which are housed in a stainless-steel capsule body (Figure 4). This design leads to four temperature control gas gaps: Gap 1 between the fuel stack and inner surface of the matrix ring, Gap 2 between the matrix ring and inner surface of the graphite sleeve, Gap 3 (inner gap) between the graphite sleeve and inner surface of the graphite sink, and Gap 4 (outer gap) between the graphite sink and inner surface of the capsule retainer. Gaps 1 and 2 are too small, which are not shown in Figure 4.

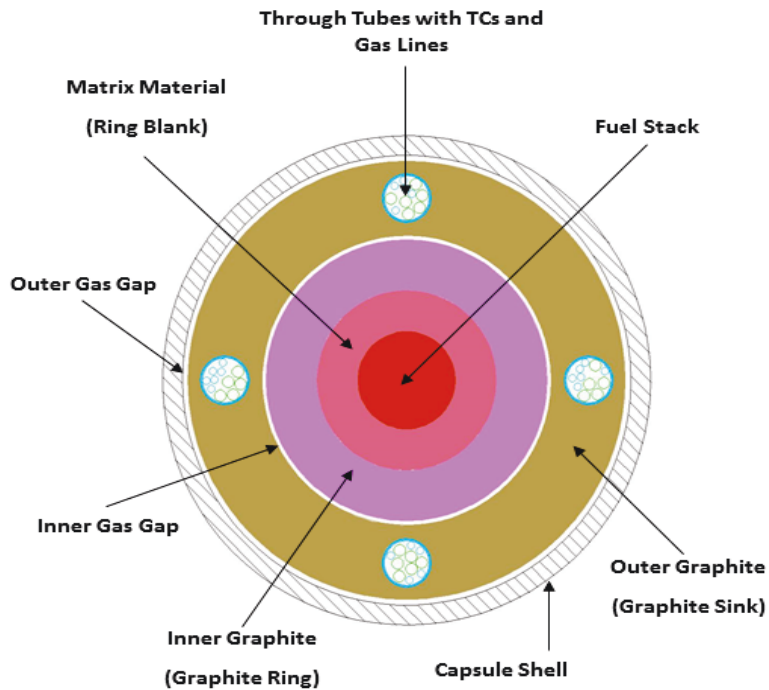


Figure 4. Schematic of radial cut of Advanced Gas Reactor-3/4 capsule.

2.2.2 Thermal Model

One ABAQUS-based (Version 6.14-2), three-dimensional finite-element thermal model is created for each of the 12 AGR-3/4 capsules to predict daily average temperatures of fuel compacts, graphite rings, and TC locations for the entire irradiation period when the ATR core is at power. The ABAQUS thermal model uses about 400,000 eight-node hexahedral brick finite element mesh to estimate capsule temperature profiles as shown in Figure 5 (Hawkes et al. 2015). Validation of ABAQUS, Version 6.14-2, was performed and reported in Hawkes (2015). It comprised 10 thermal models validating different aspects of ABAQUS' heat transfer abilities. The maximum difference between ABAQUS-calculated values and exact theoretical values is just under 2.0%. The governing equation of steady-state conductive heat transfer is expressed as (Hawkes et al. 2015):

$$0 = \frac{\partial}{\partial x} \left(k(T) \frac{\partial T}{\partial x} \right) + \frac{\partial}{\partial y} \left(k(T) \frac{\partial T}{\partial y} \right) + \frac{\partial}{\partial z} \left(k(T) \frac{\partial T}{\partial z} \right) + \dot{q} \quad (1)$$

where

T = temperature

$x, y,$ and z = direction

$k(T)$ = thermal conductivity varying with temperature and neutron fluence

q = heat source.

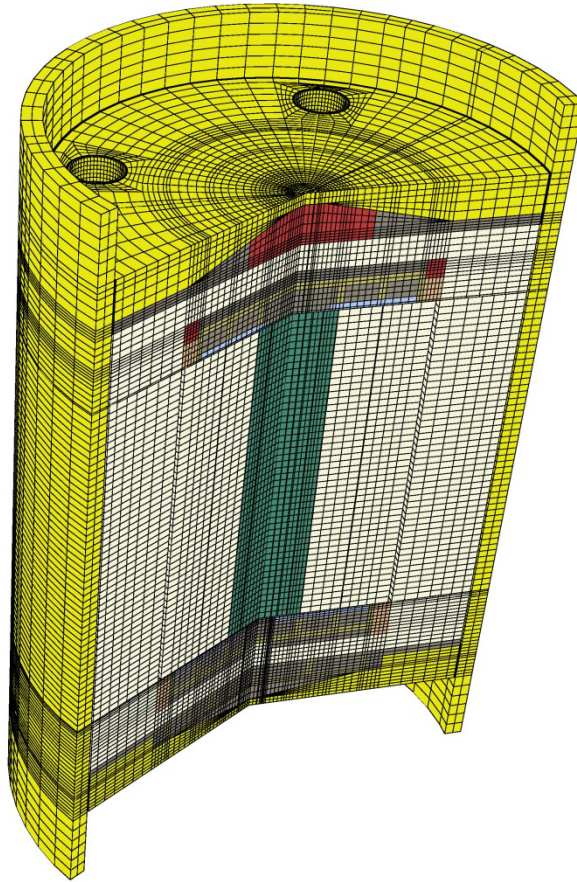


Figure 5. Cutaway view of finite element of Advanced Gas Reactor-3/4 capsule (Hawkes et al. 2015).

The heat transfer through the four gas gaps occurs only by conduction (about 80 to 85%) and radiation (about 15 to 20%); there is negligible advection (<0.01%) due to the very low flow rate of gas (30 cm³/min). The governing equation for radiation heat transfer across the control gas gap is:

$$q_{net} = \frac{\sigma(T_1^4 - T_2^4)}{\frac{(1-\varepsilon_1)}{\varepsilon_1 A_1} + \frac{1}{A_1 F_{12}} + \frac{(1-\varepsilon_2)}{\varepsilon_2 A_2}} \quad (2)$$

where

- q_{net} = net heat flux
- σ = Stephan Boltzmann constant
- T_1 and T_2 = surface temperatures
- ε_1 and ε_2 = emissivity of Surfaces 1 and 2
- A_1 and A_2 = areas of Surfaces 1 and 2
- F_{12} = view factor from Surface 1 to 2.

The main time-series inputs to the model are daily component (fuel compacts, graphite rings, and other components) heat rates (Q) and neutron fast fluences calculated from the as-run depletion analysis (Sterbentz 2015); and daily gas composition of the helium-neon mixture (neon fraction). The fast neutron fluence is needed for calculation of the components' thermal conductivity and estimation of the gas gap sizes. The thermal model estimates capsule temperature profiles as shown in Figure 6 for the whole capsule. While no direct measurements of FTs are available, the graphite holder temperature from the TCs in the AGR capsules was used to validate computer codes.

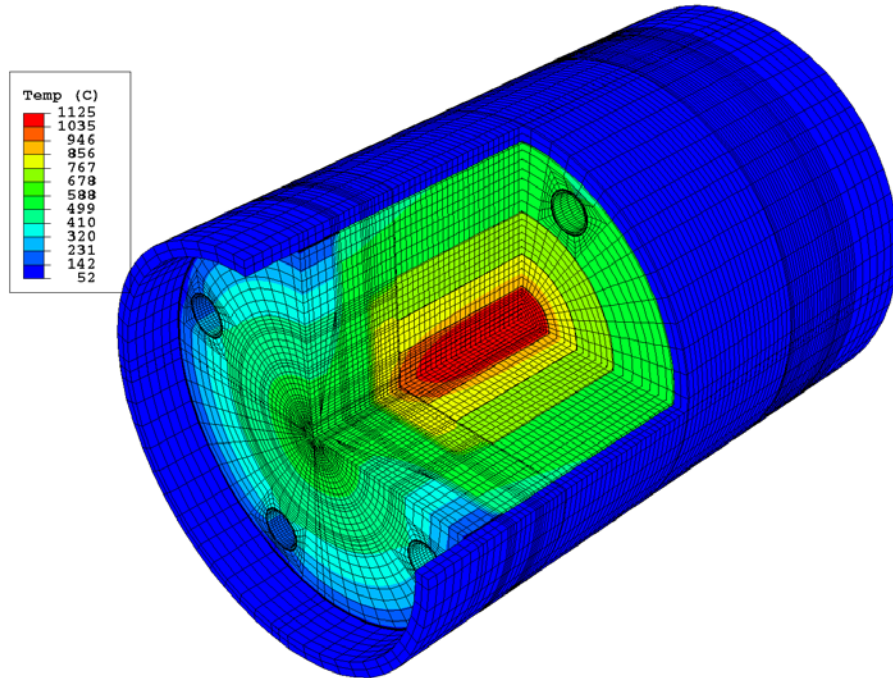


Figure 6. Temperature distribution in cutaway view of Capsule 5.

However, uncertainty remains because of a lack of knowledge about phenomena such as heat- and neutron-induced changes in the capsule gas gaps. All gas gaps were modeled as changing with fast neutron fluence due to fuel compact and graphite material shrinkage. The dimensional changes of compacts and graphite rings are used for estimating gap sizes as a function of fast fluence and matrix temperature. These data were obtained from the following documents (Hawkes et al. 2015): (1) Demkowicz et al. (2011), (2) Gontard and Nabielek (1990), (3) Hrovat et al. (2008), and (4) Windes (2012).

Besides the gas gap assumptions, the following factors and model assumptions may also contribute to predicted temperature uncertainties (Hawkes 2015):

1. Graphite and compact thermal conductivity vary with fluence and temperature, which are taken from legacy experiment correlations and scaled for AGR-3/4 material density.
2. The gas mixture (helium, neon) thermal conductivity is taken from a report from Brown University.
3. Radiation heat transfer occurs from the gaps between surfaces of fuel stack, graphite rings, and the stainless-steel retainer; and graphite sink to thru tubes. An emissivity of 0.4 was assumed for the stainless-steel retainer and an emissivity of 0.9 for the graphite and thru tubes. Thru tubes are considered to be covered with graphite dust.
4. There is no axial heat conduction from one capsule to the next.

Figure 6 presents temperature distribution in a cutaway view of Capsule 5, which is typical for all capsules and time steps (Hawkes 2015). The compact temperature is hottest and peaked along the capsule vertical center line (up to 1125°C in this instance), where the designed-to-fail fuel particles were located. The graphite ring temperature is radially decreasing in the range of 500 to 850°C, with highest temperature in the matrix ring, following by the sleeve ring, and then the graphite sink. Figure 7 and Figure 8 show the calculated daily average fuel compact maximum, average, and minimum temperatures for all capsules (Hawkes 2015).

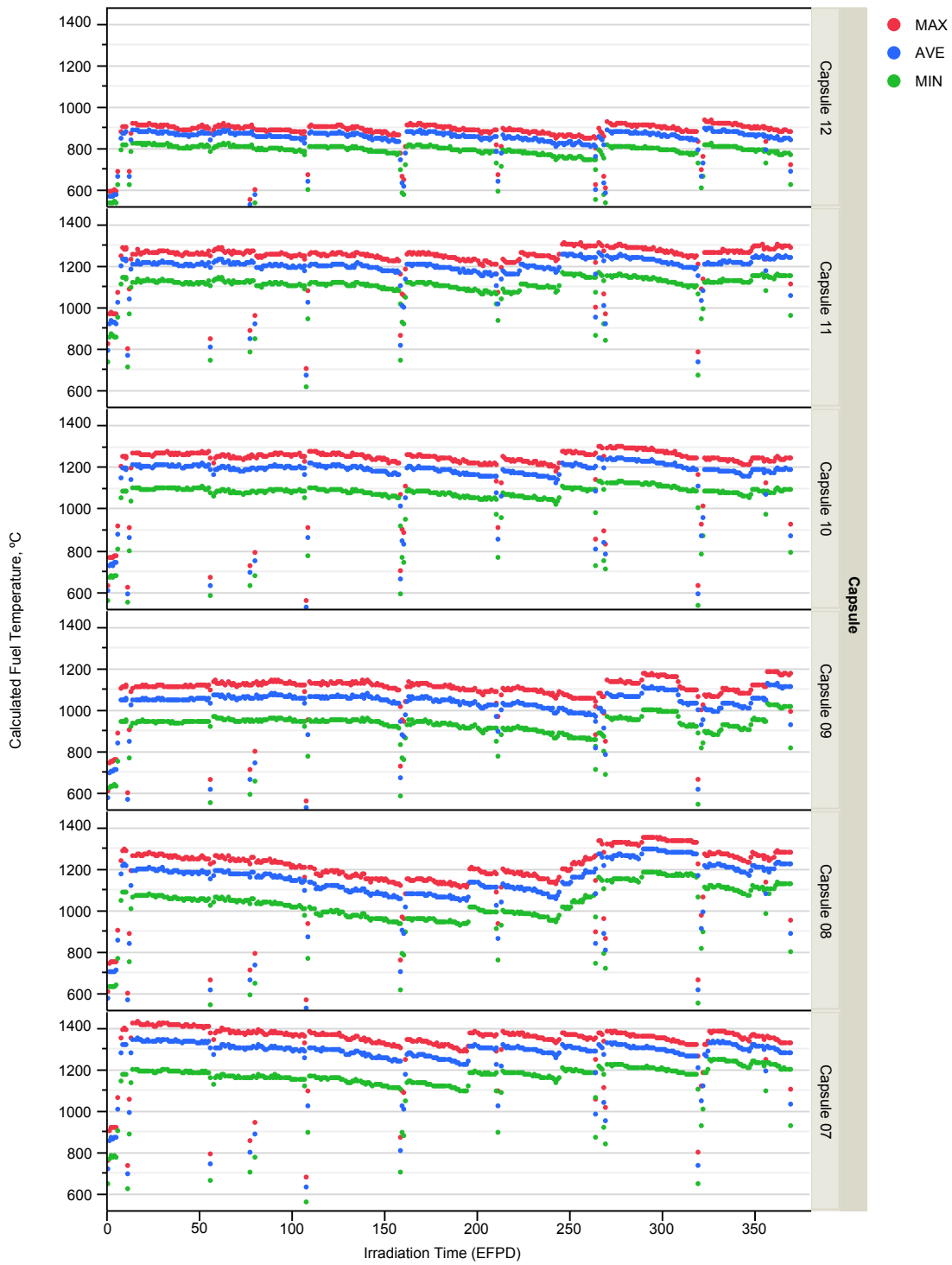


Figure 7. Calculated history of daily minimum, maximum, and volume-averaged temperatures for Capsules 7 through 12.

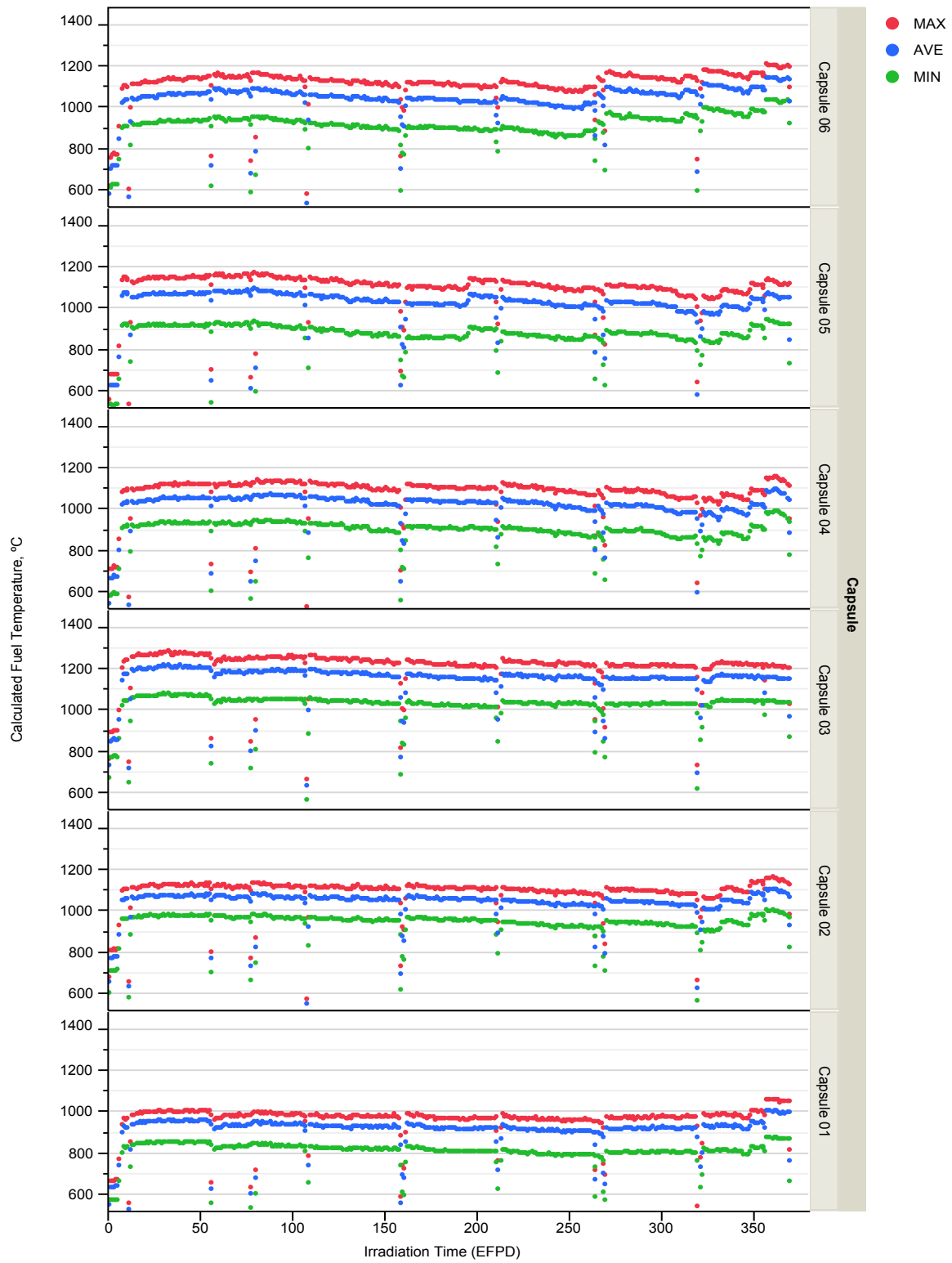


Figure 8. Calculated history of daily minimum, maximum, and volume-averaged temperatures for Capsules 1 through 6.

3. UNCERTAINTY QUANTIFICATION OF MODEL PREDICTED TEMPERATURE

3.1 Technical Approach

In general, uncertainty in the prediction of a simulation model arises from two main sources: input uncertainty and model uncertainty. This is assuming that the numerical errors can be eliminated using sufficient resolution of the finite element mesh in computing code. Subsequently, the overall uncertainty of simulation model predictions in terms of variance can be expressed as:

$$\sigma_T^2 = \sigma_P^2 + \sigma_B^2 \quad (3)$$

where

σ_T^2 = overall uncertainty of predicted temperature in terms of variance

σ_P^2 = input uncertainty in terms of variance

σ_B^2 = model form uncertainty in terms of variance.

The uncertainty quantification process for temperatures predicted by the thermal model includes the following steps:

1. Estimate thermal model form uncertainty.
2. Quantify parameter uncertainty:
 - a. Identify model inputs and quantify parameter uncertainties based on input from modelers and subject matter experts.
 - b. Rank inputs based on parameter influence on output temperatures as a product of input sensitivity and input uncertainty using one time step calculation and select the set of most influential inputs
 - c. Estimate daily uncertainty, sensitivity, and correlation coefficient of selected inputs for the entire AGR-3/4 irradiation period.
 - d. Calculate temperature parameter uncertainty from input uncertainties and sensitivities.
3. Quantify overall uncertainty for instantaneous calculated temperatures (daily average) from model form uncertainty and parameter uncertainty using *Equation (3)*.

The daily uncertainty (in terms of relative and absolute standard deviation at each time step) is estimated for the following calculated temperatures:

- TC temperature
- Instantaneous volume-averaged FT
- Peak FT
- Volume-averaged temperature for the middle 50% of the (outer) graphite ring
- Volume-averaged temperature for the middle 50% of the (inner) matrix ring.

The uncertainties of corresponding time-averaged fuel and graphite temperatures are calculated using uncertainties for instantaneous temperatures.

3.2 Thermal Model Uncertainty

Model uncertainty usually arises from assumptions associated with the mathematical form or structure of the model. This section discusses the rationale of the model form uncertainty of AGR-3/4 calculated temperatures using model performance in predicting temperatures at TC locations. The residuals for all TCs (measured minus calculated TC temperature) in 12 AGR-3/4 capsules are presented in Figure 9 and Figure 10. The average and standard deviation values of TC1 and TC2 residuals for Capsules 5, 7, 11, and 12 are presented in Table 1. According to the plots in Figure 9 and Figure 10, the TC residuals largely remain at the same level and stay within a 100°C range for all TCs over the entire irradiation period, and the standard deviations of TC residuals are small. This fact increases confidence in the assumed gas gap variation models. This is also consistent with findings for the AGR-1 capsule thermal models, which demonstrated that the capsule variable gap size models led to a better fit between calculated and measured TC temperatures (Pham et al. 2014).

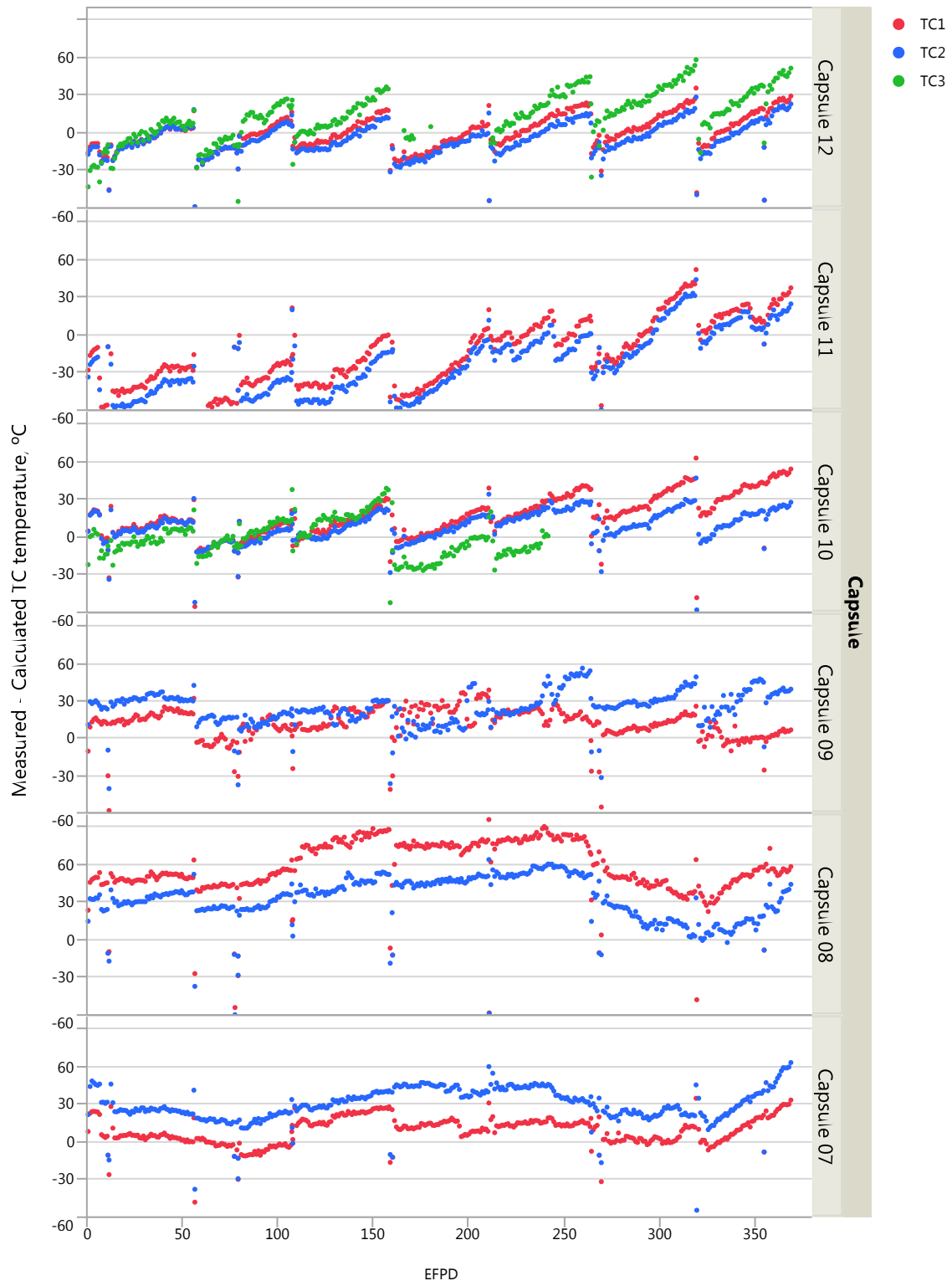


Figure 9. Difference between measured and predicted thermocouple temperatures for Capsules 7 through 12.

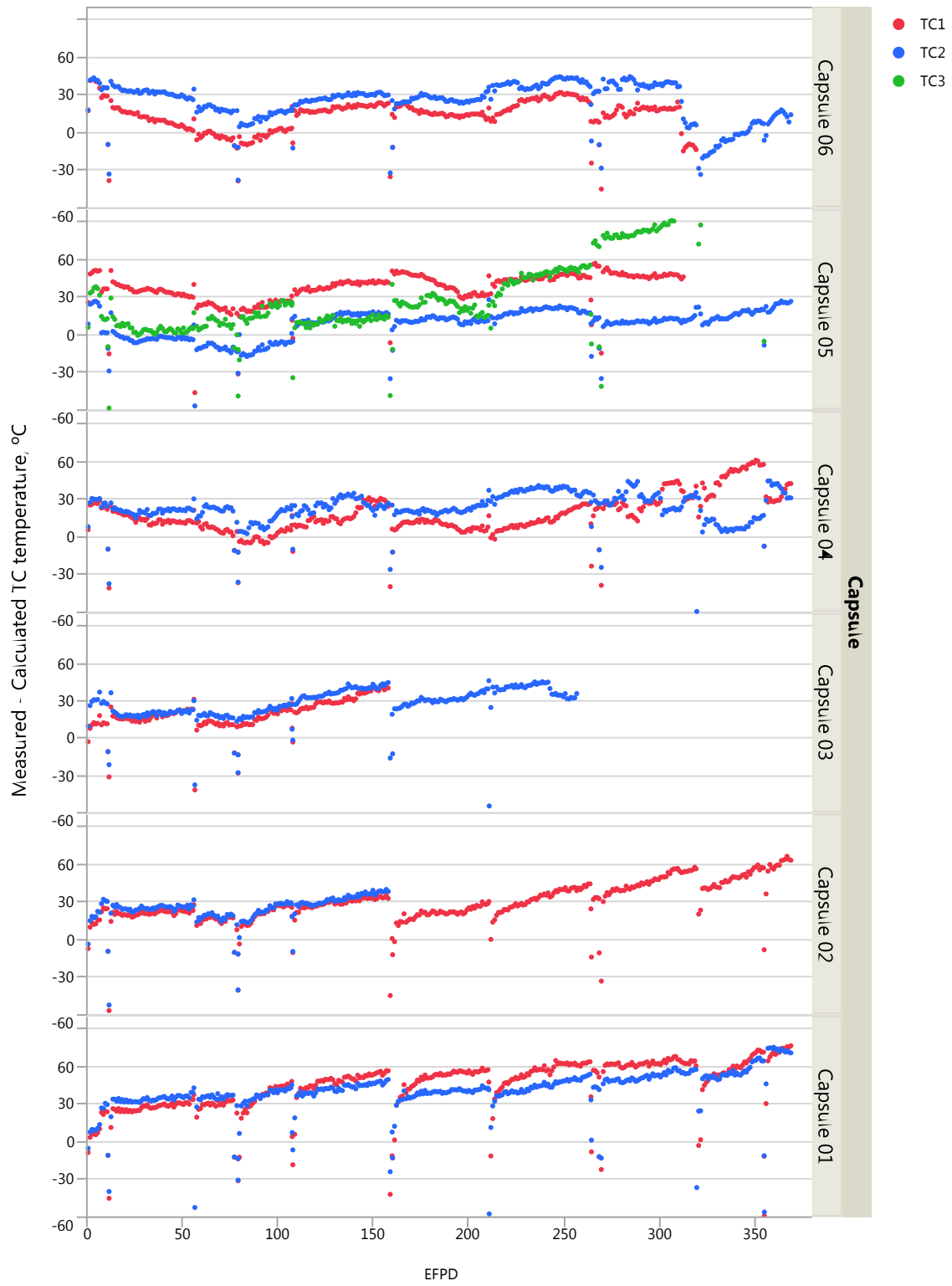


Figure 10. Difference between measured and predicted thermocouple temperatures for Capsules 1 through 6. Itinerary

Table 1. Averaged and standard deviation values of thermocouple residuals for Advanced Gas Reactor-3/4 capsules.

Capsule	Residuals			Standard Deviation		Averaged TC (°C)	Bias (%)
	TC1	TC2	Average	TC1	TC2		
Capsule 12	1	-4	-1	13	11	496	0
Capsule 11	-15	-25	-20	26	27	717	2.8
Capsule 7	9	31	20	10	11	631	3.2
Capsule 5	39	9	24	10	11	556	4.3

As seen in Table 1, Capsule 12 has the smallest average TC residual (-1°C); additionally, as seen in Figure 9, the residuals are lying on both sides of the zero horizontal line, indicating negligible model form uncertainty (or unbiased model) for this capsule. On other hand, Capsules 5, 7, and 11 have average TC residuals of approximately 24°C , 20°C , and -20°C , respectively. As a result, the model form uncertainty (or bias) in terms of relative standard deviation for Capsules 5, 7, 11, and 12 for the entire irradiation period can be estimated as the ratio between average TC residuals and average TC readings, which are presented in the Bias column in Table 1.

3.3 Parameter Uncertainty

Model parameter uncertainty refers to incomplete knowledge of correct values of model inputs, which exists independently with any model, but will impact the uncertainty of model prediction. To quantify the parameter uncertainty of AGR calculated temperatures, ABAQUS model input parameters of potential importance are identified. Identification has two parts: (1) using expert judgment, determine parameters with the largest uncertainties and estimate these uncertainties, and (2) using sensitivity analysis, determine parameters that the modeling is most sensitive to, and refine the estimates of these sensitivities.

The input uncertainties and sensitivity coefficients are combined and propagated to quantify the parameter uncertainty using the following equation, given the predicted temperature can be assumed to be the weighted summation of input parameters:

$$\sigma_p^2 = \sum_i^n a_i^2 \sigma_i^2 + \sum_i^n \sum_{j \neq i}^n \rho_{ij} a_i \sigma_i a_j \sigma_j \quad (4)$$

where

a_i^2 = square of the sensitivity coefficient for parameter i

σ_i^2 = uncertainty of input parameter i in terms of variance

ρ_{ij} = correlation coefficient for input parameters i and j .

This assumption is confirmed during sensitivity analysis.

3.3.1 Influential Input Selection

The selection of input parameters for uncertainty quantification of the AGR-3/4 calculated temperatures is based on the ranking of their influences on variation of temperature predictions. The influence ranking is highest for parameters with large uncertainty and/or large sensitivity. The sensitivity evaluation of the temperature calculations was performed by the modeler (Hawkes 2015a) for the AGR-3/4 experiment on an individual capsule (Capsule 5). A series of cases was compared to a base case by varying different input parameters to the ABAQUS finite element thermal model for Capsule 5 at time step 43 of ATR Cycle 147A. The tornado plots in Figure 11 show the most sensitive input parameters on peak fuel temperature and in Figure 12 for VA fuel temperature, sorted from largest to smallest. Figure 13

shows parameter sensitivities for TC1 temperature. Based on these results, the most sensitive parameters for fuel temperatures are heat rate in the fuel, control gas composition (e.g., neon fraction), and four gap sizes. The next four are heat rate in the graphite, graphite thermal conductivity, fuel conductivity, and gap conductivity between compact and graphite holder. These parameters have different impacts on the temperature at TC locations in the outer graphite ring (TC1). The outer gas gap (Gap 4) has the most impact followed by neon fraction and heat rate. The fuel conductivity has much more influence on peak fuel temperatures, while the heat rate in graphite has a bigger impact on TC1 temperature.

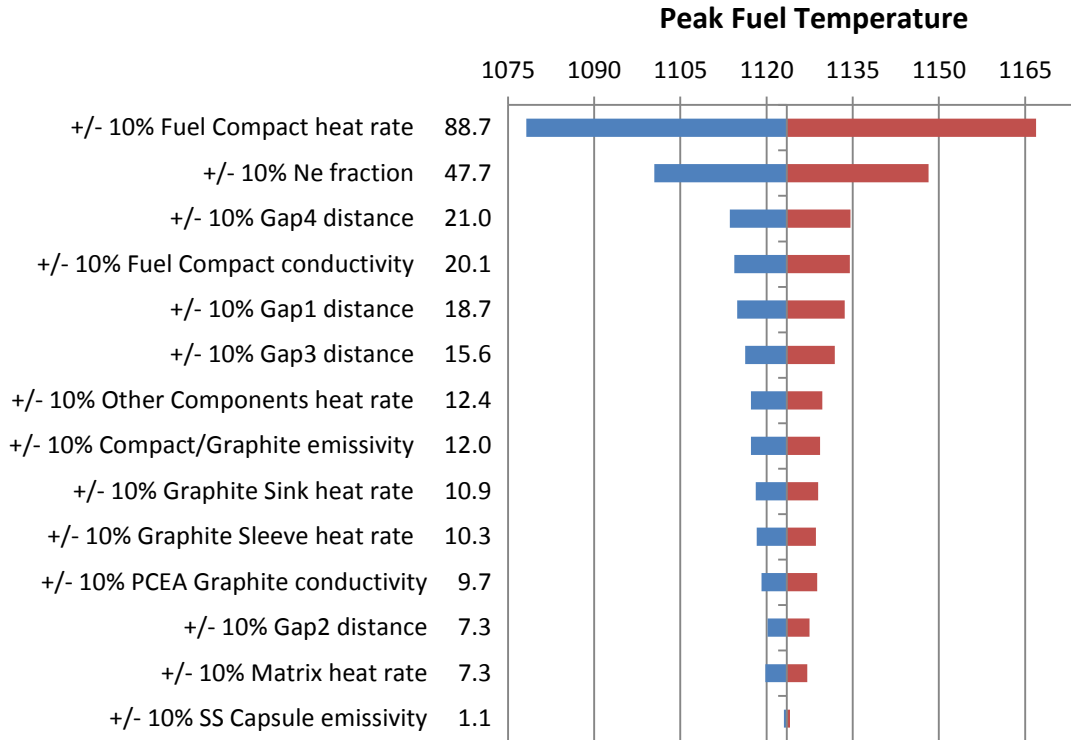


Figure 11. Parameter sensitivities for Capsule 5 peak fuel temperatures.

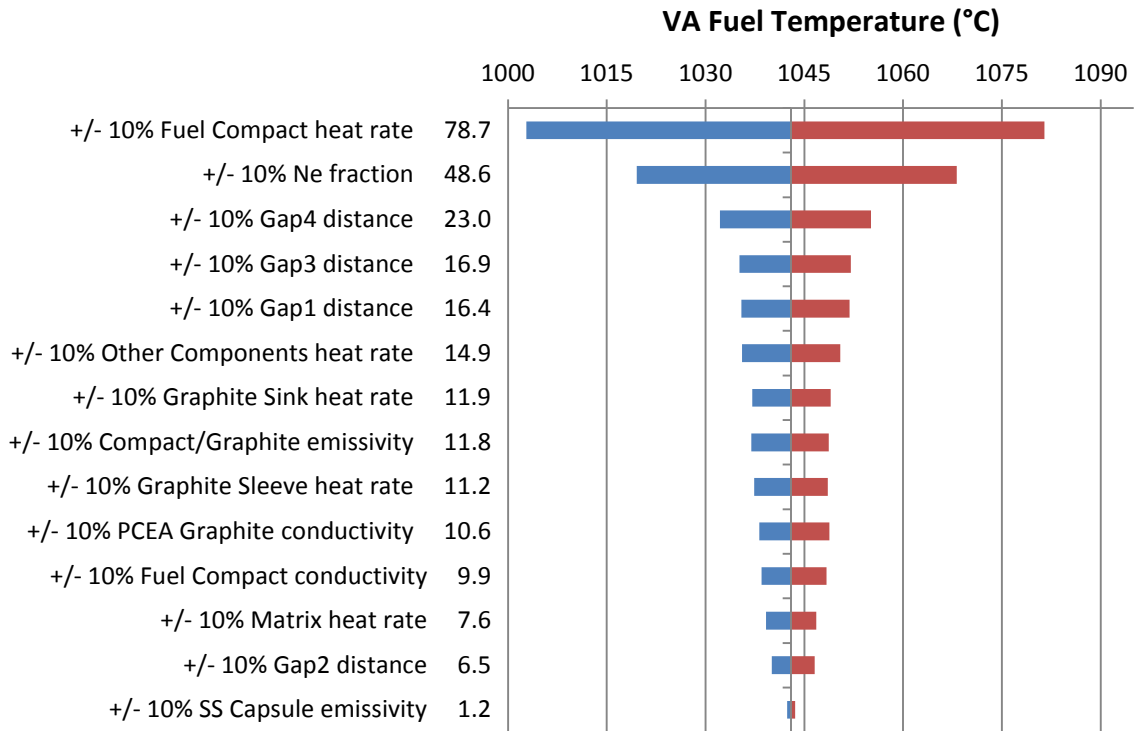


Figure 12. Parameter sensitivities for Capsule 5 volume-averaged fuel temperatures.

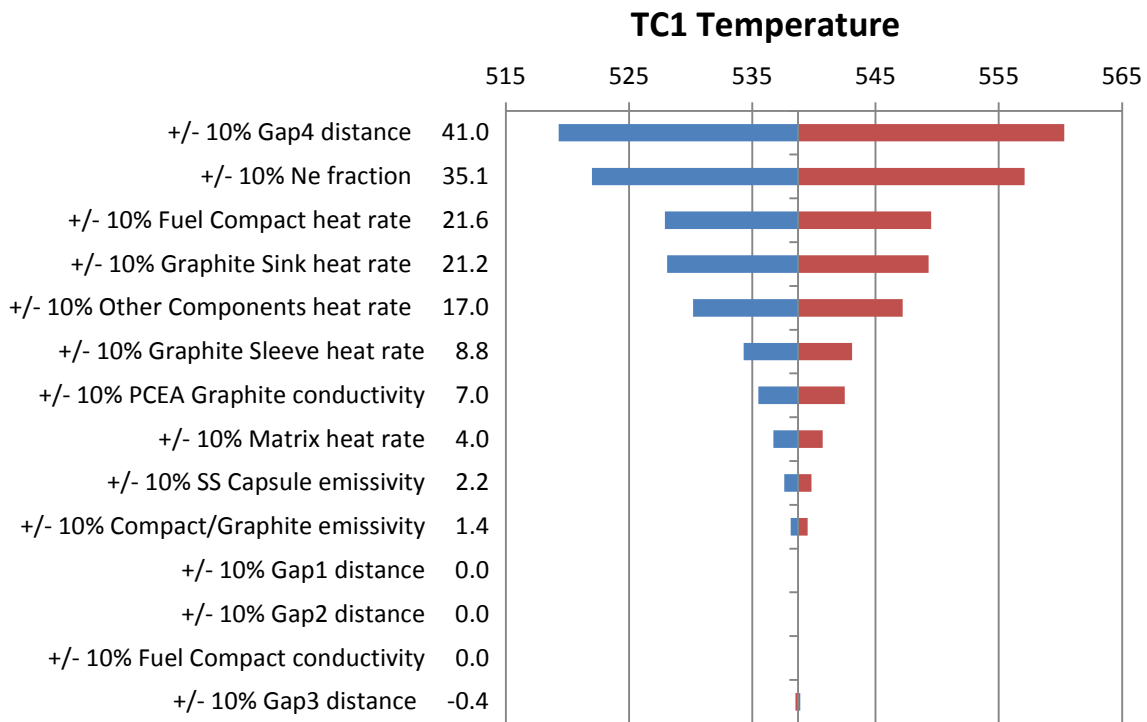


Figure 13. Parameter sensitivities for Capsule 5 calculated TC1 temperatures.

The range of uncertainties for identified inputs to thermal model is determined by ART AGR experts (Petti et al. 2015). Expert judgment takes into account machining tolerances for capsule geometry, measurement uncertainty of mass flow controllers, model uncertainty of neutronics analysis results, and legacy experience for fuel compact and graphite conductivity and emissivity.

After combining input parameter uncertainties with sensitivities, the nine most influential input parameters on AGR-3/4 calculated temperatures are the four gas gap sizes, neon fraction, heat rate in fuel compacts, heat rate in three graphite rings, graphite thermal conductivity (three rings), and fuel compact thermal conductivity as presented in Table 2. The first three parameters were chosen because of high sensitivity and the last two, having much lower sensitivity, were chosen because of their significantly higher input uncertainty. The four gas gap sizes have high impact on all temperatures of interest because of their high uncertainties. The emissivity is not included because of insignificant sensitivity on calculated temperatures.

Table 2. Uncertainties of identified significant inputs to thermal model for AGR-3/4 capsules.

Parameter	Uncertainty	Rationale
Gap 1 about 3 mil	[1 to 1.3 mil]	Uncertainty at start of irradiation is 1 mil based on fabrication tolerance. Uncertainty over course of irradiation is time dependent because of graphite holder shrinkage, which is proportional to the reaction rate in the graphite. This leads to a physics-based gas gap model. Thus, the absolute gap uncertainty is assumed to be a linear function of fluence. By the end of irradiation, gap uncertainty is estimated using uncertainty of the AGR-1 and AGC-1 PIE compact and graphite dimensional change data (Subsection 3.3.2.1).
Gap 2 [3 to 39 mil]	[1 to 1.9 mil]	
Gap 3 [8 to 150 mil]	[1 to 2.7 mil]	
Gap 4 [12 to 85 mil]	[1 to 4.4 mil]	
Neon fraction	Function of neon fraction	Uncertainty is based on 1-sccm flow rate tolerance and estimated from neon fraction prediction equation (Subsection 3.3.2.2).
Fuel compacts' heat rate	5%	Based on AGR-1 comparison done by J. Harp with additional input from J. Sterbentz (Subsection 3.3.2.3).
Graphite rings' (matrix, sleeve, and sink) heat rate	3%	
Graphite conductivity	15%	Additional conductivity data for the test graphite allows a lower uncertainty estimate for graphite than for fuel.
Fuel conductivity	20%	Uncertainty is based on work done on surrogate compacts by C. Folsom at Utah State University.

3.3.2 Input Uncertainties

Table 2 summarizes the uncertainties for the nine most influential input parameters in terms of impact on calculated temperatures as determined by ART AGR experts. However, the input uncertainties over the course of irradiation are dynamic, accounting for the effect of unplanned events and changes in thermal properties of capsule components (e.g., changes in distances of four gas gaps) over extended exposure to high temperatures and fast neutron irradiation. This section lays out the basis for determination of the input uncertainty for the nine selected parameters for each time step over the entire AGR-3/4 irradiation.

3.3.2.1 Gap Sizes. Each AGR-3/4 capsule has a stack of four fuel compacts in the center surrounded by three graphitic annuli: proceeding from the compact out are the matrix ring (inside), graphite sleeve, and graphite sink (outside). This design leads to four temperature control gas gaps: Gap 1 between the fuel stack and inner surface of the matrix ring, Gap 2 between the matrix ring and inner surface of the graphite sleeve, Gap 3 between the graphite sleeve and inner surface of the graphite sink, and Gap 4 between the graphite sink and inner surface of capsule wall (Figure 4). At the beginning of irradiation, the as-fabricated compacts' and graphite rings' diameters and capsule retainer sleeve inner diameter are adjusted, taking into account the thermal expansions when capsules are brought up to temperature. The initial "hot" gap sizes, equal to a half of the difference between the corresponding adjusted diameters, is used in the ABAQUS model to predict temperatures in each capsule for the first time step of irradiation. At this point in time, the associated uncertainties of all four gap sizes were based on machining tolerance and assumed to be about 0.001" (1 mil) for all 12 capsules. The initial gap sizes for four gaps in each of the 12 capsules are presented in Table 3, Columns 2 through 5, and Figure 14. The associated uncertainties in terms of percentage of 1-mil gap error and initial gap size are presented in Table 3, Columns 6 through 9. For all capsules, Gaps 1 and 2 have the smallest distance, leading to the highest relative uncertainty. Gaps 3 and 4 have the largest distances, especially in Capsules 1 and 11; subsequently they have the least relative uncertainty.

Table 3. Initial gap sizes and uncertainties for AGR-3/4 capsules.

Capsule	Initial Gap Size (in.)				Initial Gap Uncertainty (%)			
	Gap 1	Gap 2	Gap 3	Gap 4	Gap 1	Gap 2	Gap 3	Gap 4
1	0.00265	0.01445	0.14995	0.06123	37.7	6.9	0.7	1.6
2	0.00295	0.00350	0.06005	0.05171	33.9	28.6	1.7	1.9
3	0.00295	0.00225	0.15010	0.01502	33.9	44.4	0.7	6.7
4	0.00250	0.00250	0.01005	0.02099	40.0	40.0	10.0	4.8
5	0.00285	0.00235	0.00800	0.01237	35.1	42.6	12.5	8.1
6	0.00295	0.00335	0.00750	0.02114	33.9	29.9	13.3	4.7
7	0.00295	0.00300	0.04050	0.01152	33.9	33.3	2.5	8.7
8	0.00270	0.00275	0.02150	0.01039	37.0	36.4	4.7	9.6
9	0.00295	0.00350	0.01060	0.02473	33.9	28.6	9.4	4.0
10	0.00320	0.00200	0.04025	0.02114	31.2	50.0	2.5	4.7
11	0.00270	0.03925	0.15025	0.08519	37.0	2.5	0.7	1.2
12	0.00295	0.00350	0.09950	0.06048	33.9	28.6	1.0	1.7

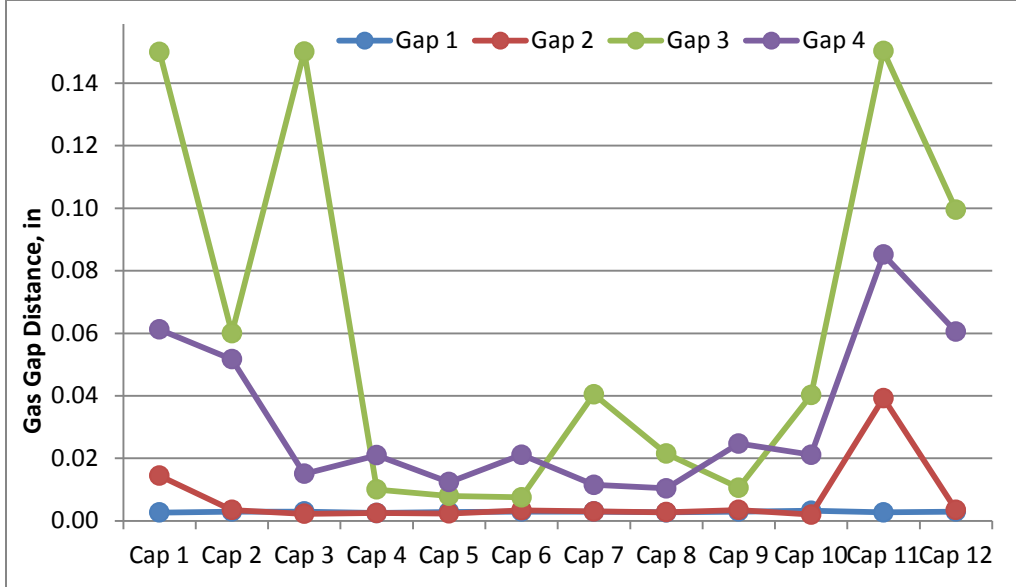


Figure 14. Initial gap sizes for all 12 AGR-3/4 capsules.

As the experiment progresses, the material properties of capsule components are changing because of high temperatures and neutron fluence exposure. It is well-known that under neutron irradiation graphite materials typically shrink leading to dimension changes of fuel compacts and the three graphite rings. The dimensional change data for AGR-3/4 capsules are obtained from the following documents (Hawkes et al. 2015): (1) Demkowicz et al. (2011), (2) Gontard and Nabielek (1990), (3) Hrovat et al. (2008), and (4) Windes (2012). Table 4 summarizes radius changes for the fuel compacts and matrix ring and volume changes for the graphite sleeve and graphite sink (PCEA and IG-110). These dimensional changes vary with fast neutron fluence and temperature, and are used for estimation of the daily distances for four gas gaps in each capsule.

Table 4. Compact, matrix, and graphite rate of change varying with fast fluence and temperature.

Fast Fluence, 10^{25} n/m ²	Compact	Matrix				Graphite	
		430°C	900°C	1160°C	1430°C	PCEA	IG-110
		$\Delta r/r$	$\Delta r/r$	$\Delta r/r$	$\Delta r/r$	$\Delta V/V$	$\Delta V/V$
0	0.0000	0.0000	0.0000	0.0000	0.0000	0.0000	0.0000
1	-0.0059	-0.0046	-0.0020	-0.0046	-0.0064	-0.0062	-0.0077
2	-0.0095	-0.0088	-0.0037	-0.0081	-0.0121	-0.0125	-0.0146
3	-0.0110	-0.0125	-0.0051	-0.0105	-0.0169	-0.0187	-0.0209
4	-0.0110	-0.0158	-0.0061	-0.0121	-0.0209	-0.0249	-0.0264
5	-0.0110	-0.0186	-0.0069	-0.0129	-0.0242	-0.0311	-0.0313
6	-0.0110	-0.0209	-0.0073	-0.0130	-0.0266	-0.0374	-0.0354
7	-0.0110	-0.0227	-0.0074	-0.0124	-0.0283	-0.0436	-0.0388
8	-0.0110	-0.0241	-0.0072	-0.0114	-0.0292	-0.0498	-0.0416

The gap sizes used in the ABAQUS models are calculated as follows:

$$\text{For Gap 1: } G_1 = G_{10} - \Delta r_{compact} + \Delta r_{in_matrix} \quad (5)$$

$$\text{For Gap 2: } G_2 = G_{20} - \Delta r_{out_matrix} + \Delta r_{in_sleeve} \quad (6)$$

$$\text{For Gap 3: } G_3 = G_{30} - \Delta r_{out_sleeve} + \Delta r_{in_sink} \quad (7)$$

$$\text{For Gap 4: } G_4 = G_{10} - \Delta r_{out_sing} + \Delta r_{in_capsule} \quad (8)$$

where

G_{10} = initial distance of Gap 1

$\Delta r_{compact}$ = radius change of compact

Δr_{in_matrix} = inner radius change of matrix ring

Δr_{out_matrix} = outer radius change of matrix ring

Δr_{in_sleeve} = inner radius change of sleeve ring

Δr_{out_sleeve} = outer radius change of sleeve ring

Δr_{in_sink} = inner radius change of sink ring

Δr_{out_sink} = outer radius change of sink ring

$\Delta r_{in_capsule}$ = radius change of capsule wall.

Note that all radius changes are negative due to material shrinkage of fuel compacts and matrix, sleeve, and sink rings. Figure 15 shows the actual gap sizes used in the ABAQUS thermal models as a function of EFPDs for four gaps in each of the four capsules included in this report, Capsules 5, 7, 11, and 12. The complex dimensional change of the matrix ring leads to non-linear variation of Gaps 1 and 2 as a function of irradiation time.

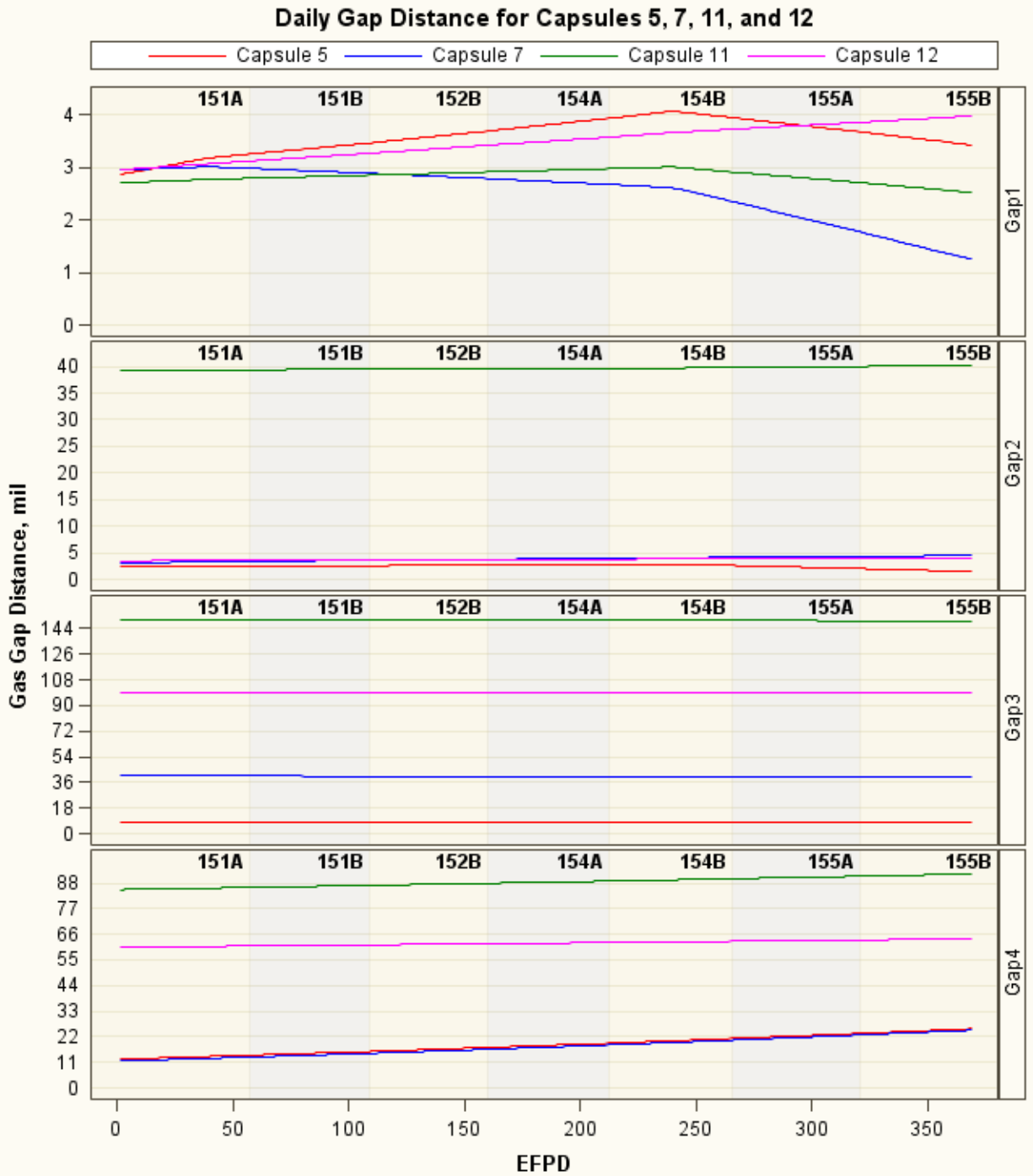


Figure 15. ABAQUS gap size as function of effective full-power days for Capsules 5, 7, 11, and 12.

For Gap 1, the gap uncertainty is estimated by propagating the uncertainty of each term in Equation (5) as follows:

$$\sigma_{G1e} = \sqrt{\sigma_{G10}^2 + \sigma_{\Delta r_{compact}}^2 + \sigma_{\Delta r_{in_matrix}}^2} \quad (9)$$

where

σ_{G10} = initial gap 1 uncertainty estimated as 1 mil in Table 2

$\sigma_{\Delta r_{compact}}$ = uncertainty of the change in compact radius

$\sigma_{\Delta r_{in_matrix}}$ = uncertainty of the change in matrix inner radius.

As stated above, the compact dimensional change is estimated using metrology data obtained during PIE of the AGR-1 experiment as shown in Figure 16 (Hawkes 2015). The rate of radius change in AGR-1 compacts at the end of irradiation (green triangles in Figure 16) is applied for AGR-3/4 compacts as the averaged value of radius changes. Therefore, uncertainty of the estimated radius change is caused by the variation of radius changes from compact to compact and by the uncertainty of each radius change measurement. According to Hawkes (2015), the uncertainty of each radius change measurement (each green triangle) is 10%. Looking at one level of fluence in Figure 16, the widest variation of compact radius changes is approximately $\pm 20\%$ around the mean value of 1.1%. As a result, the uncertainty in compact dimensional change ($\frac{\Delta r}{r}$) can be estimated as:

$$\sigma_{\frac{\Delta r}{r}} = \sqrt{\sigma_{\Delta r_{AGR-1\ compact}}^2 + \sigma_{AGR-1\Delta r_{compact\ variance}}^2} = \sqrt{10\%^2 + 20\%^2} = 22\% \quad (10)$$

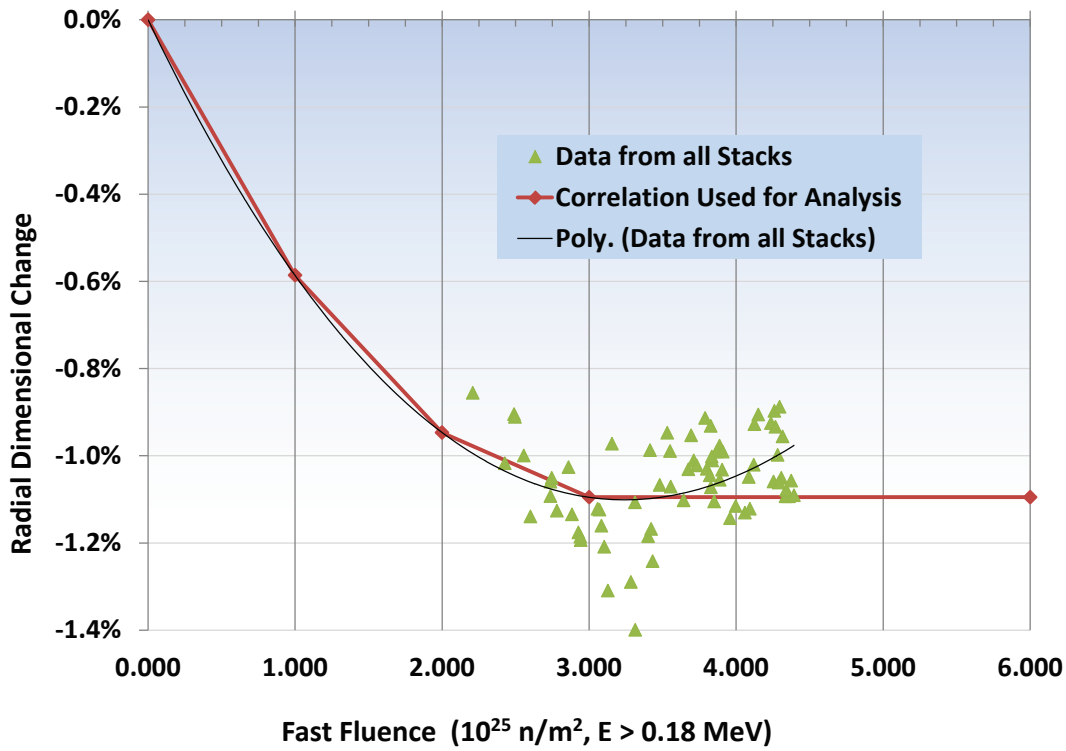


Figure 16. Radius changes of Advanced Gas Reactor-1 fuel compacts (Hawkes 2015).

The uncertainty in terms of absolute value in mils of the compact radius change will be:

$$\sigma_{\Delta r_{compact}} = \frac{\Delta r}{r} * r_{compact} * \sigma_{\frac{\Delta r}{r}} = 1.1\% * 243 \text{ (mil)} * 22\% = 0.58 \text{ (mil)} \quad (11)$$

where

$r_{compact}$ = compact radius, which is equal to 243 mil.

The maximum change in compact radius used in the AGR-3/4 capsule is 1.1%. Assuming the same uncertainty for changes of the inner matrix radii, the uncertainty of changes in Gap 1 in terms of absolute value at the end of irradiation can be estimated using *Equation (9)*:

$$\sigma_{G_{1e}} = \sqrt{1 + 0.58^2 + 0.58^2} = 1.3 \text{ (mil)} \quad (12)$$

That is, the uncertainty in Gap 1 increases from the initial gap uncertainty (σ_{G_1}) of 1 mil at the beginning of irradiation to the end gap uncertainty ($\sigma_{G_{1e}}$) of 1.3 mil by the end of irradiation. For time steps between the beginning and the end of irradiation, the daily Gap 1 uncertainty in terms of absolute value (in mils) is estimated as a linear interpolation of initial and end Gap 1 uncertainty as follows:

$$\sigma_{G_{1i}} = \sigma_{G_1} + \frac{fluence_i}{fluence_e} (\sigma_{G_{1e}} - \sigma_{G_1}) \quad (13)$$

Assuming the same uncertainty for changes of both inner and outer matrix radii, sleeve, and sink rings, and capsule shell, the uncertainty in terms of absolute value for the remaining gaps, Gap 2 through Gap 4, can be estimated using *Equations (9) through (13)*. The relative uncertainty of the gaps is calculated as the ratio of absolute uncertainty and the gap size as shown in Figure 17. Since the radii of the fuel compacts, three graphite rings, and capsule shell are similar in all capsules, it is reasonable to assume the same gap uncertainties for all 12 AGR-3/4 capsules. The absolute initial and end gap uncertainties (in mils) for four gaps are presented in Table 2. As seen in Figure 17, Gap 2 in Capsule 5 reached 128% relative uncertainty in terms of standard deviation at the end of irradiation, and Gap 1 in Capsule 7 reached 104% relative uncertainty. This is because the decrease in gap sizes at the end of irradiation caused a large increase in relative uncertainty.

The assumption that the uncertainty of changes in the inner and outer matrix radii, sleeve, and sink rings are the same as the uncertainty in the compact radius will be reconsidered when the uncertainty analysis is repeated for the remaining capsules.

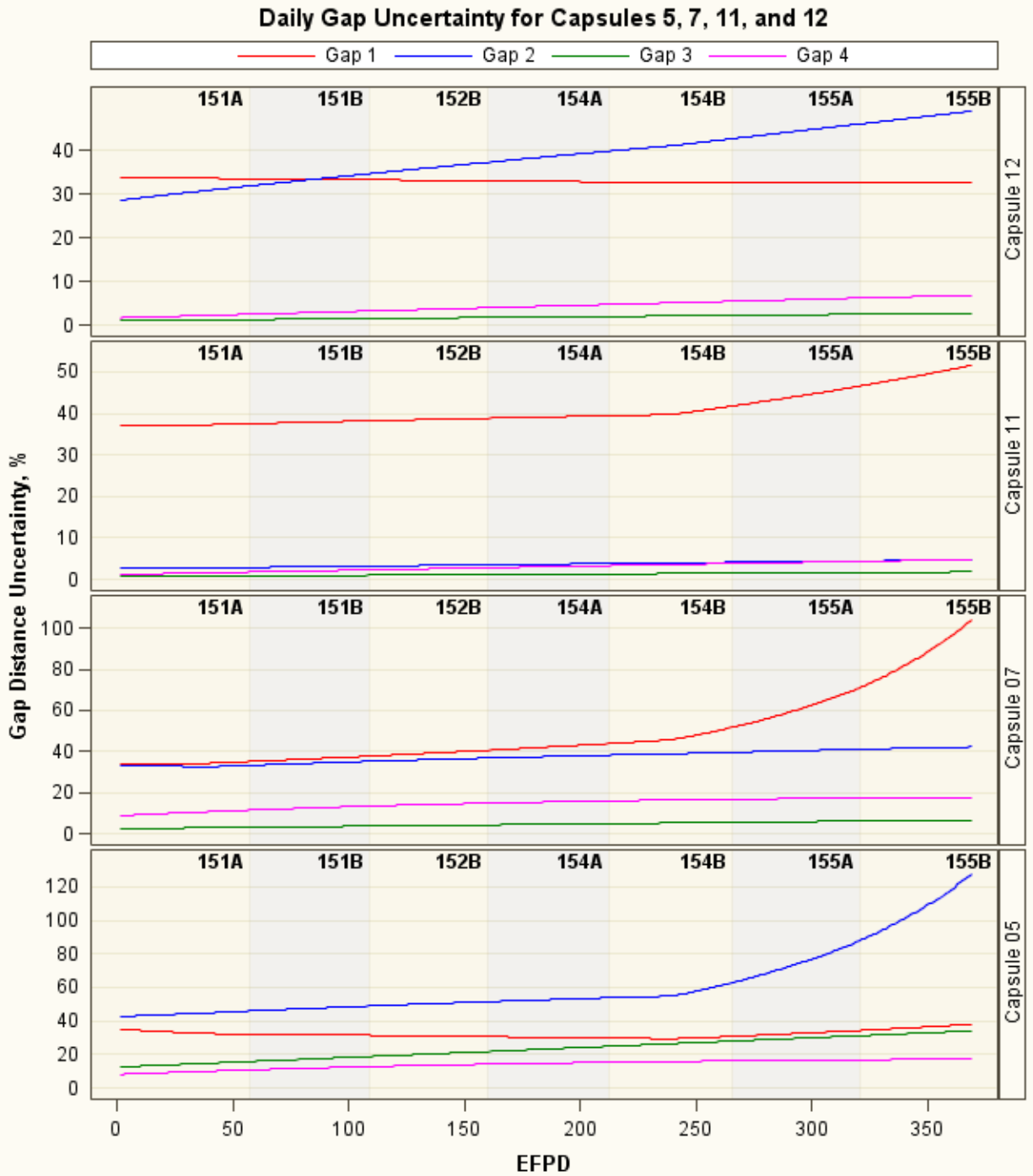


Figure 17. Daily uncertainty of distances of Gaps 1 through 4 in Capsules 5, 7, 11, and 12.

3.3.2.2 Neon Fraction. Heat produced mainly in the fuel compacts and graphite rings transfers through the control gas gaps via a gap conductance modelled as a function of the gap size and the conductivity of the sweep gas (Hawkes 2014). The neon fraction of the capsule control gas mixture is, in turn, used in the correlation taken from a report from Brown University to determine the gas mixture conductivity. As designed, the capsule gas lines do not cross-talk with each other either before or after gas enters an individual capsule, and the amount of gas leaking out from a capsule gas line to the leadout is

negligible; any gas leaking in to a capsule is assumed to come only from the leadout flow. As a result, the calculation formula for the neon fraction in each capsule, including potential gas leakage to and from the leadout flow, is expressed as:

$$Fr_{Ne} = \frac{Q_{Ne} + \max(Q_{outlet} - Q_{Ne+He}, 0) * \frac{Q_{Neleadout}}{Q_{Ne+Heleadout}}}{\max(Q_{outlet}, Q_{Ne+He})} \quad (14)$$

where

Fr_{Ne} = neon fraction

Q = gas flow in sccm.

The main source of neon fraction uncertainty is the measurement error in the gas flow meters, which have a 1-sccm tolerance (Table 2) based on engineering assessment. A neon fraction simulation of Equation (14), with neon and helium flows taken randomly from a normal distribution with mean value and standard deviation of 1 sccm, was performed for different neon fraction levels. The neon fraction uncertainty for each neon fraction level is equal to the standard deviation calculated from 100,000 random neon fraction results. Figure 18 plots the relative neon fraction standard deviations (uncertainty) as a function of the neon fraction values. The power equation option of the trend line feature of the Microsoft Excel platform is used to estimate a function that results in a good fit to the data ($R^2=0.9924$). Therefore, the relative neon fraction uncertainty can be expressed as a function of neon fraction as:

$$\sigma_{Fr_{ne}} = \frac{2.5487}{Fr_{Ne}^{1.047}} \quad (15)$$

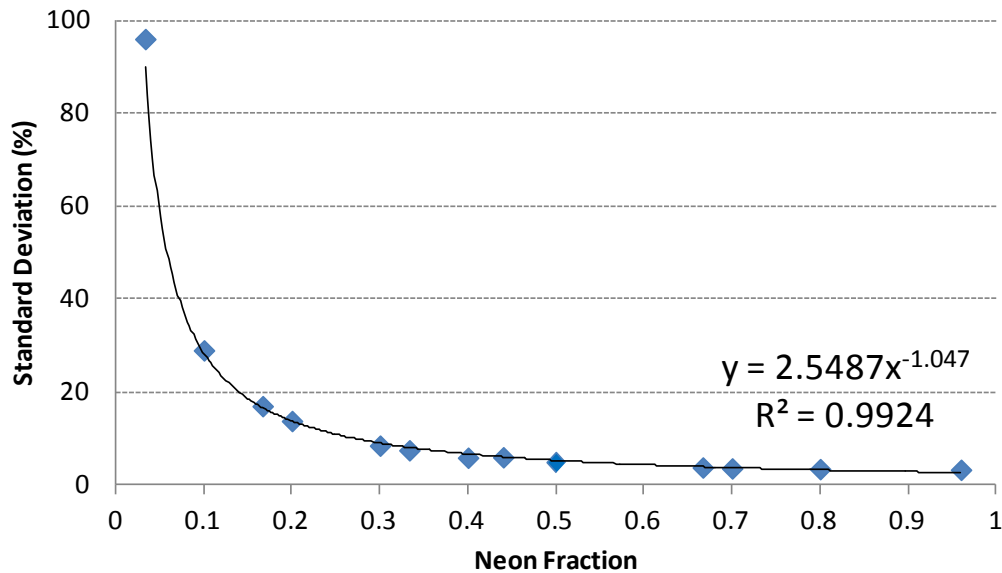


Figure 18. Neon fraction uncertainty and trend line.

Neon fraction uncertainty is estimated well using a power function of neon fraction. Thus, the relative uncertainty is high at low neon fraction (about 100% at 0.03 neon fraction) because of high relative uncertainty of the mass flow controllers at lower neon flow rates. However, when AGR-3/4 runs on pure helium (i.e., capsule neon flow rate is 0 sccm), it becomes certain that $FR_{Ne} \approx 0$, resulting in a drop in neon fraction uncertainty to about 3% ($\pm 1/30$) due to 1-sccm uncertainty of neon flow rate. Conversely, when the capsule and leadout gas flows are pure neon (i.e., capsule neon flow rate is 30 sccm), then it is also certain that $FR_{Ne} \approx 1$, but the neon fraction uncertainty is near 0% [about $1/(30 \cdot 30)$] due to lower relative uncertainty of neon flow rate ($1/30$).

3.3.2.3 Fuel and Graphite Heat Rates. The fuel compacts' and graphite rings' heat rates are taken from the as-run physics calculation (Sterbentz 2015). The uncertainty in the calculated fuel heat rate is caused by a collection of several factors from ATR measured data input parameters that go into the physics calculation and Monte Carlo statistical uncertainties associated with calculated parameters. However, good agreement between burnup calculated by the physics depletion model (ECAR-958 Burnup Simulation) and PIE measurements for AGR-1 experiment as shown in Figure 19 (Harp 2014), where the difference is less than 10% for the worst compact, indicates that the instantaneous (daily) fuel fission power uncertainty should be small. These specific uncertainties include:

1. ATR total core or lobe power of $\pm 4.1\%$
2. Fuel compact uranium beginning-of-life number densities of $\pm 0.5\%$
3. Calculated irradiation flux of $\pm 1.0\%$
4. Calculated reaction rates or a one group cross section of $\pm 2.0\%$
5. Power normalization factors of $\pm 1.0\%$
6. Outer shim control cylinder hafnium and beryllium reflector poison number densities of $\pm 1.0\%$
7. Outer shim control cylinder rotational position of $\pm 0.5\%$.

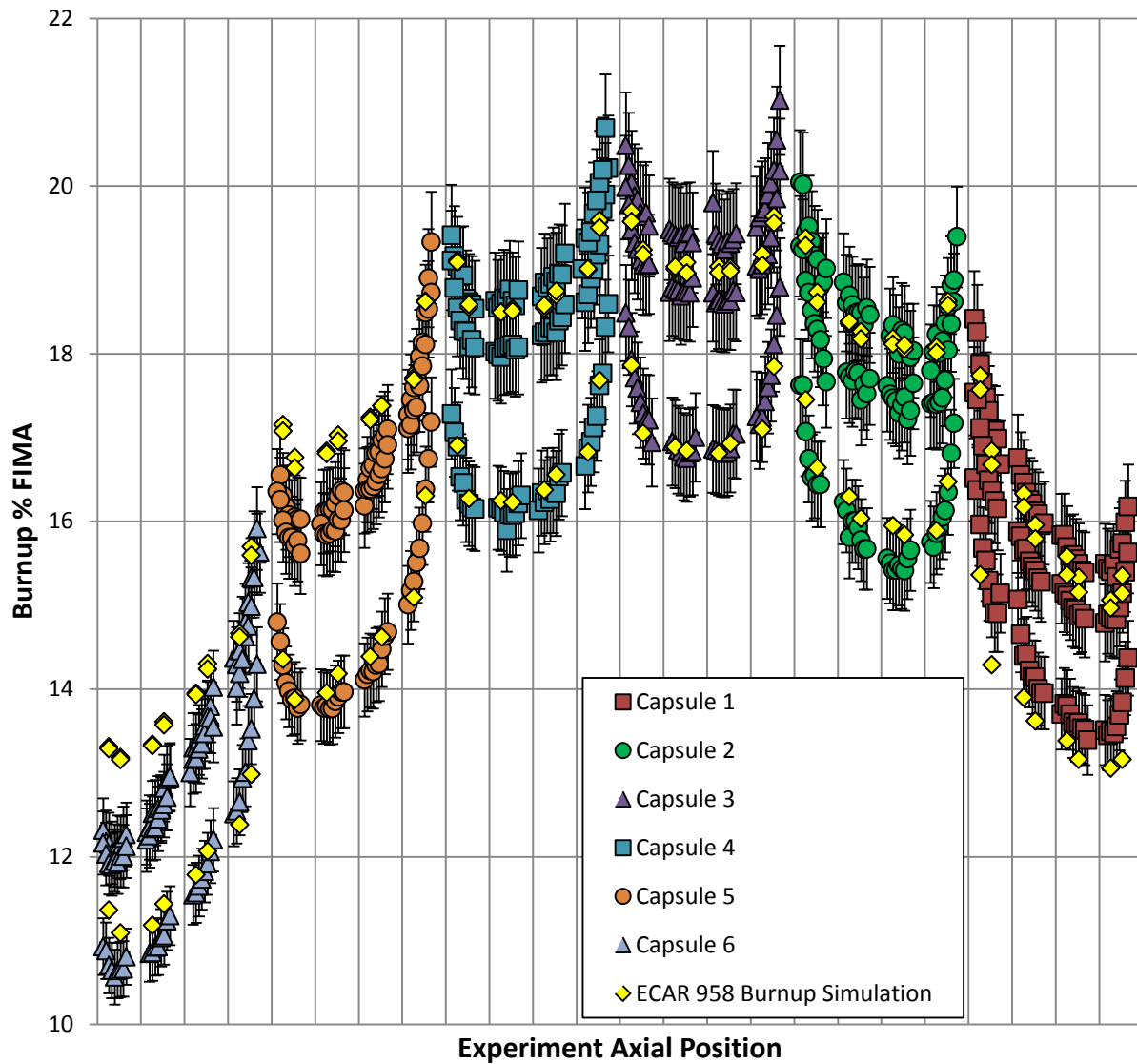


Figure 19. Burnup derived from Cs-134/Cs-137 activity ratio for each measured precision gamma scanner slice for all AGR-1 capsules compared to simulations from ECAR-958. Each vertical tick mark represents a separate level in each capsule (Harp 2014).

Assuming these individual uncertainties to be random, the overall fuel heat rate uncertainty can be estimated to be $\pm 5.0\%$ for all capsules and all cycles, which is similar for AGR-2 capsules. Figure 20 shows the averaged fuel compact heat rate for each of 12 capsules versus the time of irradiation in EFPDs. In contrast to AGR-1 and AGR-2 experiments, the fuel compact heat rates in the 12 AGR-3/4 capsules have remained relatively steady throughout the entire irradiation, thanks to the ability to regulate the necessary power of the ATR core near the NEFT location, where the AGR-3/4 experiment was located. During each cycle, the fuel heat rates in the middle capsules (5 to 9) decrease by approximately 20%.

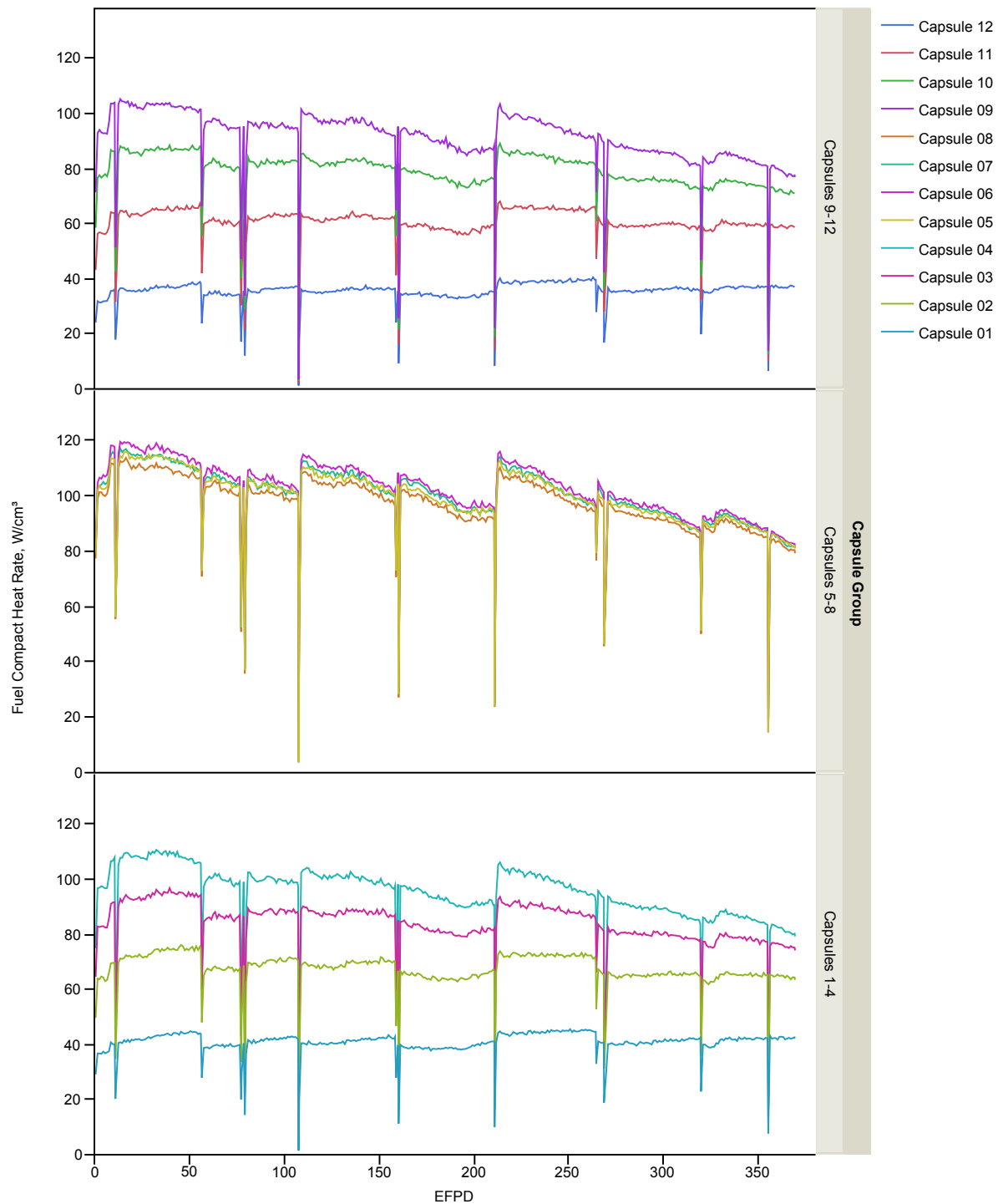


Figure 20. Capsule average fuel compact heat rate versus irradiation time in effective full-power days.

The graphite heat rates shown in Figure 21 are an order of magnitude lower than fuel heat rates. However, the total volume of the three graphite rings in each capsule is much larger than total volume of the four fuel compacts, which leads to significant influence of the graphite heat rate on calculated temperatures, especially at TC locations in the graphite sink. Thus, the heat rate of the three graphite rings is included in this calculated temperature uncertainty.

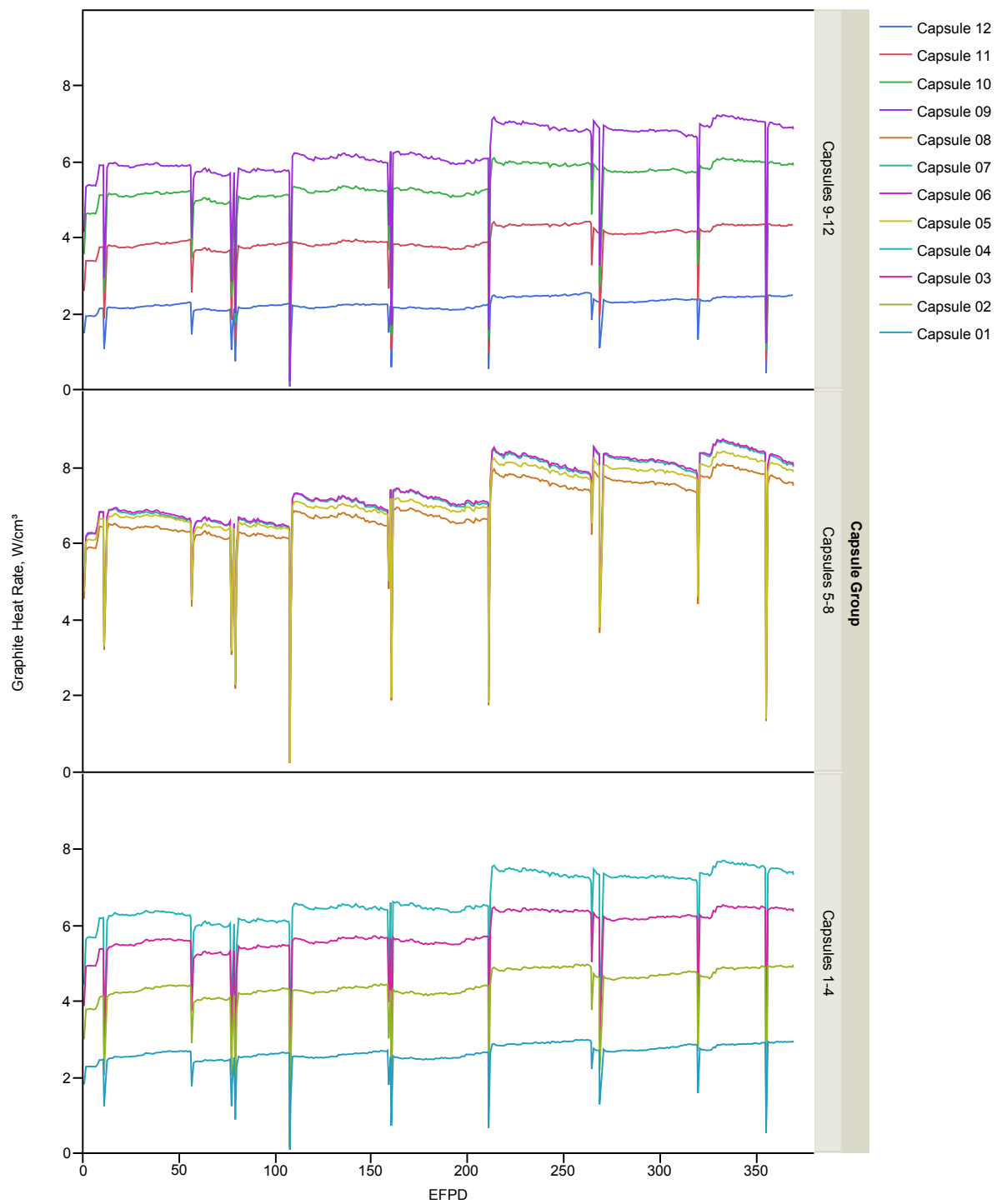


Figure 21. Capsule average graphite ring heat rate versus irradiation time in effective full-power days.

According to the physics modeler, James Sterbentz (2015a), the heat rate uncertainty in the graphite rings surrounding the AGR-3/4 compacts should be much smaller than the uncertainty in the compact heat rates. This is because the graphite heating is due primarily to ATR core neutron and gamma radiation interaction, the calculated transport of which is relatively straightforward and accurate and directly scalable to the ATR core power. The heat rates are also relatively constant as a function of burnup, whereas the fission compact heat rates are a complex function of burnup, ATR core heating radiation, and fission from the compacts themselves that does not deposit all fission radiation components in the compacts. Subsequently, the uncertainty in the AGR-3/4 compact heat rates would be a factor of 2 greater than the graphite ring heat rate uncertainties. Therefore, for this uncertainty quantification, the graphite heat rate uncertainty can be estimated to be equal $\pm 3.0\%$ for all capsules and all cycles.

3.3.2.4 Fuel Compact Thermal Conductivity. The fuel compact thermal conductivity was taken from correlations of conductivity with temperature, temperature of heat treatment, neutron fluence, and TRISO-coated particle packing fraction (Gontard and Nabelek 1990). These correlations were further adjusted to account for differences in fuel compact density and packing fraction. The given correlations were developed for a fuel compact matrix density of 1.75 g/cm^3 , whereas the compact matrix used in AGR-3/4 had a density of approximately 2.01 g/cm^3 (Collin 2015). Thus, the thermal conductivities for AGR-3/4 compacts were scaled according to the ratio of densities to correct for this difference. Figure 22 shows a three-dimensional plot of the fuel compact thermal conductivity varying with fluence and temperature. The lack of experimental data for AGR-3/4 fuel compact thermal properties leads to high uncertainty of compact thermal conductivity, which is estimated to be 20% for the entire AGR-3/4 irradiation (Table 2).

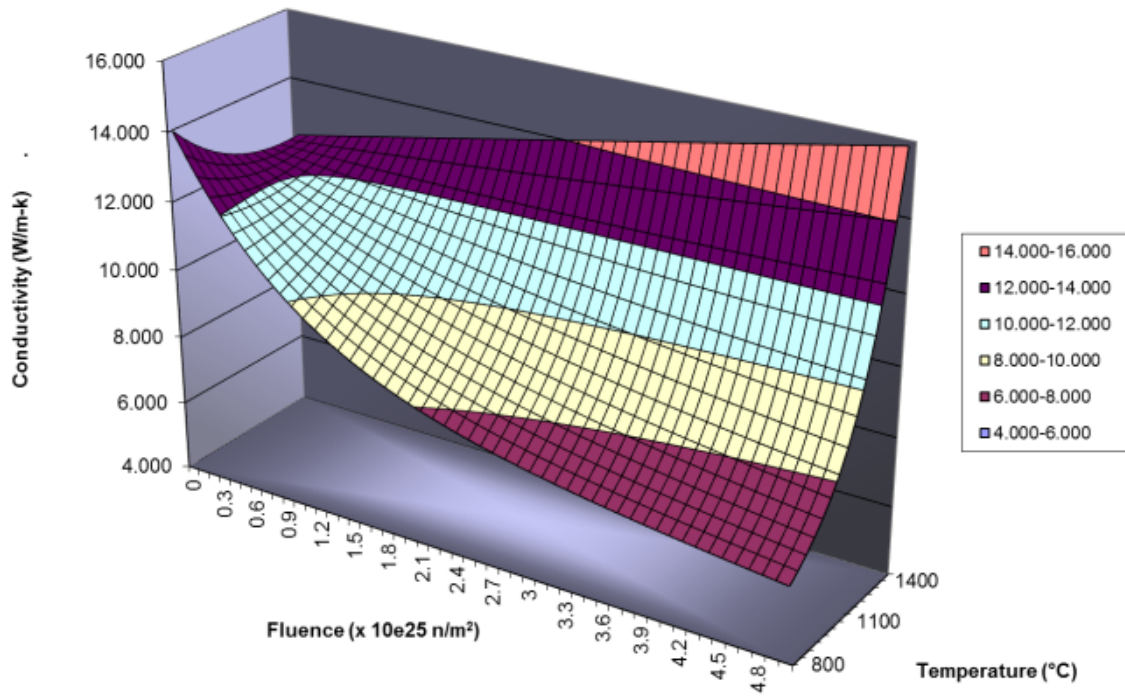


Figure 22. Uranium oxycarbide compact thermal conductivity varying with fluence and temperature (ECAR-2807).

3.3.2.5 Graphite Thermal Conductivity. Unirradiated graphite thermal conductivity data for the holders were provided by GrafTech as a function of temperature and the weight percent of boron carbide present in the material (Snead and Burchell 1995). The effect of irradiation on the thermal conductivity of the graphite was accounted for in this analysis using the correlation:

$$\frac{k_{irr}}{k_0} = (0.25 - 0.00017 * T_{irr}) * A * \log(dpa) + 0.000683 * T_{irr}$$

$$A = -1.0$$
(16)

where

- k_{irr} = thermal conductivity of irradiated graphite
- k_0 = thermal conductivity of unirradiated graphite
- T_{irr} = irradiation temperature (°C)
- dpa = displacements per atom.

The multiplier used to convert fast fluence (>0.18 MeV) to dpa is 8.23×10^{-26} dpa/(n/m²). Figure 23 shows a three-dimensional plot of this ratio (k_{irr}/k_0) varying with dpa and temperature. The ratio of irradiated to unirradiated thermal conductivity is increasing with higher temperatures and decreasing with higher dpa (or fast neutron irradiation). These correlations are obtained based on different graphite properties than the graphite employed in the AGR-3/4 test train. The fact that the thermal conductivity for the actual AGR-3/4 graphite rings has to be extrapolated from given correlations also leads to higher parameter uncertainty. According to expert assessment, the existence of one data point for validation of the correlation helps to reduce the graphite thermal conductivity uncertainty from an original value of 20 to 15% for the entire AGR-3/4 irradiation, as shown in Table 2.

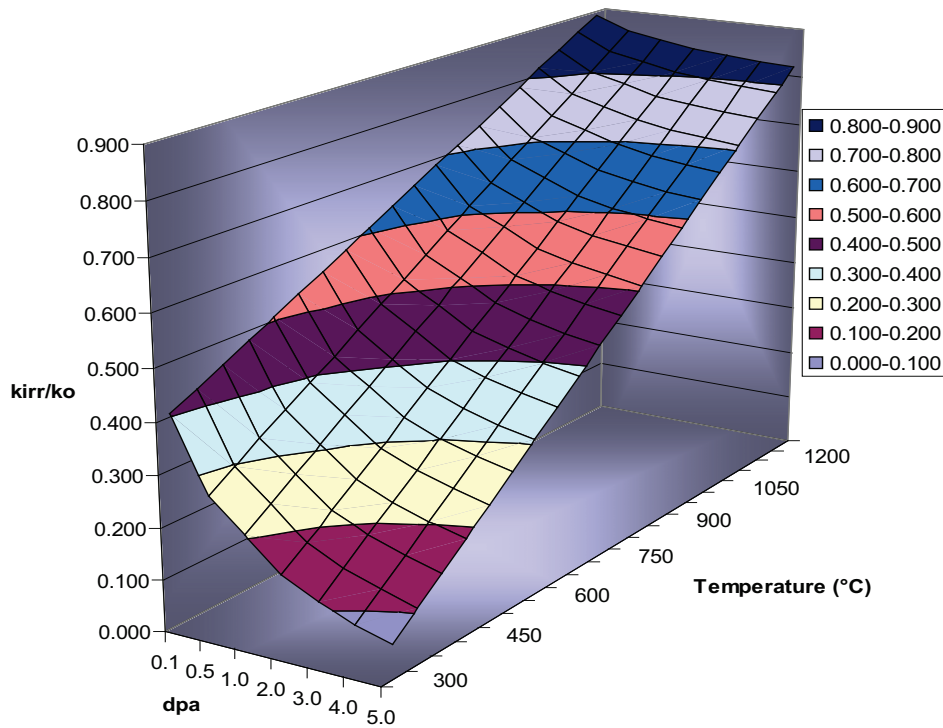


Figure 23. Ratio of irradiated over unirradiated graphite thermal conductivity (k_{irr}/k_0) varying with temperature and displacements per atom.

3.3.3 Input Parameter Sensitivity

The governing equations for steady-state conduction and radiation heat transfer models (Equations [1] and [2]) used for AGR-3/4 capsule temperature calculation show complex nonlinear relationships between output temperature and input parameters over the wide variation of experimental conditions. This makes it impossible to derive a unique analytical formula to calculate output uncertainty from input variations over the whole AGR-3/4 experimental condition domain. Additionally, the standard Monte Carlo technique is impractical because of the necessity of requiring hundreds of thousands of simulations to estimate the overall output temperature uncertainty with satisfactory accuracy. The AGR-3/4 thermal model sensitivity analysis results given in Section 3.3.1 represent parameter sensitivities within only a small experimental condition domain of $\pm 10\%$ of the nominal values used in the analysis. Also, the existing sensitivity analysis in (Hawkes et al. 2015) does not include the investigation of interactive effects of input variables.

3.3.3.1 Statistical Experimental Design for Sensitivity Analysis. To be computationally efficient, a statistical experimental design was used to develop the set of simulation runs necessary to estimate all main effects and pairwise interactions of the selected nine important input variables. To overcome the nonlinearity of the temperature function (e.g., Equation [1]), the AGR-3/4 thermal condition domain is divided into multiple smaller ranges, within which the output temperature can be estimated as a linear combination of selected input variables. Subsequently, the temperature uncertainty can be calculated from given input uncertainty using standard error propagation of the linear combination (Ostle and Mensing 1975). Capsules 5, 7, 11, and 12 were included for this sensitivity analysis.

Table 5 lists the required 163 runs of the ABAQUS code to be completed for Scenarios 1–12 in Table 6. These scenarios cover a wide range of the thermal conditions such as fuel heat rate, neon fraction, and fast neutron fluence (subsequently, fuel compact and graphite holder conductivities).

Table 5. Experimental design matrix for AGR-3/4 thermal model sensitivity analysis.

Run	Gap 1	Gap 2	Gap 3	Gap 4	Neon Fraction	Graphite Conductivity	Fuel Conductivity	Fuel Heat Rate	Graph. Heat Rate
0	N	N	N	N	N	N	N	N	N
1–2	+/-	NN	NN	NN	NN	NN	NN	NN	NN
3–4	NN	+/-	NN	NN	NN	NN	NN	NN	NN
5–6	NN	NN	+/-	NN	NN	NN	NN	NN	NN
7–8	NN	NN	NN	+/-	NN	NN	NN	NN	NN
9–10	NN	NN	NN	NN	+/-	NN	NN	NN	NN
11–12	NN	NN	NN	NN	NN	+/-	NN	NN	NN
13–14	NN	NN	NN	NN	NN	NN	+/-	NN	NN
15–16	NN	NN	NN	NN	NN	NN	NN	+/-	NN
17–18	NN	NN	NN	NN	NN	NN	NN	NN	+/-
19–22	+/-/+/-	-/+/-/+	NNNN	NNNN	NNNN	NNNN	NNNN	NNNN	NNNN
23–26	+/-/+/-	NNNN	-/+/-/+	NNNN	NNNN	NNNN	NNNN	NNNN	NNNN
27–30	+/-/+/-	NNNN	NNNN	-/+/-/+	NNNN	NNNN	NNNN	NNNN	NNNN
31–34	+/-/+/-	NNNN	NNNN	NNNN	-/+/-/+	NNNN	NNNN	NNNN	NNNN
35–38	+/-/+/-	NNNN	NNNN	NNNN	NNNN	-/+/-/+	NNNN	NNNN	NNNN
39–42	+/-/+/-	NNNN	NNNN	NNNN	NNNN	NNNN	-/+/-/+	NNNN	NNNN
43–46	+/-/+/-	NNNN	NNNN	NNNN	NNNN	NNNN	NNNN	-/+/-/+	NNNN
47–50	+/-/+/-	NNNN	NNNN	NNNN	NNNN	NNNN	NNNN	NNNN	-/+/-/+
51–54	NNNN	+/-/+/-	-/+/-/+	NNNN	NNNN	NNNN	NNNN	NNNN	NNNN
55–58	NNNN	+/-/+/-	NNNN	-/+/-/+	NNNN	NNNN	NNNN	NNNN	NNNN

Table 5. (continued).

Run	Gap 1	Gap 2	Gap 3	Gap 4	Neon Fraction	Graphite Conductivity	Fuel Conductivity	Fuel Heat Rate	Graph. Heat Rate
59–62	NNNN	+/-+/-	NNNN	NNNN	-/+/-+	NNNN	NNNN	NNNN	NNNN
63–66	NNNN	+/-+/-	NNNN	NNNN	NNNN	-/+/-+	NNNN	NNNN	NNNN
67–70	NNNN	+/-+/-	NNNN	NNNN	NNNN	NNNN	-/+/-+	NNNN	NNNN
71–74	NNNN	+/-+/-	NNNN	NNNN	NNNN	NNNN	NNNN	-/+/-+	NNNN
75–78	NNNN	+/-+/-	NNNN	NNNN	NNNN	NNNN	NNNN	NNNN	-/+/-+
79–82	NNNN	NNNN	+/-+/-	-/+/-+	NNNN	NNNN	NNNN	NNNN	NNNN
83–86	NNNN	NNNN	+/-+/-	NNNN	-/+/-+	NNNN	NNNN	NNNN	NNNN
87–90	NNNN	NNNN	+/-+/-	NNNN	NNNN	-/+/-+	NNNN	NNNN	NNNN
91–94	NNNN	NNNN	+/-+/-	NNNN	NNNN	NNNN	-/+/-+	NNNN	NNNN
95–98	NNNN	NNNN	+/-+/-	NNNN	NNNN	NNNN	NNNN	-/+/-+	NNNN
99–102	NNNN	NNNN	+/-+/-	NNNN	NNNN	NNNN	NNNN	NNNN	-/+/-+
102–106	NNNN	NNNN	NNNN	+/-+/-	-/+/-+	NNNN	NNNN	NNNN	NNNN
107–110	NNNN	NNNN	NNNN	+/-+/-	NNNN	-/+/-+	NNNN	NNNN	NNNN
111–114	NNNN	NNNN	NNNN	+/-+/-	NNNN	NNNN	-/+/-+	NNNN	NNNN
115–118	NNNN	NNNN	NNNN	+/-+/-	NNNN	NNNN	NNNN	-/+/-+	NNNN
119–122	NNNN	NNNN	NNNN	+/-+/-	NNNN	NNNN	NNNN	NNNN	-/+/-+
123–126	NNNN	NNNN	NNNN	NNNN	+/-+/-	-/+/-+	NNNN	NNNN	NNNN
127–130	NNNN	NNNN	NNNN	NNNN	+/-+/-	NNNN	-/+/-+	NNNN	NNNN
131–134	NNNN	NNNN	NNNN	NNNN	+/-+/-	NNNN	NNNN	-/+/-+	NNNN
135–138	NNNN	NNNN	NNNN	NNNN	+/-+/-	NNNN	NNNN	NNNN	-/+/-+
139–142	NNNN	NNNN	NNNN	NNNN	NNNN	+/-+/-	-/+/-+	NNNN	NNNN
143–146	NNNN	NNNN	NNNN	NNNN	NNNN	+/-+/-	NNNN	-/+/-+	NNNN
147–150	NNNN	NNNN	NNNN	NNNN	NNNN	+/-+/-	NNNN	NNNN	-/+/-+
151–154	NNNN	NNNN	NNNN	NNNN	NNNN	NNNN	+/-+/-	-/+/-+	NNNN
155–158	NNNN	NNNN	NNNN	NNNN	NNNN	NNNN	+/-+/-	NNNN	-/+/-+
159–162	NNNN	NNNN	NNNN	NNNN	NNNN	NNNN	NNNN	+/-+/-	-/+/-+

N is nominal value (Run 0).

+ is 1.1 time of nominal value (+10%).

- is 0.9 time of nominal value (-10%).

Runs 1 to 18 are used to estimate main effect of nine inputs.

Runs 19 to 162 are used to estimate the pairwise interaction of 36 possible pairs from nine inputs.

Table 6. Thermal conditions for 12 selected cases.

Case	Capsule	ATR Cycle	Time Step	EFPDs	Neon Fraction	Fluence, 10^{25} n/m ²	Fuel Heat Rate, w/cm ³	Graphite Heat Rate, w/cm ³	Gap1, 10^{-3} in.	Gap2, 10^{-3} in.	Gap3, 10^{-3} in.	Gap4, 10^{-3} in.
1	5	151A	42	40	0.74	0.49	112.9	6.8	3.2	2.4	8.0	13.6
2	5	154B	30	240	0.31	3.17	104.2	8.2	4.1	2.9	7.9	20.3
3	5	155B	31	350	0.43	4.88	88	8.6	3.5	1.7	7.9	24.7
4	7	151A	42	40	0.92	0.49	113.9	6.9	3.0	3.4	40.5	12.7
5	7	154B	30	240	0.58	3.21	104.9	8.4	2.6	4.1	40.2	19.5
6	7	155B	31	350	0.86	4.96	88.5	8.8	1.5	4.4	40.1	24.0
7	11	151A	42	40	0.68	0.28	65.2	3.9	2.8	39.4	150.2	85.8
8	11	154B	30	240	0.41	1.79	65.1	4.5	3.0	39.7	149.7	89.4
9	11	155B	31	350	0.81	2.70	59.7	4.5	2.6	40.1	149.5	91.5
10	12	151A	42	40	0.84	0.15	36.8	2.3	3.1	3.5	99.5	60.8
11	12	154B	30	240	0.48	0.94	39.3	2.6	3.7	3.8	99.3	62.7
12	12	155B	31	350	0.63	1.41	37.5	2.6	3.9	3.9	99.2	63.8

3.3.3.2 Parameter Sensitivity Analysis. From the ABAQUS output for each of the 12 scenarios, multiple temperatures of interest are obtained such as VA FT, peak FT, VA and peak matrix and graphite sleeve rings, and TC1, TC2, and TC3 temperatures. These results are used for a sensitivity analysis of the input parameters on model predicted temperatures. The JMP[®] module “Fit Model” (JMP[®] 10.0.0) of SAS[®] (SAS[®] 2009) is used to build a surrogate response surface model for each of the calculated temperatures to determine which input terms have significant impacts. The parameter coefficients are treated as sensitivities that estimate the rate of change of temperature with regard to the input. Subsequently, they can be used to propagate the parameter uncertainty to the output temperatures.

As stated in the previous section, nine thermal model input parameters are included in this sensitivity analysis, namely the fuel heat rate (*FHR*), graphite rings’ heat rate (*GHR*), the four distances of the gas gaps (*G1 to G4*), the neon fraction (*NeF*) of the capsule gas mixture, fuel thermal conductivity (*FC*), and graphite compact thermal conductivity (*GC*). The experimental design provides estimation of main input effects and second order term effects (noted as *Term*²), which are pairwise interactions among inputs and square terms of inputs. The following response surface model containing 55 terms is constructed and studied for each of calculated temperature response measures using the JMP[®] platform:

$$f_T = a_0 + a_1 FHR + a_2 GHR + a_3 G1 + a_4 G2 + a_5 G3 + a_6 G4 + a_7 NeF + a_8 FC + a_9 GC + \sum_{i=10}^{55} a_i Term^2 \quad (17)$$

Both input variables and output responses are transformed to a relative value (0.9 is 10% less, 1.0 is nominal, and 1.1 is 10% more) by dividing by the nominal values prior to response surface model fitting. This transformation does not impact the parameter sensitivities. Results of Case 1 are plotted here for discussion because they are similar to the other cases. Figure 24 presents the actual versus predicted plots for VA FT indicating near-perfect fit of the response surface regression model (R square nearly 1).

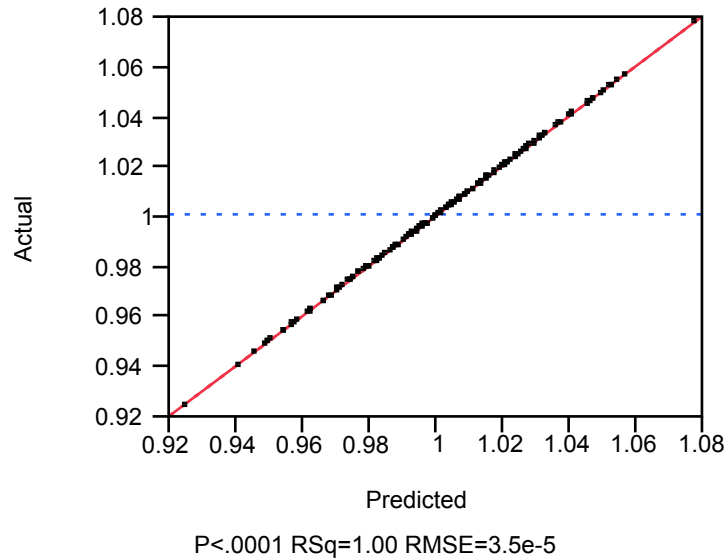


Figure 24. Actual by predicted plot for VA FT for Case 1 (Capsule 5).

Figure 25 lists all parameter estimates ($a_1 - a_{55}$ in *Equation [9]*) sorted from the largest to the smallest for VA fuel temperature in Case 1 (they are almost in the same order for other temperatures and other cases). Apparently, most of the coefficients (parameter estimates) in the model are significantly different from zero. However, the bar chart showing the temperature variation due to input change indicates that only the nine main effects are dominant. The square of the neon fraction (the most significant among the second order terms) has insignificant influence on output temperature. Similarly, Figure 26 shows the leverage plots for the nine main effects (variables) and squared neon fraction for VA FT. The significant slopes of fuel heat rate, gas gap, and neon fraction are further indications of influence on VA FT variation. Although the estimate of the squared neon fraction term is significantly different from zero, its contribution to fuel temperature variation is small, as shown by the almost horizontal line in the leverage plot on bottom right. All other second-order terms in the regression model (*Equation [17]*) have even smaller contributions to the capsule temperature variations.

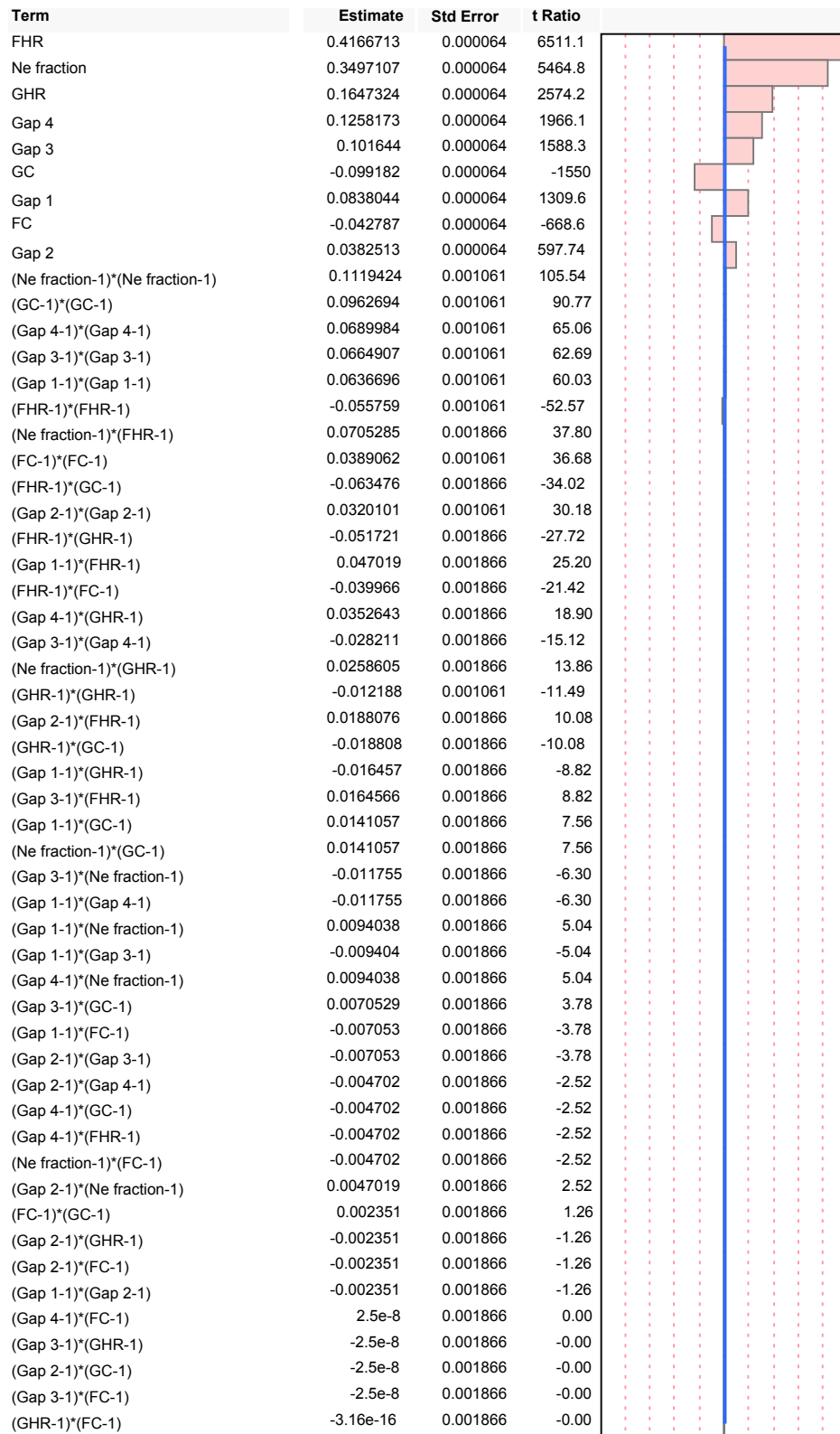


Figure 25. Parameter estimates (*Equation [17]*) sorted from largest to smallest for volume-averaged fuel temperature of Scenario 1.

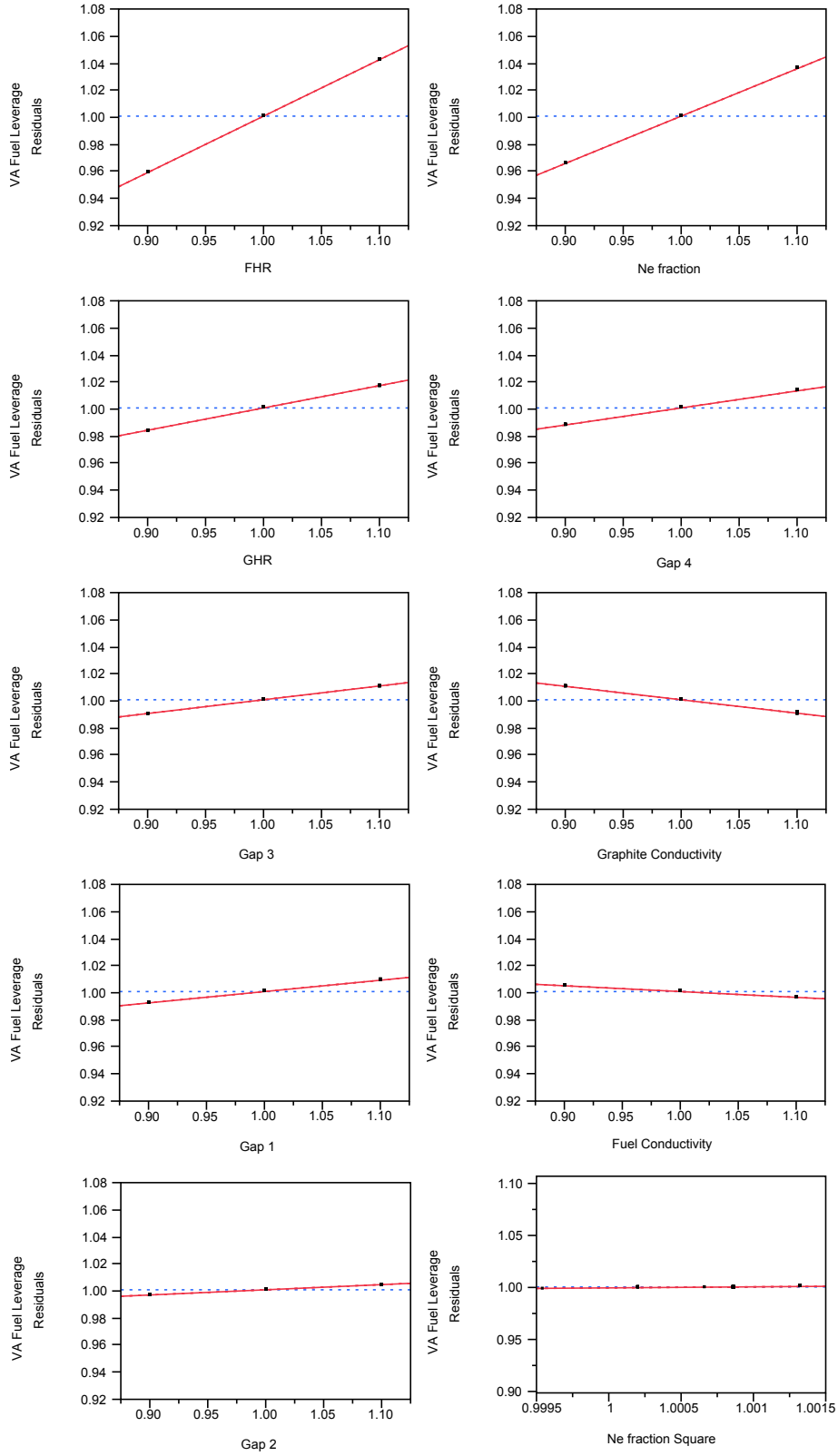


Figure 26. Leverage plots for nine main effects and square term of neon fraction for volume-averaged fuel temperatures (parameters are relative ratios to their nominal values and in order of sensitivity from largest to smallest indicated by the slope of the plots).

Additionally, the prediction profilers in the JMP “fit model” platform displays profile traces for each independent variable, as seen in Figure 27 for fuel, graphite (volume-averaged and peak), and TC temperatures. A profile trace is the predicted response as one variable is changed while the others are held constant at their current values. The absence of curvature in the prediction profiles for all variables confirms the linear relationship between response measures and input variables within 10% of input variations. The bar plots in Figure 28 show the parameter sensitivities of nine inputs for all interested calculated temperatures for Case 1(Capsule 5).

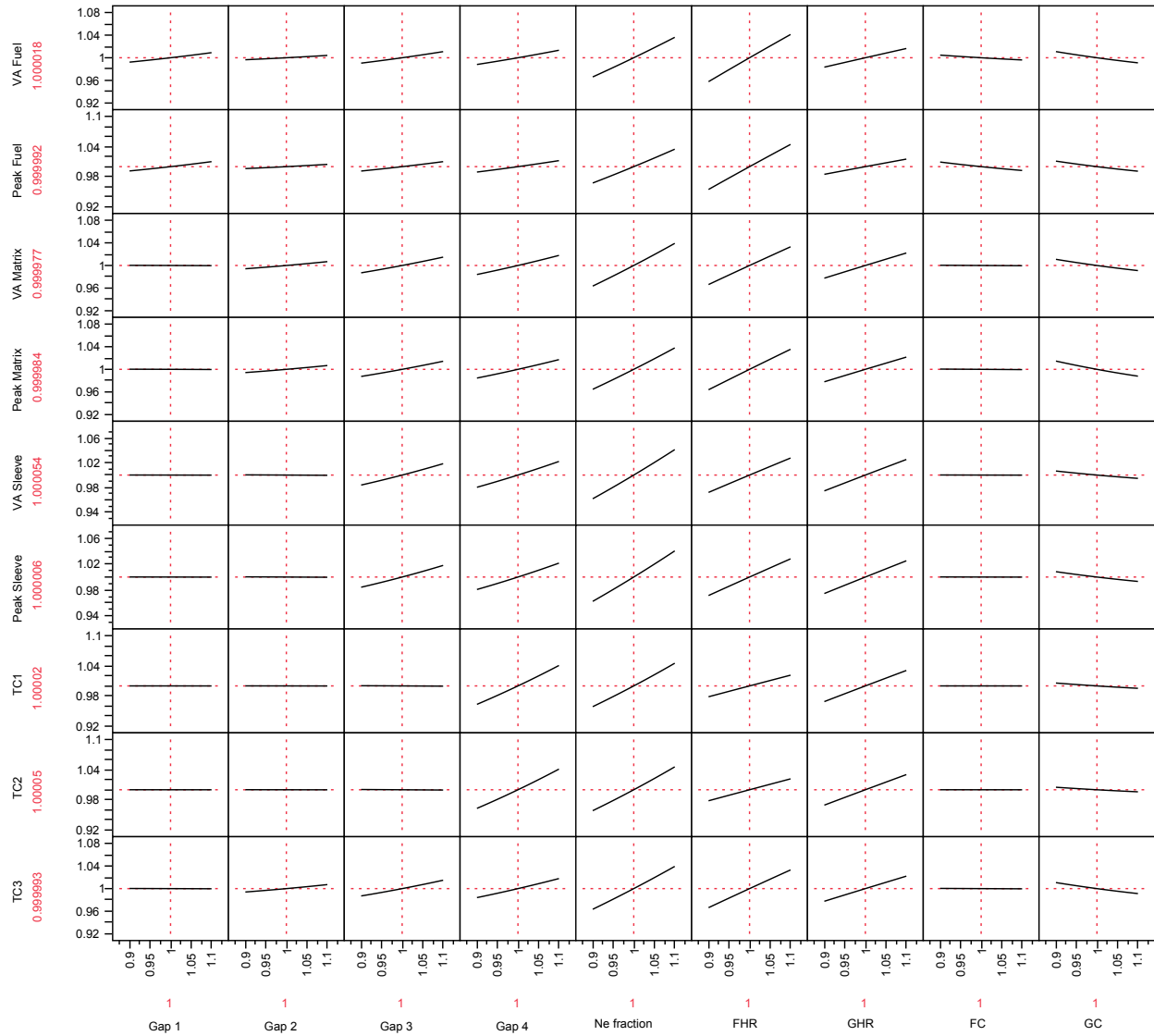


Figure 27. Prediction profiles of functions for volume-averaged fuel, peak fuel, volume-averaged matrix, peak matrix, volume-averaged sleeve, peak sleeve, and thermocouple temperatures.

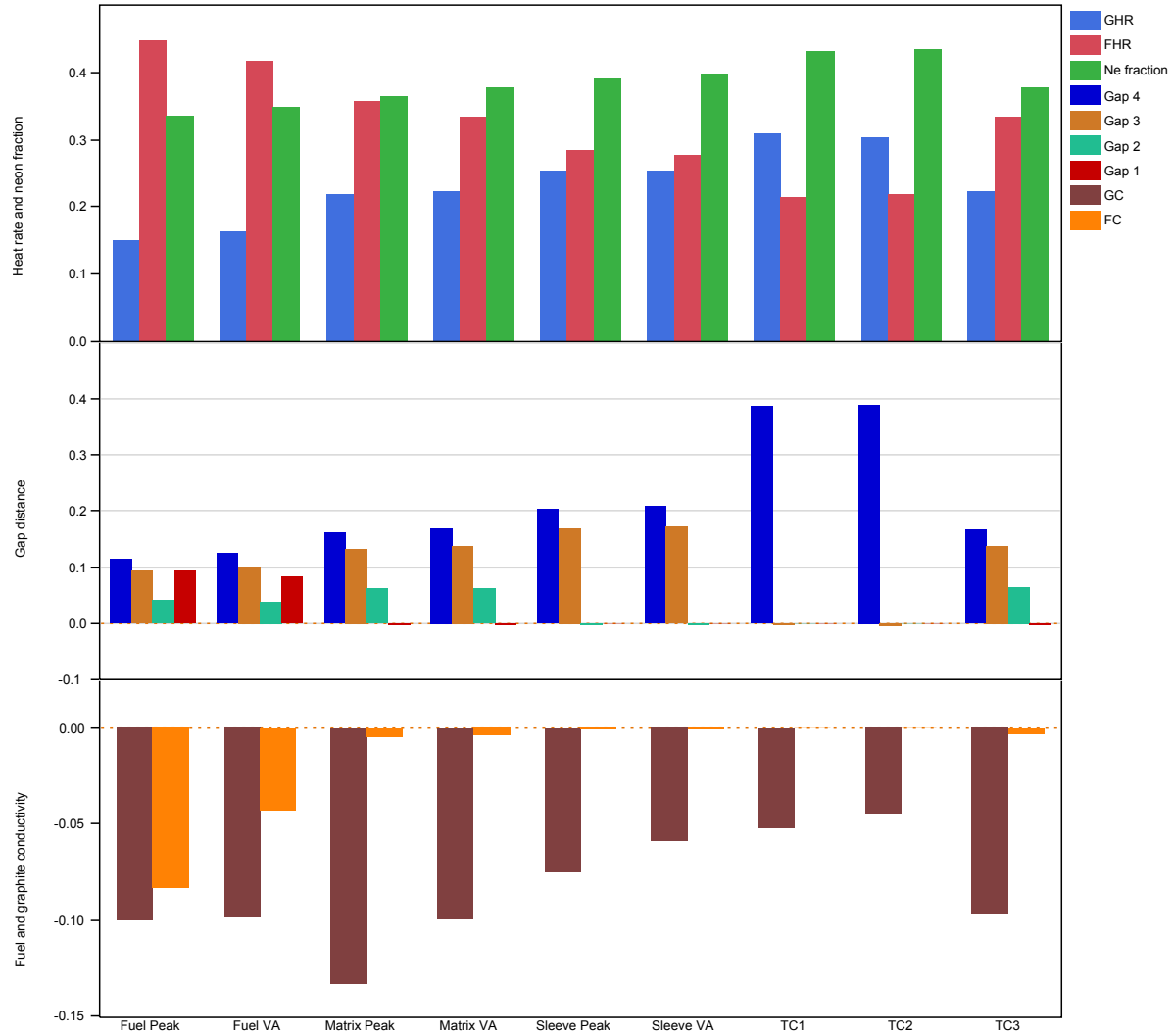


Figure 28. Sensitivity coefficients for fuel, matrix, sleeve (both peak and volume-averaged), and thermocouple temperatures for Case 1.

The sensitivity analysis results presented in Figure 25, Figure 26, and Figure 27 allow for exclusion of all second order terms (square terms of five variables and their pairwise interactions) in the regression model (*Equation [17]*) because of their relatively negligible contributions to temperature variation. As a result, the regression model of *Equation (17)* can be reduced to a linearized approximation of model temperature as:

$$f_T = a_0 + a_1 FHR + a_2 GHR + a_3 G1 + a_4 G2 + a_5 G3 + a_6 G4 + a_7 Nef + a_8 FC + a_9 GC \quad (18)$$

All calculated temperature results provided by Grant Hawkes (Hawkes 2015a) and resulted sensitivity coefficients of nine selected inputs for 12 cases listed in Table 6 were committed to the NDMAS subversion repository, \\isasapp\NGNP_Data\AGR34\PHY\Calc_temperature\Sensitivity\.

3.3.3.3 Sensitivity Coefficients for Capsules 5, 7, 11, and 12. The *Equation (18)* model's coefficient estimates (a_1 – a_9) for VA FT, peak FT, mid-50%-VA matrix (MA), mid-50%-VA sleeve (SA), TC1 and TC3 temperatures for the 12 cases listed in Table 6 are presented in Figure 29 through Figure 31. Capsules 7 and 11 do not have TC3; therefore, there are two empty spaces in each figure. Sensitivity of TC1 temperatures is also applied to TC2 temperatures because they are located in a similar peripheral

location of the graphite holder. The variation of sensitivities reflects the nonlinear relationship between the temperature and the thermal model inputs over the wide thermal condition range of the entire AGR-3/4 irradiation. Therefore, the model input sensitivities for other time steps will be estimated by interpolation from sensitivities of these three data sets for each capsule depending on their actual thermal condition input parameters. The input sensitivity coefficients in each capsule will apply to corresponding calculated temperatures in that capsule.

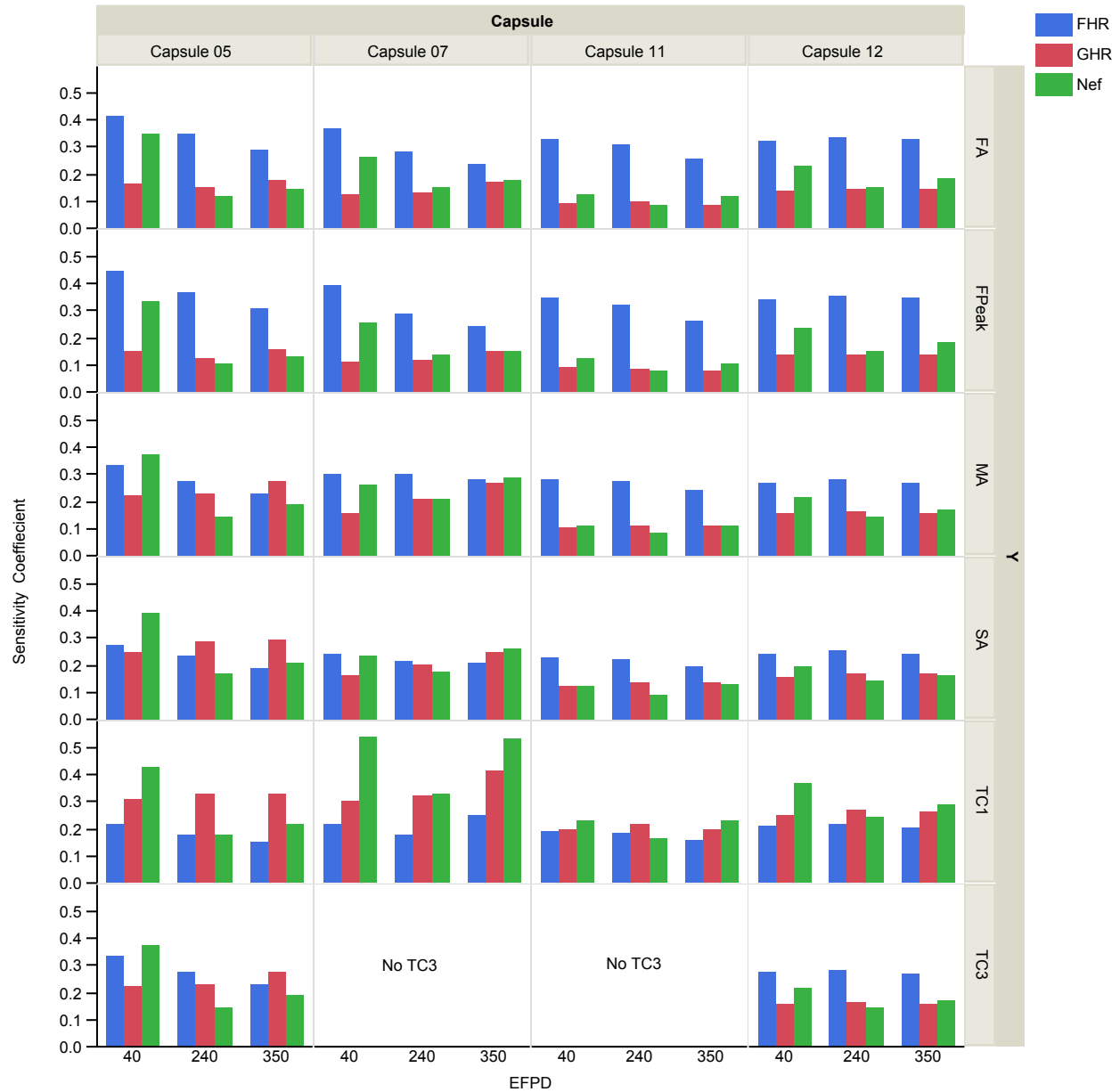


Figure 29. Sensitivity coefficients of fuel heat rate, graphite heat rate, and neon fraction for Capsules 5, 7, 11, and 12.

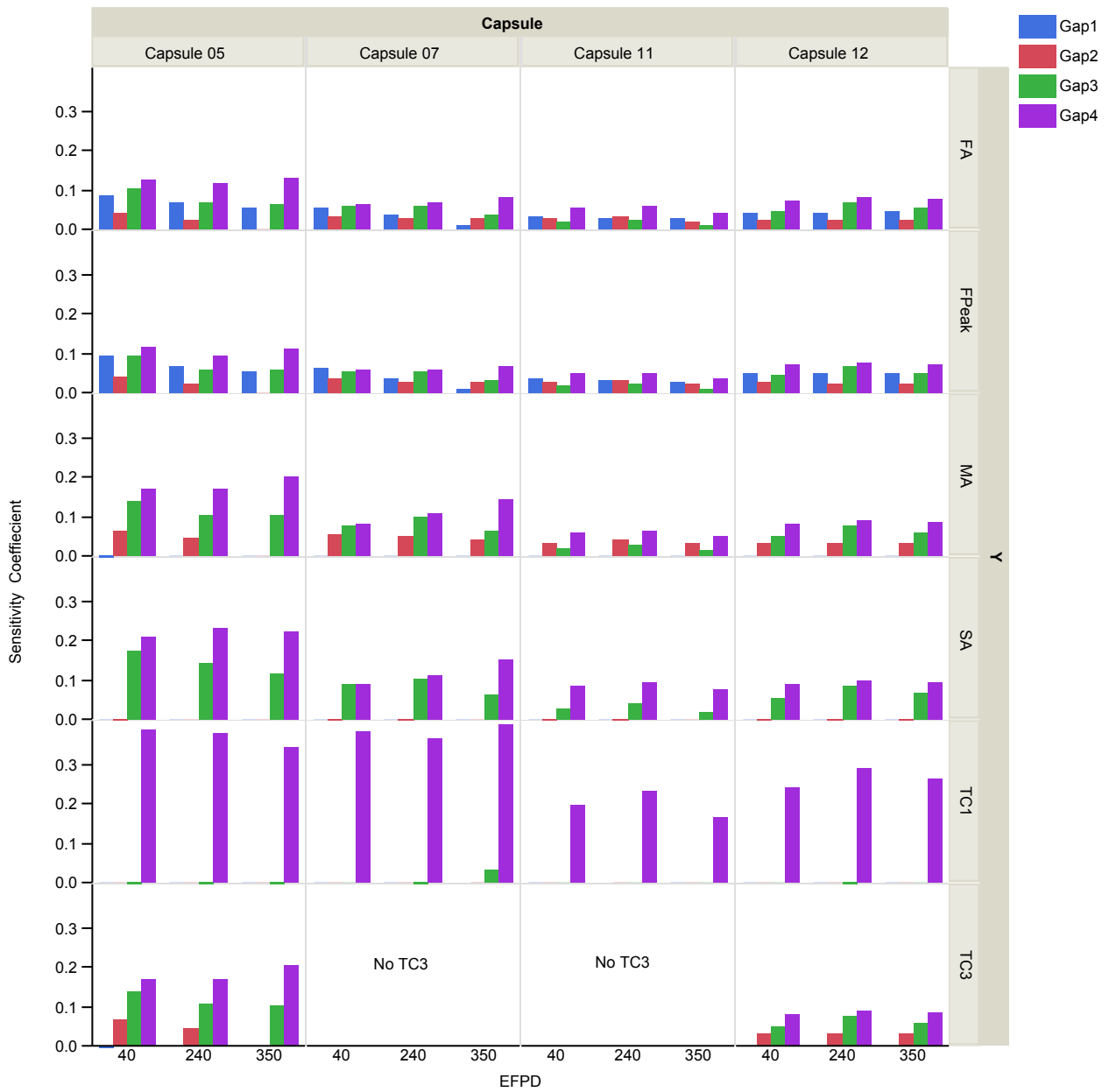


Figure 30. Sensitivity coefficients of four gap sizes for Capsules 5, 7, 11, and 12.

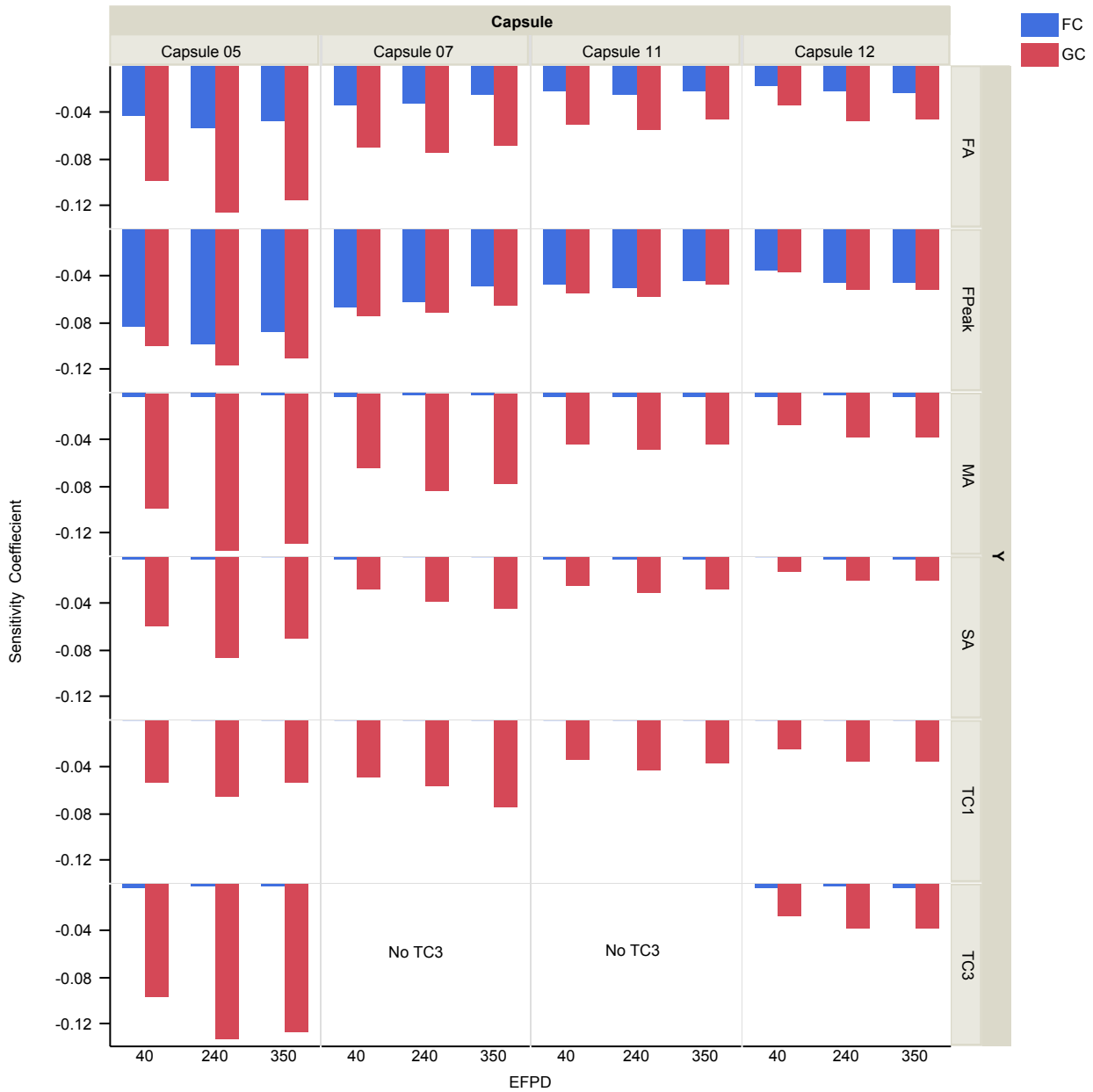


Figure 31. Sensitivity coefficients of fuel and graphite conductivities for Capsules 5, 7, 11, and 12.

Figure 29 presents sensitivity coefficients of the three most sensitive inputs, (i.e., fuel heat rate, graphite heat rate, and neon fraction for calculated temperatures in Capsules 5, 7, 11, and 12). The fuel heat rate sensitivity is the highest for VA FT and peak FT, and the graphite heat rate sensitivity is higher for TC temperatures. The neon fraction sensitivity varies the most because of the large variation in neon fraction for the three points in time. Notably, the neon fraction sensitivity for Capsule 11 is significantly lower than for the other three capsules even though the neon fractions were similar.

Figure 30 presents sensitivity coefficients of four gap sizes for calculated temperatures in Capsules 5, 7, 11, and 12. Among these four gaps, Gap 4 (the outermost gap) is the most sensitive input especially for TC1 temperature, which is taken adjacent to this gap, while the three remaining gap sizes (1 – 3) have almost no impact on TC1 temperature. On the other hand, Gap 1 (the innermost gap) impacts

only VA FT and peak FT, but does not have any impact on graphite temperatures. Gap 2 impacts mostly VA matrix temperature and Gap 3 has a moderate impact for all temperatures.

Finally, Figure 31 shows negative sensitivity coefficients for the two least sensitive inputs, fuel and graphite thermal conductivities, for calculated temperatures in Capsules 5, 7, 11, and 12. The fuel conductivity only impacts VA and peak FTs, but had almost no influence on graphite temperatures, whereas the graphite conductivity impacts both fuel compact and graphite ring temperatures.

3.3.4 Correlation Coefficients of Thermal Model Input Parameters

3.3.4.1 Uncorrelated Parameter Errors. The correlation coefficient between two input parameters equals zero when their error sources are independent or uncorrelated. In other words, the variation of one parameter due to its random error does not affect the error of the other parameter. For example, initial gas gap size and neon fraction are both the result of measurements performed by different tools and procedures. The flow rate is measured by the flow meter, and the control gas gap is based on measuring physical dimensions of capsule components. Therefore, the error of the gas gap measurement does not affect the error in flow rate measurement, thus, these errors are considered independent. As a result, the correlation coefficient of neon fraction and gas gap size is zero. For the same reason, correlation coefficients between the two measured parameters, gas gap size and neon fraction, and three calculated parameters, fuel heat rate, graphite, and fuel compact thermal conductivities, are zero.

3.3.4.2 Correlated Parameter Errors. This section estimates the correlation coefficients between error sources of three calculated parameters: fuel heat rate, graphite conductivity, and fuel compact conductivity. The error associations of these calculated parameters are caused by the fact that their formulas contain common factors such as temperature and fast neutron fluence.

3.3.4.2.1 Fuel and Graphite Compact Thermal Conductivities. The fuel thermal conductivity and graphite compact thermal conductivity plots varying with temperature and fast fluence (expressed in neutrons per square centimeter or equivalent displacements per atom) are presented in Figure 22 and Figure 23, respectively. From available data provided by the look-up tables for fuel and graphite conductivities as functions of fast fluence and temperature (Hawkes et al. 2011), the relationship of fuel and graphite compact thermal conductivities as functions of fast fluence (converted into displacements per atom) and temperature (T) are constructed using JMP®. The functional relationship given for fuel compact thermal conductivity is:

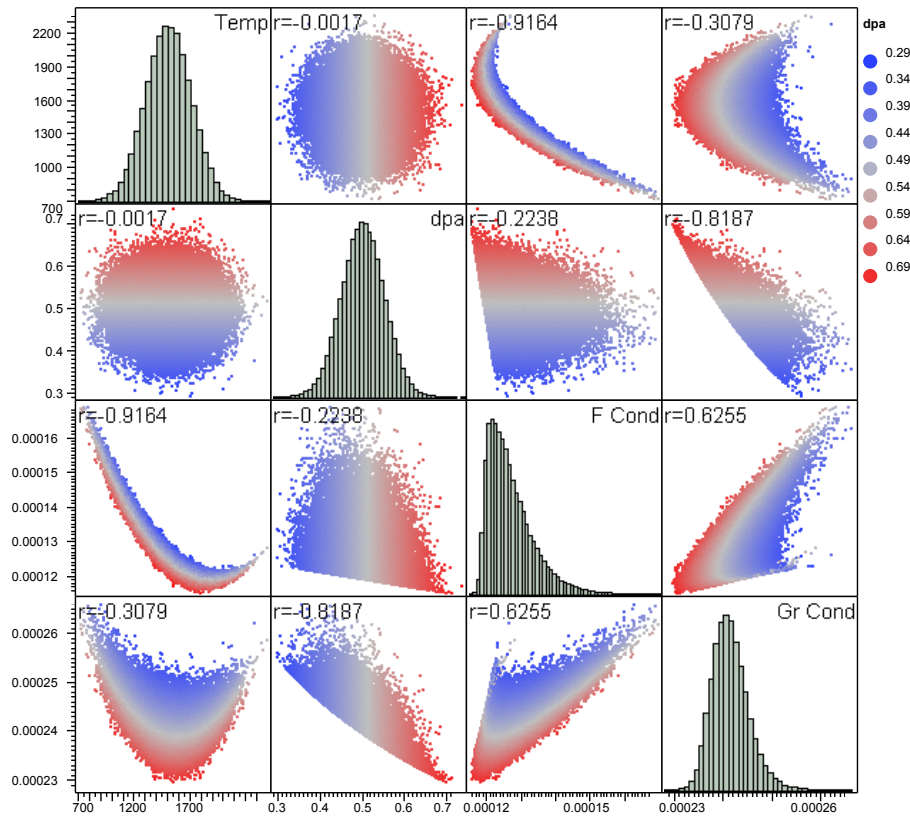
$$FC = 3.72 \cdot 10^{-5} + 4.07 \cdot 10^{-8} T - 9.44 \cdot 10^{-6} dpa + 3.74 \cdot 10^{-11} (T - 2030)^2 + 2.31 \cdot 10^{-8} (T - 2030)(dpa - 1.82) + 2.85 \cdot 10^{-6} (dpa - 1.82)^2 \quad (19)$$

and for graphite conductivity is:

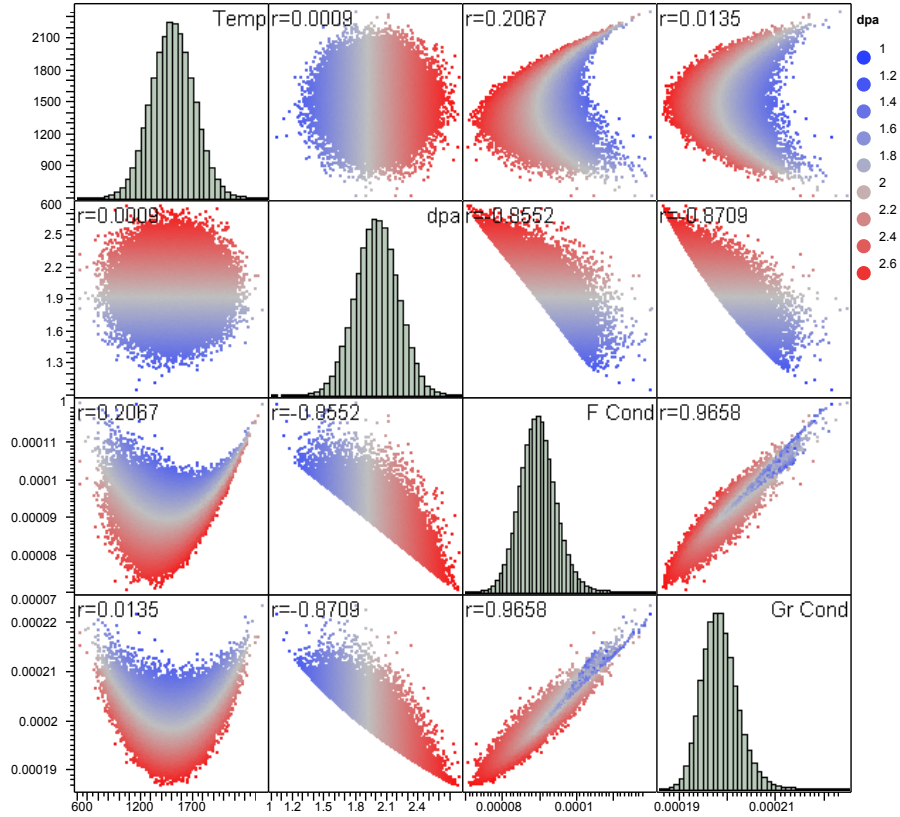
$$GC = 3.36 \cdot 10^{-4} - 3.85 \cdot 10^{-8} T + 1.02 \cdot 10^{-8} (T - 1449.5)(\log(dpa) + 5.05) - 4.499 \cdot 10^{-5} \log(dpa) - 2.36 \cdot 10^{-6} (\log(dpa) + 5.05)^2 \quad (20)$$

Using JMP®, a total of 100,000 data points was collected from normal distributions of AGR-3/4 FT (1500 ± 200 K), graphite temperature (1200 ± 200 K), and displacements per atom ($\mu_{dpa} \pm 10\%$) for five levels of the mean displacements per atom, $\mu_{dpa} = 0.5, 1, 2, 3, 4$ corresponding to fast neutron fluence. The multiplier used to convert fast fluence to displacements per atom is $0.823 \times 10^{25} \text{ dpa}/(\text{n}/\text{m}^2)$ (Hawkes 2015).

To compute the noise correlation coefficient between fuel and graphite conductivities, the fuel and graphite temperatures of one data point (a pair of temperatures and displacements per atom) are sampled with the same noise components. The sampled displacements per atom and temperature values are inserted in (Equation [19]) and (Equation [20]) to compute the fuel thermal conductivity and the graphite compact thermal conductivity for each data point. The correlation coefficient between graphite and fuel compact thermal conductivities is estimated using the JMP® “multivariate” function. Figure 32 shows the scatter plot matrix of FT, displacements per atom, fuel and graphite thermal conductivities together with their distribution and correlation coefficients of each pair of variables for displacements per atom levels 0.5 and 2.0.



$$\mu_{dpa} = 0.5$$



$$\mu_{dpa} = 2.0$$

Figure 32. Scatter plot matrix showing correlation between fuel and graphite thermal conductivities at one fuel temperature and two displacements per atom levels (0.5 and 2.0).

The noise correlation coefficients between fuel and graphite thermal conductivities $\rho_{FC,GC}$ for five levels of fast neutron fluence (converted from displacements per atom) are presented in Table 7 and Figure 33. The second order polynomial function of the fast fluence (f) in $\text{n/m}^2 \times 10^{25}$ was used to fit the correlation coefficients in Table 7 as:

$$\rho_{FC,GC} = -0.0708f^2 + 0.3585f + 0.4464 \quad (21)$$

Table 7. Correlation coefficients between fuel and graphite thermal conductivities.

Fluence ($\text{n/m}^2 \times 10^{25}$)	0.6075	1.215	2.430	3.645	4.860
Correlation coefficient	0.6255	0.7739	0.9658	0.7355	0.544

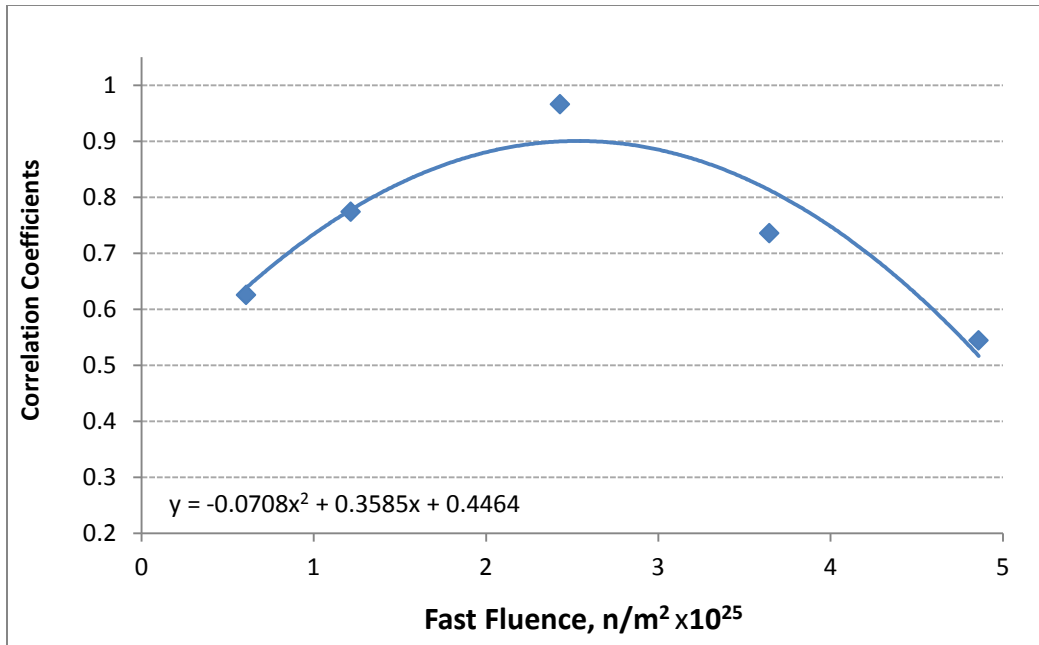


Figure 33. Correlation coefficients between fuel and graphite thermal conductivities varying with fast neutron fluence.

3.3.4.2.2 Fuel Compact/ Graphite Thermal Conductivity and Fuel Compact/Graphite Heat Rate. The value of fuel compact heat rate (Q) depends on the daily neutron flux, FT , and material properties such as cross-section and fuel burnup. The graphite and fuel compact thermal conductivity, as mentioned earlier, is a function of temperature and neutron fast fluence. Based on the functional dependence of fuel compact and graphite thermal conductivity and fuel heat rate on neutron fast fluence and neutron flux respectively, it is reasonable to assume that the correlation coefficient between their noises should be smaller than between graphite and fuel conductivities. Since the fuel compact and graphite thermal conductivities and fuel heat rate are not possible to simulate, their noise correlation coefficients are assumed to be half of the correlation coefficient between fuel and graphite conductivities.

3.3.4.2.3 Fuel Compact/Graphite Heat Rate. The fuel compact and graphite heat rates are directly defined by neutron fast fluence, therefore, their correlation coefficient should be very high. In this study, this correlation coefficient is conservatively assumed to be 1.

3.3.5 Propagation of Parameter Uncertainties and Sensitivities

The variation of parameter estimates across three thermal condition scenarios in Capsule 5 presented in Figure 28 reflects the variation in parameter sensitivities over the entire input domain for AGR-3/4. This confirms the nonlinear nature of Capsule 5 thermal models as a function of the five input variables. However, within a small enough input range (e.g., from $[\text{nominal} \times (1-10\%)]$ to $[\text{nominal} \times (1+10\%)]$) the AGR-3/4 predicted temperature can be estimated by a linear combination of five input variables as presented in Equation (18). Subsequently, the standard parameter error propagation of the linear summation (Ostle and Mensing 1975) can be used to calculate the overall output temperature uncertainty from the variance-covariance matrix of input variables for an input range close to the nominal values. The expression of output variance for each output, T , is given here:

$$\sigma_T^2 = \sum_i^n a_i^2 \sigma_i^2 + \sum_i^n \sum_{j \neq i}^n \rho_{ij} a_i \sigma_i a_j \sigma_j \quad (22)$$

where

σ_T = overall uncertainty in terms of standard deviation

a_i = sensitivity coefficient for parameter i

σ_i = uncertainty of input parameter i in terms of standard deviation

ρ_{ij} = correlation coefficient for input parameters i and j .

The input parameter uncertainties are estimated in terms of relative standard deviations (%) in Section 3.3 and the sensitivity coefficients are estimated in Section 3.3.3. Section 3.3.4 addresses the correlation coefficients of each variable pair. The correlation coefficient of a variable pair is a measure of the degree (or intensity) of association between two variables (Ostle and Mensing 1975). For each capsule, the AGR-3/4 thermal model parameter uncertainty quantification for daily average temperatures (TC temperature, VA FT, or peak FT) is performed using the results presented in Section 2.

3.3.5.1 Daily Input Parameter Uncertainties (σ_i). The daily input parameter uncertainties in terms of relative standard deviation for the five significant input variables are estimated as discussed in Section 3.3. The details of the daily uncertainty calculations are:

- The parameter uncertainties for fuel heat rate, graphite holder thermal conductivity and fuel compact thermal conductivity are assumed to be constant random errors for all time steps and six capsules as presented in Table 2. Therefore, their plots as a function of EFPDs are flat lines for all three parameters in all capsules.
- The daily parameter uncertainties for gas gap sizes (σ_{GG_i}) are based on the error of the gap size formula of Equation (13).
- The daily parameter uncertainty for neon fraction (σ_{Nef_i}) is calculated for each time step and each capsule by substituting the actual capsule neon fraction on that time step using Equation (15) (representing a functional relationship between neon fraction uncertainties and neon fraction values). Since the capsule neon fractions vary with time to maintain the capsule specified FT, the daily uncertainties of neon fraction also vary with EFPDs.

3.3.5.2 Daily Parameter Sensitivities (a_i). The daily parameter sensitivities, a_i , of five significant input variables at time step (i) are estimated using the functional relationships between sensitivity coefficients and corresponding input parameters established in Section 3.3.3 for each output temperature in each capsule. Since the inputs to the thermal models vary with time, the resulting daily parameter sensitivities also vary with time.

3.3.5.3 Daily Correlation Coefficients (σ_{FC,GC_i}). The daily correlation coefficients between fuel compact and graphite thermal conductivities, $\rho_{FC,GC}$, at time step (i), are calculated using the function of fast neutron fluence given in Equation (21) and shown in Figure 33. Since the neutron fluence varies with time, the daily correlation coefficients also vary with time.

3.3.5.4 Parameter Uncertainty ($\sigma_{P_i}^2$). The parameter uncertainty (in terms of variance) of the thermal model output temperature at time step (i) is calculated using Equation (22). Since the input

sensitivity, correlation coefficient and uncertainty vary with time, the calculated temperature uncertainty also varies with time (EFPDs).

3.4 Overall Uncertainty Quantification

3.4.1 Uncertainty for Daily temperature

The overall uncertainty for calculated daily (instantaneous) temperature in term of variance equals the total of model form uncertainty (σ_B^2) and parameter uncertainty ($\sigma_{P_i}^2$). For each day (i), the overall uncertainty of predicted temperature is calculated as follows:

$$\sigma_{T_i}^2 = \sigma_{P_i}^2 + \sigma_B^2 \quad (23)$$

3.4.2 Uncertainty for Time Average (TA) Temperature

The capsule TA VA FT and TA peak FT at day (i) are calculated from daily average temperatures as:

$$T_{TA_i} = \frac{\sum_{k=1}^i T_k \cdot t_k}{\sum_{k=1}^i t_k} \quad (24)$$

where

T_k and t_k = daily average calculated temperature and time step at day (k).

Time step t_k equals 1 for most time steps and $t_k < 1$ for the startup or power-down days. The error standard deviation of the TA temperatures is calculated using the standard formula for error propagation of the linear combination of daily average temperatures. Assuming that the errors of daily averaged calculated temperatures are independent from each other, the error standard deviation of the TA FT (VA or peak) is calculated as:

$$\sigma_{T_{TA_i}} = \sqrt{\frac{\sum_{k=1}^i t_k \sigma_{T_k}^2}{\sum_{k=1}^i t_k}} \quad (25)$$

4. RESULTS

The overall model temperature uncertainty is estimated using the uncertainty quantification procedure described in the previous sections. The daily uncertainty (in terms of relative and absolute standard deviation at each time step) is estimated for the following calculated temperatures: all TCs, instantaneous VA FT, peak FT, VA temperature for the middle 50% of the graphite (outer – sleeve), and VA temperature for middle 50% of the matrix (inner – matrix). The uncertainty of corresponding time-averaged fuel and graphite temperatures is calculated from uncertainties for instantaneous temperatures using *Equation (25)*.

As stated in Section 3.3, the uncertainties of fuel heat rate, graphite heat rate, fuel thermal conductivity, and graphite thermal conductivity are assumed constant over the entire irradiation and are the same for all 12 AGR-3/4 capsules. Therefore, they are plotted as horizontal lines as a function of EFPDs. Among these, the fuel conductivity has highest uncertainty (20%) followed by the graphite conductivity (15%). The uncertainty for fuel heat rate (5%) is higher than graphite heat rate uncertainty (3%) because depletion of fuel is more complex than graphite material. On the other hand, the uncertainties of neon fraction and four gap sizes are dynamic over the irradiation time because they are a function of the input variations as described in the Subsections 3.3.2.1 and 3.3.2.2. Among the four gas gaps, Gap 1 and Gap 2 have very high uncertainty due to their small width (2–5 mil). For the neon

fraction, the uncertainties are unusually larger for a few time steps at the beginning and the end of each ATR cycle when the neon fractions were close to zero.

The uncertainty results include the dominant parameter of the predicted temperature uncertainty, which is the parameter that contributes to the largest temperature variance. In turn, the temperature variance due to input uncertainty is the square of the product of the sensitivity coefficient and the standard deviation for a parameter $(a_i \sigma_i)^2$. The dominant parameter varies depending on input parameter uncertainty (e.g., fuel heat rate, neon fraction) and output temperatures. The results given in the following sections identify the dominant parameter and quantify its influence on the overall uncertainty. The overall uncertainties in terms of standard deviation are given both as a range over EFPDs for instantaneous temperatures and at the end of irradiation for time-averaged temperatures.

4.1 Temperature Uncertainty Results for Capsule 12

Table 8 summarizes the temperature uncertainty results for the top capsule, Capsule 12. Figure 34 shows daily uncertainty for nine selected inputs. The daily uncertainty results for peak and VA fuel temperature are presented in Figure 35, for mid-50%-VA matrix and sleeve temperatures are in Figure 36, and for TC temperatures are in Figure 37. Note that only data for full days of power (EFPD = 1) are included in these plots because temperatures are much lower during start-up and power-down periods, making the plots look busy. The following results of calculated temperature uncertainty are observed:

- *Model bias*: negligible due to near zero TC residuals for all three TCs.
- *Input parameter uncertainty* (Figure 34): Gap 1 and Gap 2 have the highest input uncertainty (lime and magenta lines), increasing from about 30% for initial gap size up to 46% (Gap 2) at the end of irradiation. This is because these gaps are small. Gaps 3 and 4 have much lower uncertainty because they have significantly larger gaps. The neon fraction uncertainties (green line) are in the range between 3% and 6% except a few higher values for time steps at the beginning of each cycle when the neon fraction was low. Uncertainties for remaining inputs are unchanged over time of irradiation.
- *Input parameter sensitivity* (top panels in Figure 35 through Figure 37): The fuel heat rate (red lines) is the most sensitive for fuel and matrix temperatures (up to 0.35) and neon fraction is the most sensitive for TC temperatures (up to 0.41). The graphite heat rate has about half of the fuel heat rate sensitivity. The four gaps and fuel and graphite conductivities have small sensitivity coefficients, which are generally less than 0.1.
- *Weighted variance* (second panels in Figure 35 through Figure 37): The 5% uncertainty in the fuel heat rate is a dominant factor for peak and VA fuel, and mid-50%-VA matrix temperatures followed by Gap 1 for fuel temperature and Gap 2 for matrix temperature. For TC temperatures, the fuel heat rate is the most dominant factor during the beginning of irradiation period, but toward the end of irradiation Gap 4 becomes the most dominant factor. The uncertainties of neon fraction and Gap 3 contribute insignificantly to all calculated temperature variations.
- *Overall calculated temperature uncertainty* (third and fourth panels in Figure 35 through Figure 37): The overall temperature uncertainties for this capsule are the lowest among all capsules, and range between 1.5 to 3.0% (corresponding to 8 to 28°C). This is because of negligible model bias and relatively small gap uncertainties due to larger gap sizes. In terms of absolute standard deviation, the uncertainty is largest for peak fuel temperature (22°C on average) and smallest for peripheral TC1 and TC2 (12°C on average), located in the sink ring. The fourth panels show daily instantaneous and time-averaged temperatures plotted together with one standard deviation.

Table 8. Summary of temperature uncertainty results for Capsule 12.

Peak Fuel	Volume-Averaged Fuel	Volume-Averaged Matrix	Volume-Averaged Sleeve	Peak Fuel	Volume-Averaged Fuel	Volume-Averaged Matrix	Volume-Averaged Sleeve	TC1/2	TC3
Dominant factors: Fuel heat rate and Gap 1 for all temperatures; neon fraction and Gap 4 for TC1/2.									
Relative Standard Deviation, %				Standard Deviation, °C					
Instantaneous Temperature – Minimum/Maximum									
2.6/3.1	2.4/2.8	1.8/2.5	1.5/2.2	16/28	13/24	10/19	8/14	5/14	10/19
Time-Averaged Temperature – at End of Irradiation									
2.9	2.6	2.2	1.8	25	22	17	13	Not applicable (N/A)	N/A

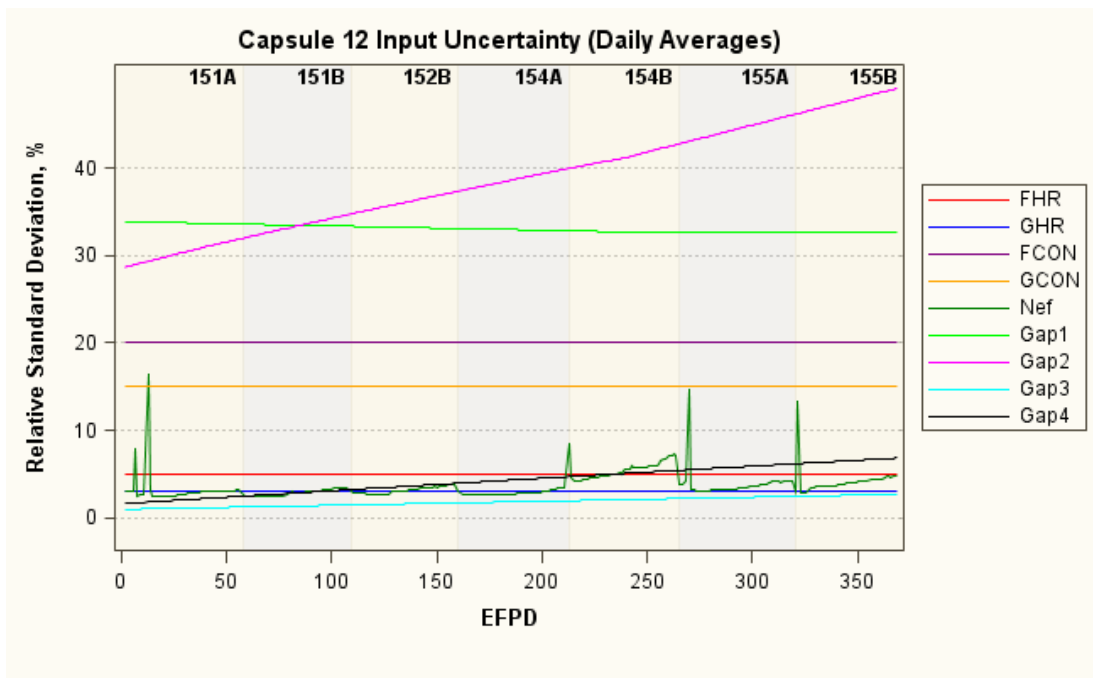


Figure 34. Daily relative standard deviations for nine inputs in Capsule 12.

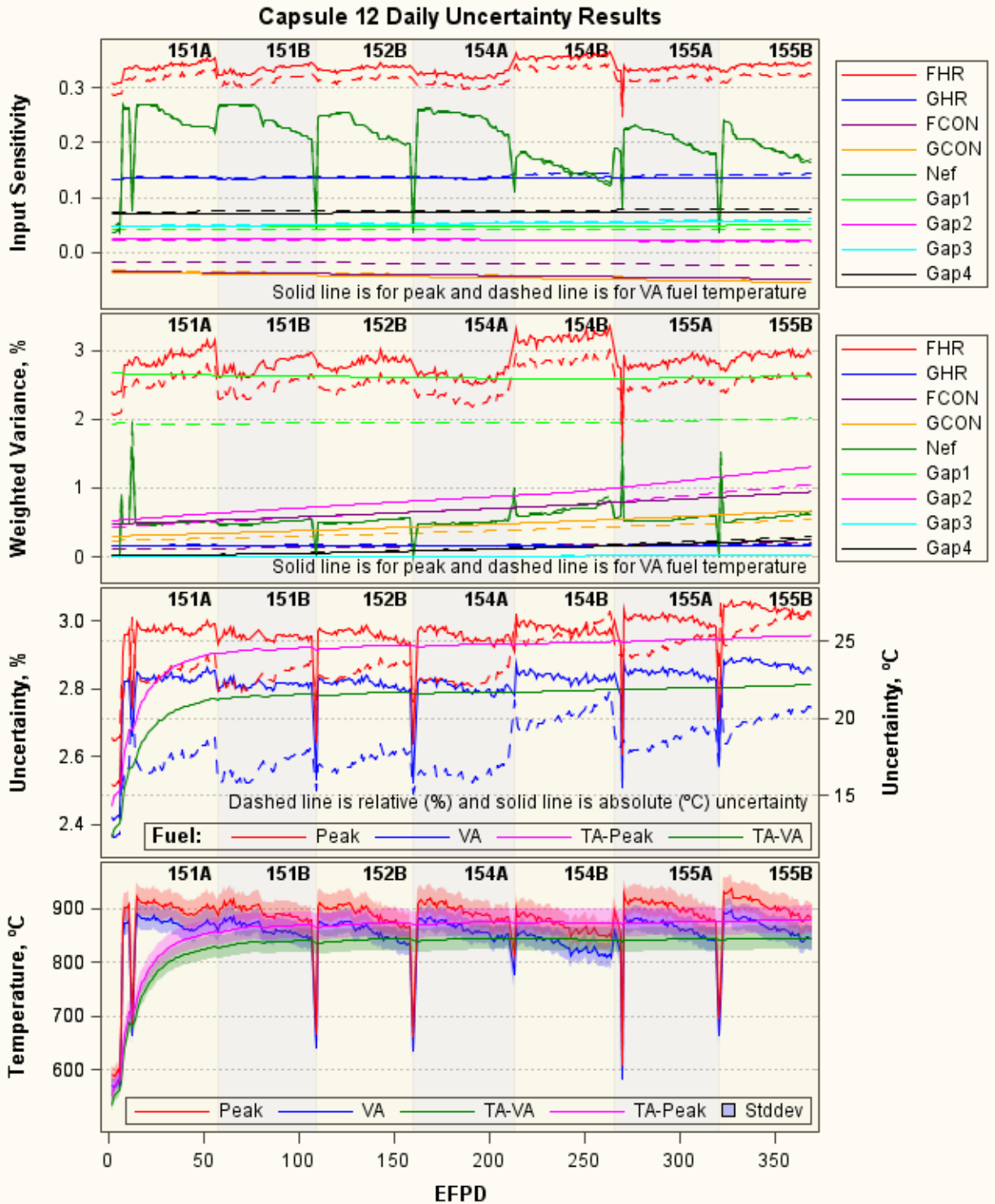


Figure 35. Daily uncertainty results for instantaneous and time-averaged peak and VA fuel temperatures in Capsule 12.

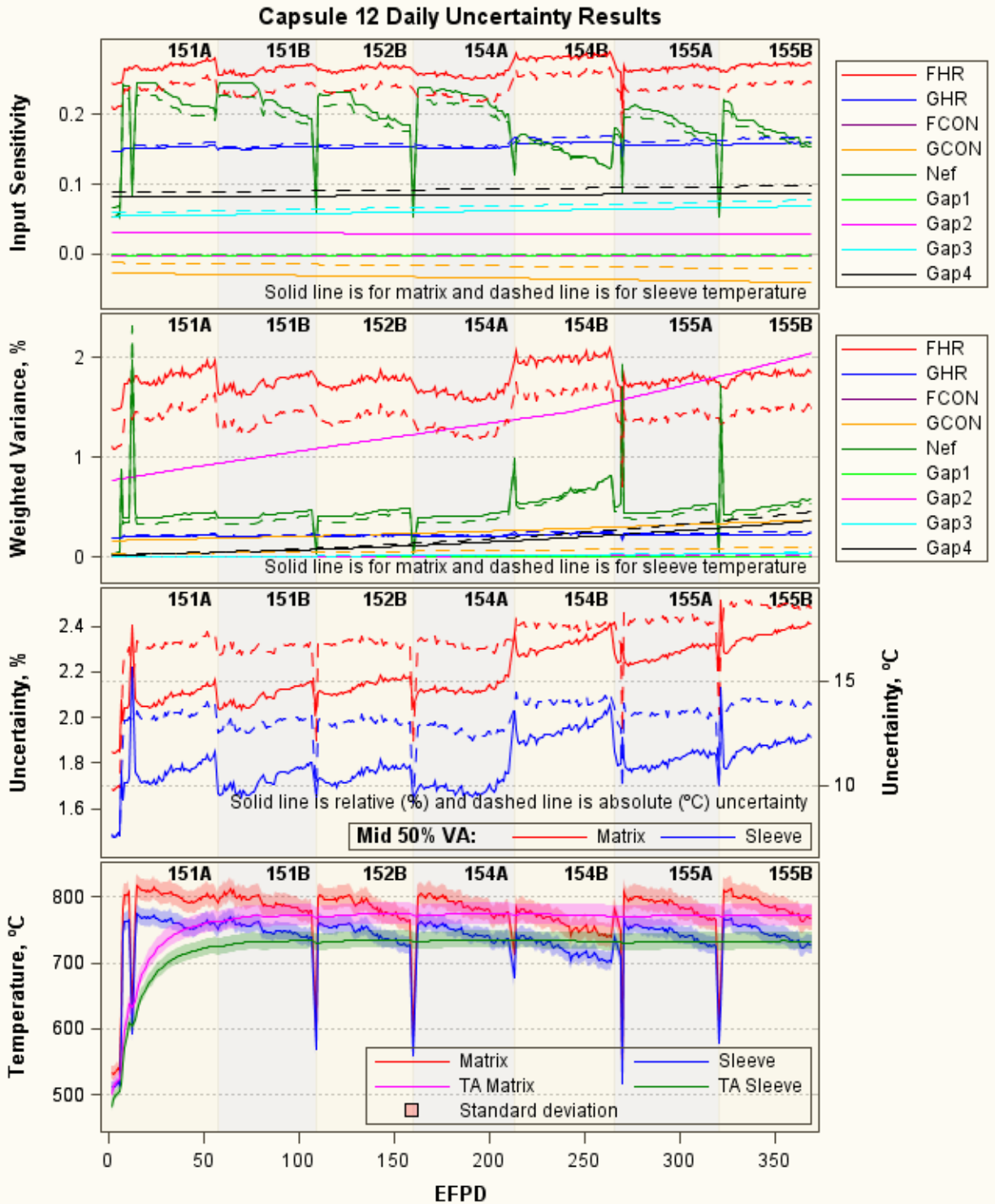


Figure 36. Daily uncertainty results for instantaneous and time-averaged mid-50%-VA matrix and sleeve temperatures in Capsule 12.

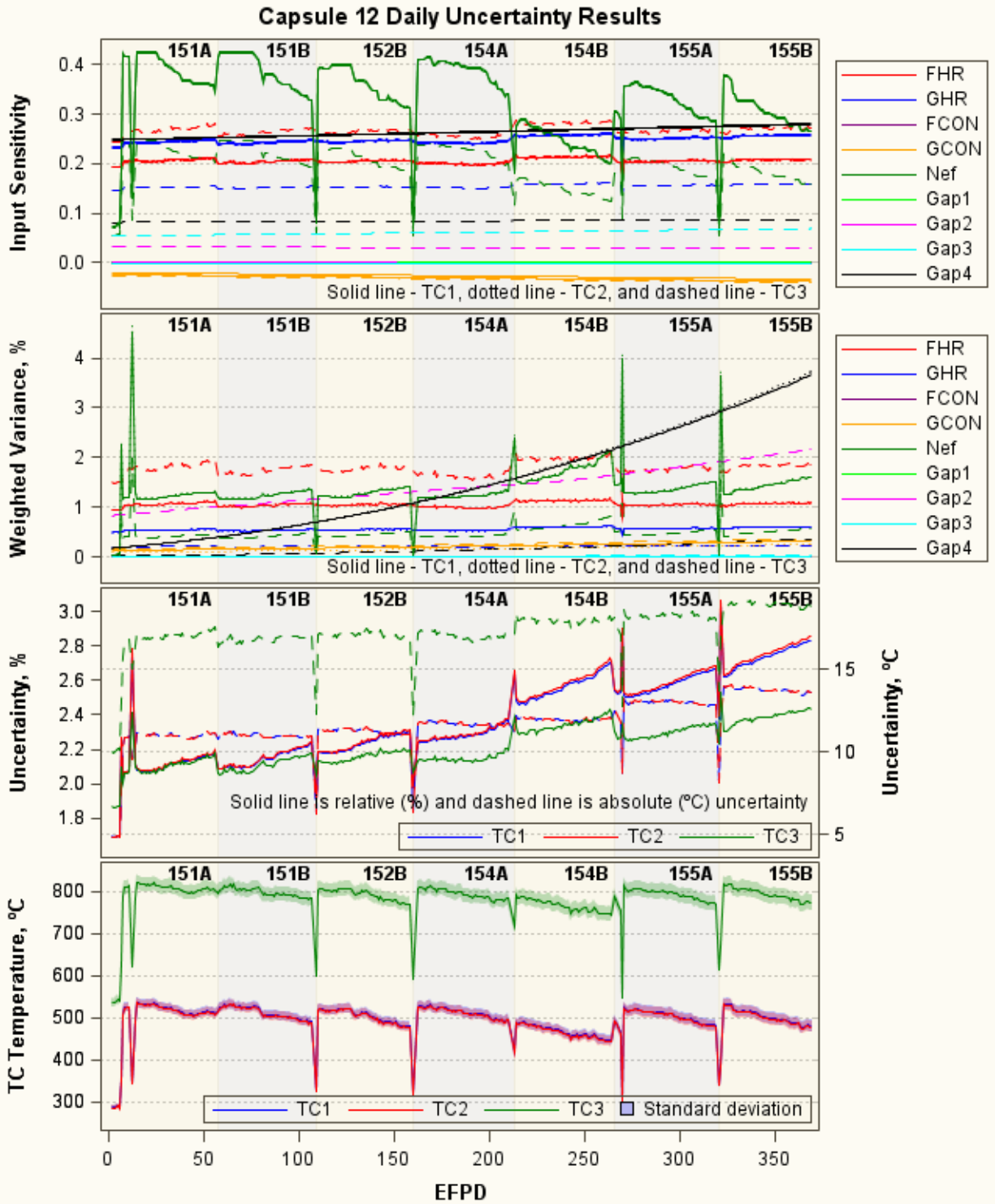


Figure 37. Daily uncertainty results for instantaneous TC temperatures in Capsule 12.

4.2 Temperature Uncertainty Results for Capsule 11

Table 9 summarizes the temperature uncertainty results for Capsule 11. Figure 38 shows daily uncertainty for nine selected inputs. The daily uncertainty results for peak and VA fuel temperature are presented in Figure 39, mid-50%-VA matrix and sleeve temperatures are in Figure 40, and TC temperatures are in Figure 41. Note that only data for full days of power (EFPD = 1) are included in these plots because temperatures are much lower during start-up and power-down periods, making the plots look busy. The following results of calculated temperature uncertainty are observed:

- *Model bias*: 2.8% due to average of -20°C TC1 and TC2 residuals.
- *Input parameter uncertainty* (Figure 38): Gap 1 has highest input uncertainty (lime line), increasing from about 38% for the initial gap size up to 48% at the end of irradiation. This is because this gap is the smallest of the four gaps. Gaps 2, 3, and 4 are largest in Capsule 11, leading to relatively small gap uncertainties. The neon fraction uncertainties (green line) are in the range between 3% and 6%, except for a few higher values for time steps at the beginning of each cycle when the neon fraction was low. Uncertainties for the remaining inputs are unchanged over the time of irradiation.
- *Input parameter sensitivity* (top panels in Figure 39 through Figure 41): The fuel heat rate (red line) is the most sensitive for the fuel, matrix, and sleeve temperatures (up to 0.32), and the neon fraction is most sensitive for TC temperatures (up to 0.25). The graphite heat rate has about half of the fuel heat rate sensitivity. The four gaps and fuel and graphite conductivities have small sensitivity coefficients, which are generally less than 0.1.
- *Weighted variance* (second panels in Figure 39 through Figure 41): The 5% uncertainty in the fuel heat rate is a dominant factor for peak and VA fuel, mid-50%-VA matrix and sleeve temperatures. This is followed by Gap 1 for fuel temperature, and graphite conductivity for matrix and sleeve temperature. For TC temperatures, the fuel heat rate and neon fraction have similar impact as the most dominant factor. Toward the end of irradiation, Gap 4 became the dominant factor for TC1/2 temperatures. The uncertainty of Gap 3 has very minor impact on all calculated temperature variations.
- *Overall calculated temperature uncertainty* (third and fourth panels in Figure 39 through Figure 41): The overall temperature uncertainties for this capsule range between 3.1 to 3.8% (corresponding to 22 to 48°C). Capsule 11 uncertainties are higher than Capsule 12 mainly because of 2.8% model bias. In terms of absolute standard deviation, the uncertainty is largest for peak fuel temperature (45°C on average) and smallest for peripheral TC1 and TC2 (23°C on average), located in the sink ring. The fourth panels show daily instantaneous and time-averaged temperatures plotted together with one standard deviation.

Table 9. Summary of temperature uncertainty results for Capsule 11.

Peak Fuel	Volume-Averaged Fuel	Volume-Averaged Matrix	Volume-Averaged Sleeve	Peak Fuel	Volume-Averaged Fuel	Volume-Averaged Matrix	Volume-Averaged Sleeve	TC1/2	TC3
Dominant factors: Fuel heat rate and Gap 1 for all temperatures; neon fraction and Gap 4 for TC1/2.									
Relative Standard Deviation, %				Standard Deviation, °C					
Instantaneous Temperature – Minimum/Maximum									
3.5/3.8	3.4/3.7	3.1/3.4	3.1/3.3	34/48	31/45	26/38	22/32	14/26	N/A
Time-Averaged Temperature – at End of Irradiation									
3.6	3.5	3.2	3.1	45	41	35	30	N/A	N/A

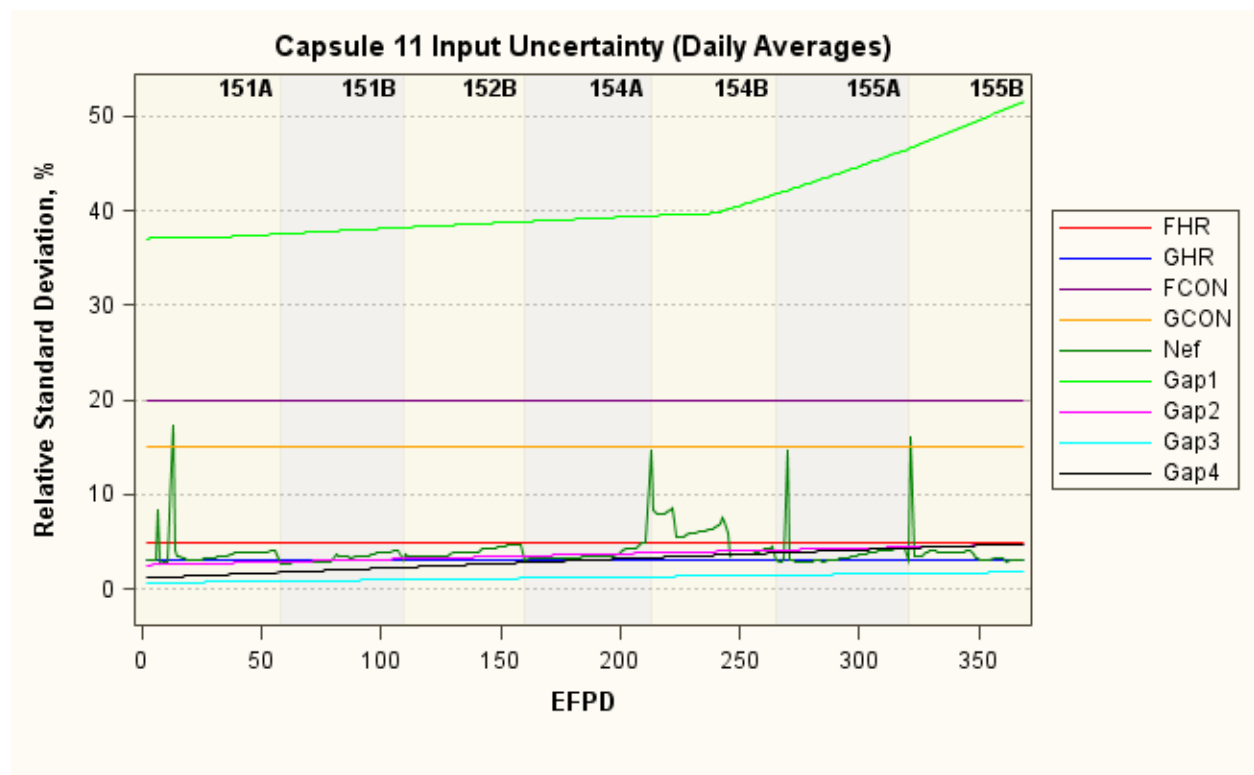


Figure 38. Daily relative standard deviations for nine inputs in Capsule 11.

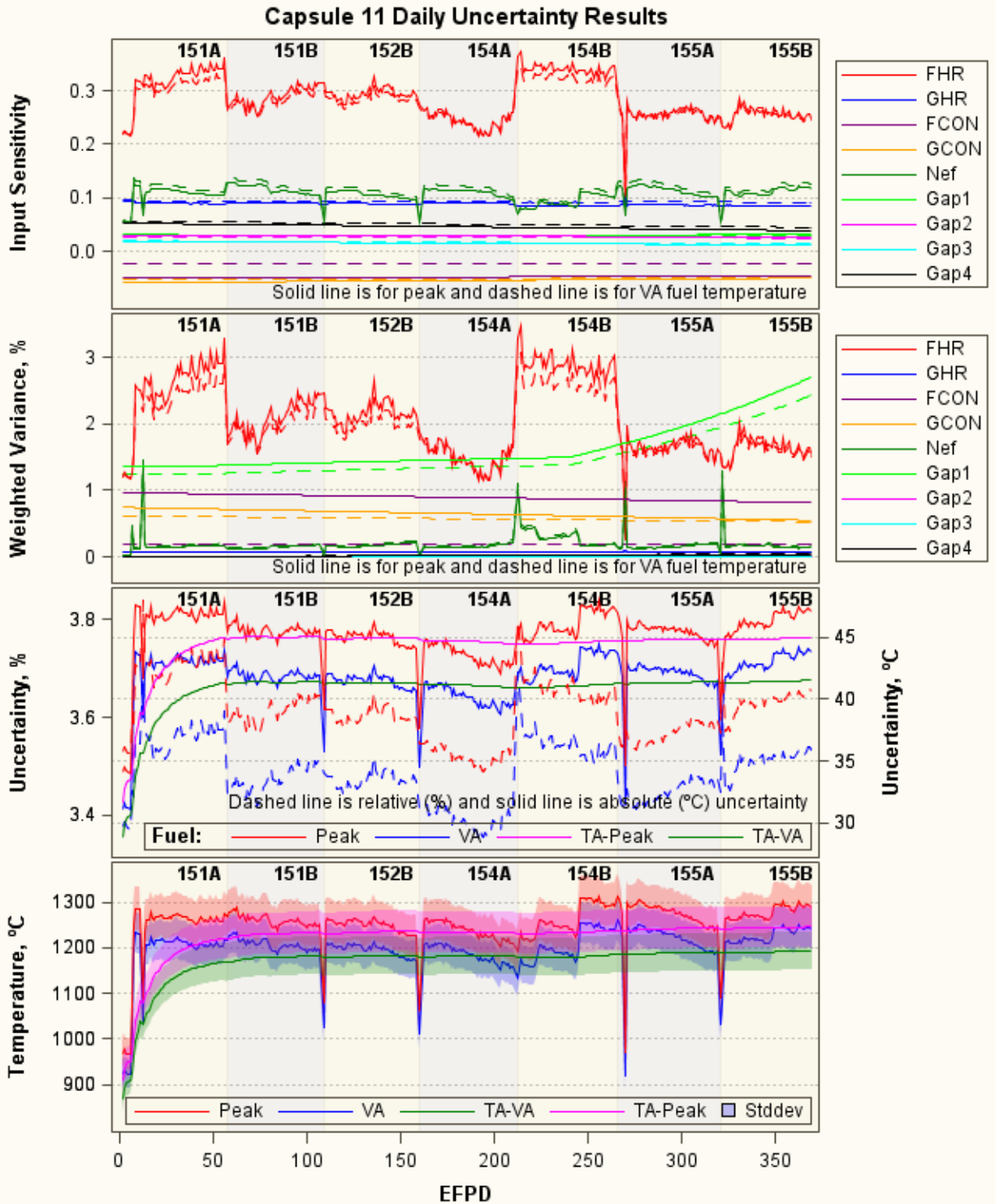


Figure 39. Daily uncertainty results for instantaneous and time-averaged peak and VA fuel temperatures in Capsule 11.

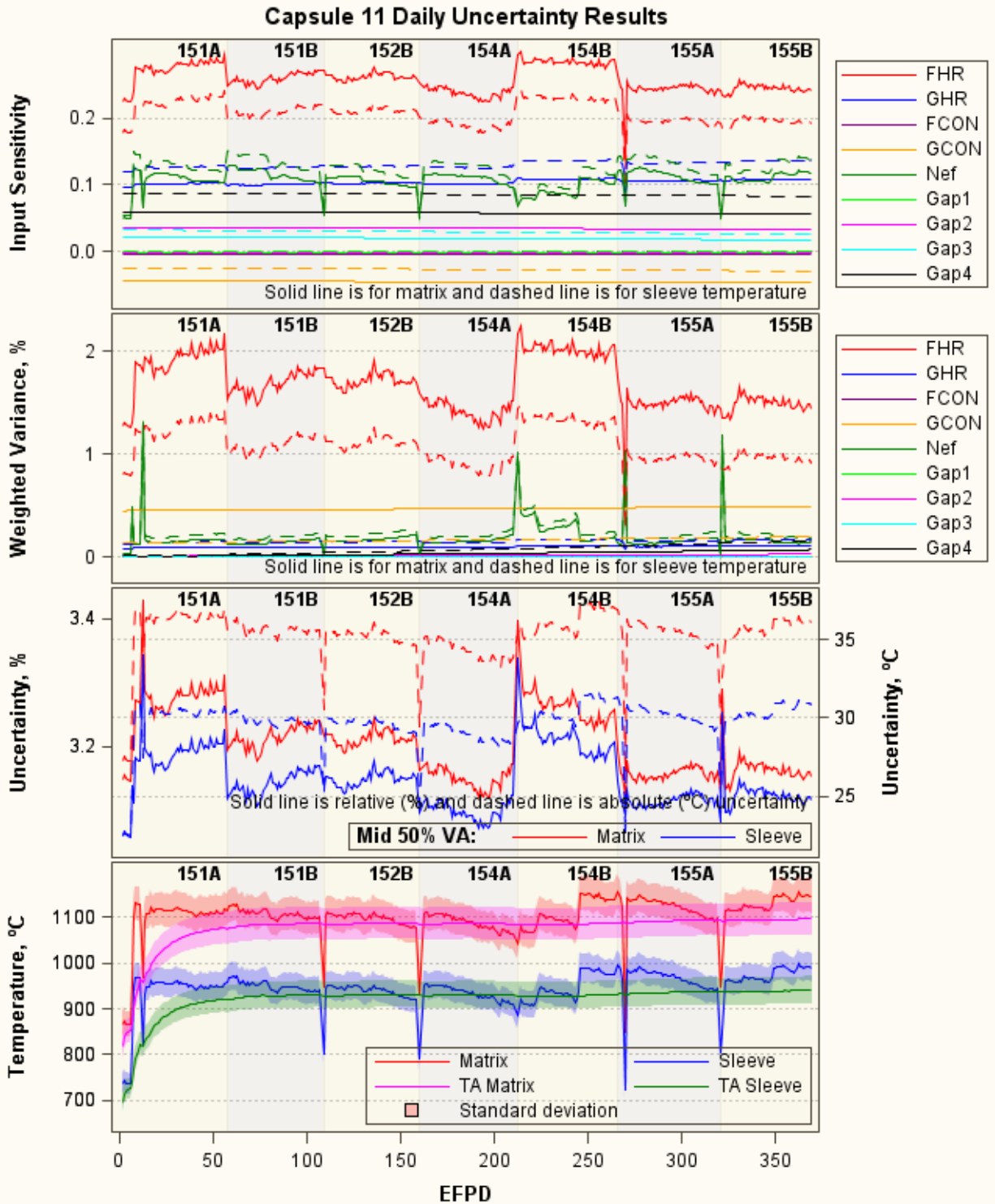


Figure 40. Daily uncertainty results for instantaneous and time-averaged mid-50%-VA matrix and sleeve temperatures in Capsule 11.

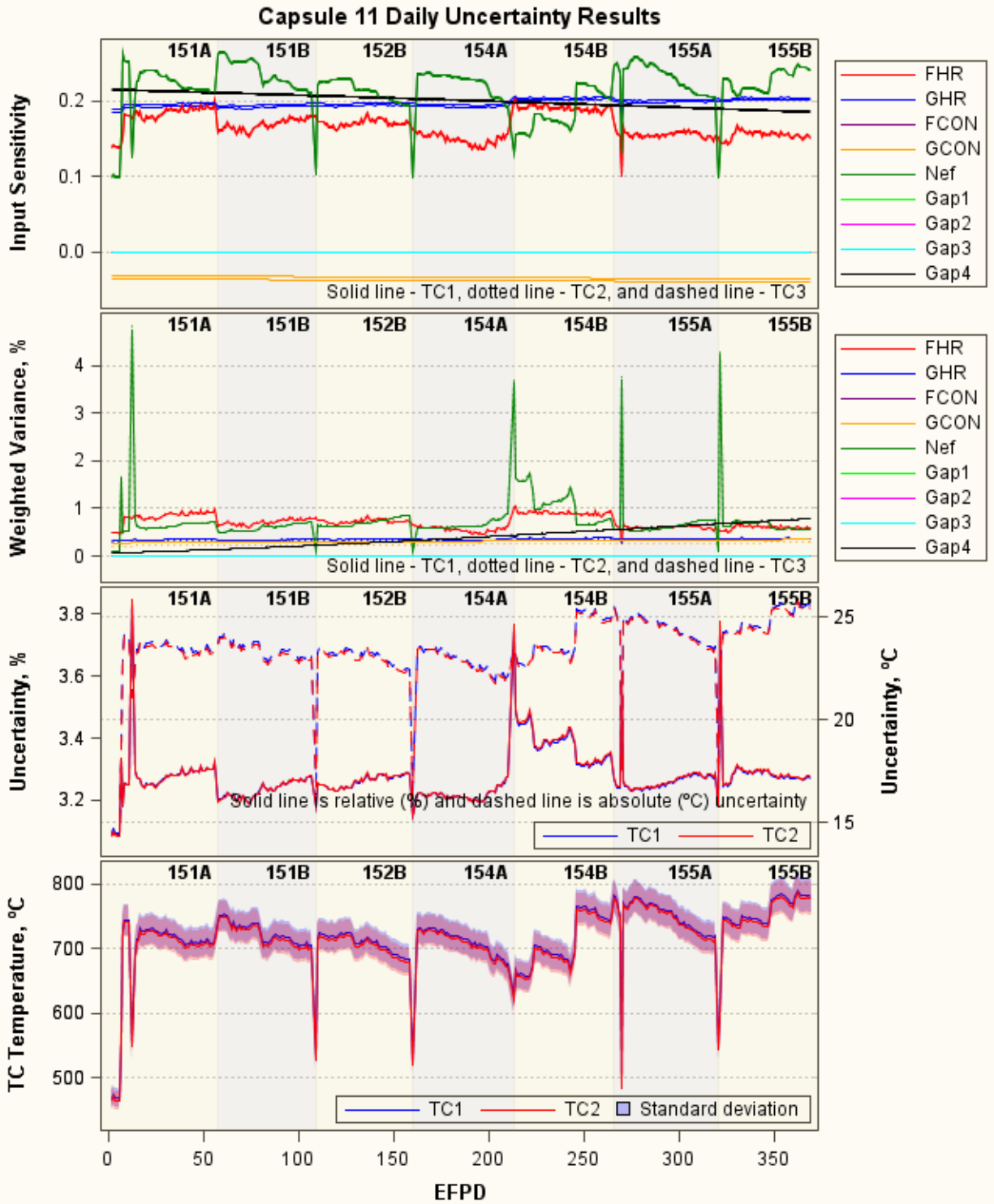


Figure 41. Daily uncertainty results for instantaneous TC temperatures in Capsule 11.

4.3 Temperature Uncertainty Results for Capsule 7

Table 10 summarizes the temperature uncertainty results for Capsule 7. Figure 42 shows daily uncertainty for nine selected inputs. The daily uncertainty results for peak and VA fuel temperature are presented in Figure 43, mid-50%-VA matrix and sleeve temperatures are in Figure 44, and TC temperatures are in Figure 45. Note that only data for full days of power (EFPD = 1) are included in these plots because temperatures are much lower during start-up and power-down periods, making the plots look busy. The following results of calculated temperature uncertainty are observed:

- *Model bias*: 3.2% due to average of 20°C TC1 and TC2 residuals.
- *Input parameter uncertainty* (Figure 42): Gap 1 has highest input uncertainty (lime line), increasing from about 33% for initial gap size up to 105% at the end of irradiation. This is because Gap 1 was narrowing by the end of irradiation to only 1.25 mil width. Gap 2 uncertainty is the second highest up to about 40%. Gaps 3 and 4 have much lower uncertainty because they have significantly larger widths. The neon fraction uncertainties (green line) are in the range between 3% and 6%, except a few higher values for time steps at the beginning of each cycle when the neon fraction was low. Uncertainties for remaining inputs are unchanged over time of irradiation.
- *Input parameter sensitivity* (top panels in Figure 43 through Figure 45): The fuel heat rate (red line) is the most sensitive for fuel and matrix temperatures (up to 0.36), and neon fraction and Gap 4 are most sensitive for TC temperatures (up to 0.55). The graphite heat rate has about half of the fuel heat rate sensitivity for matrix and sleeve temperatures. The four gaps and fuel and graphite conductivities have small sensitivity coefficients, which are generally less than 0.1.
- *Weighted variance* (second panels in Figure 43 through Figure 45): The 5% uncertainty in the fuel heat rate and Gap 1 are both dominant factors for peak and VA fuel temperatures. For mid-50%-VA matrix and sleeve temperatures, Gap 2 uncertainty is the dominant factor: although Gap 1 has much higher uncertainty, it has sensitivity coefficients near zero. Gap 3 and Gap 4 also have significant impact on matrix and sleeve temperatures. For TC temperatures, Gap 4 uncertainty is ultimately dominant due to its high sensitivity (up to 0.4), and other the three gaps contribute insignificantly to TCs' temperature variation.
- *Overall calculated temperature uncertainty* (third panels in Figure 43 through Figure 45): The overall temperature uncertainties for this capsule range between 3.6 to 4.7% (corresponding to 14 to 67°C). This is because of 3.2% model bias and relatively high gap size uncertainties. Temperature uncertainties in Capsule 7 are the second highest among 4 capsules reported here. In terms of absolute standard deviation, the uncertainty is largest for peak fuel temperature (61°C on average) and smallest for peripheral TC1 and TC2 (43°C on average), located in the sink ring. The fourth panels show daily instantaneous and time-averaged temperatures plotted with one standard deviation.

Table 10. Summary of temperature uncertainty results for Capsule 7.

Peak Fuel	Volume-Averaged Fuel	Volume-Averaged Matrix	Volume-Averaged Sleeve	Peak Fuel	Volume-Averaged Fuel	Volume-Averaged Matrix	Volume-Averaged Sleeve	TC1/2	TC3
Dominant factors: Fuel heat rate and Gap 1 for all temperatures; neon fraction and Gap 4 for TC1/2.									
Relative Standard Deviation, %				Standard Deviation, °C					
Instantaneous Temperature – Minimum/Maximum									
4.2/4.7	4.2/4.5	4.2/5.3	3.6/4.6	41/67	37/60	31/63	24/51	14/65	N/A
Time-Averaged Temperature – at End of Irradiation									
4.5	4.4	4.6	4.1	61	56	52	41	N/A	N/A

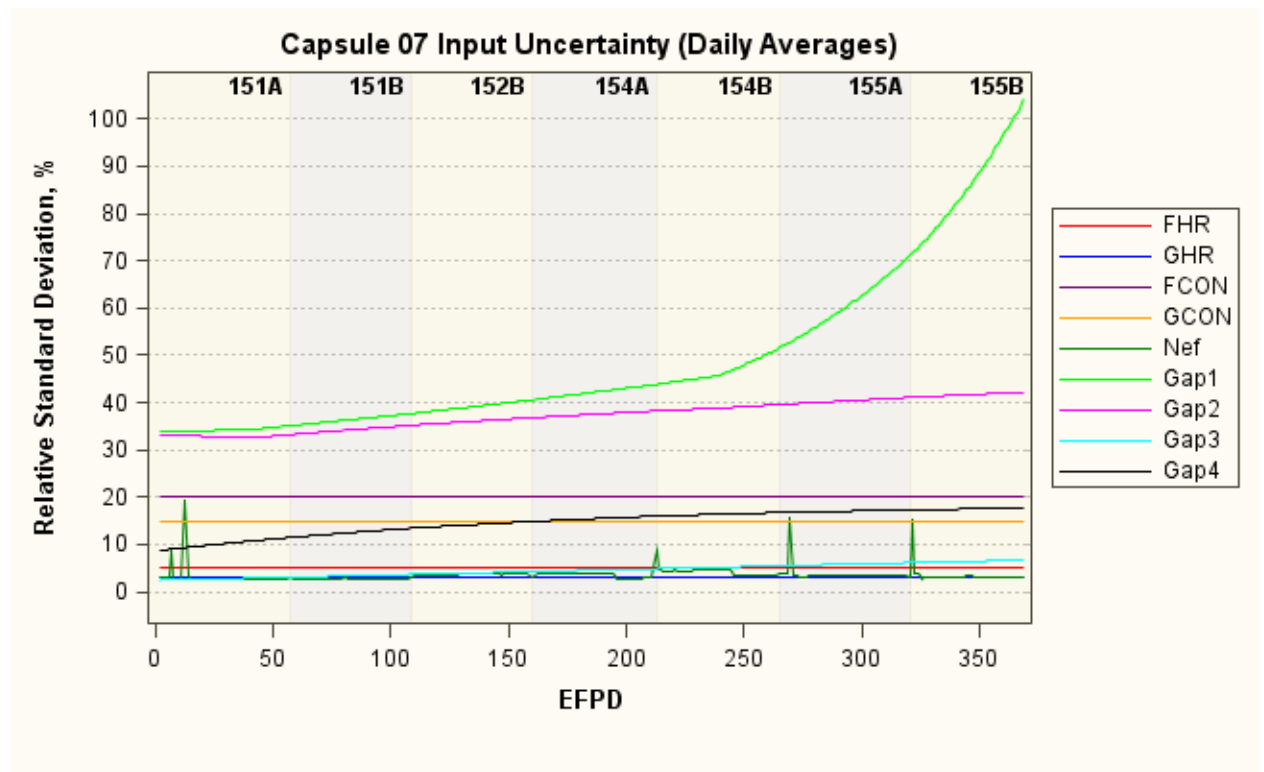


Figure 42. Daily relative standard deviations for nine inputs in Capsule 7.

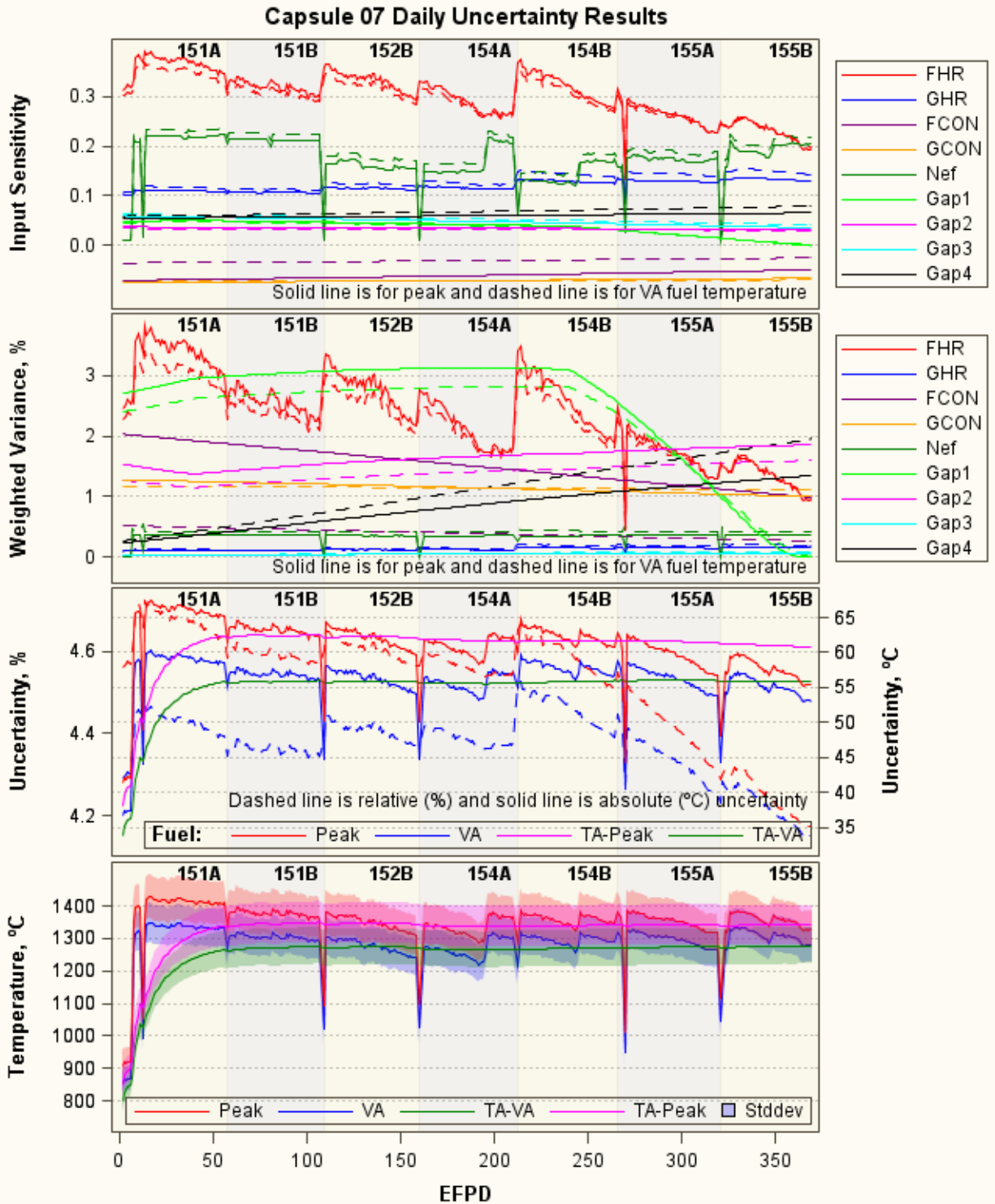


Figure 43. Daily uncertainty results for instantaneous and time-averaged peak and VA fuel temperatures in Capsule 7.

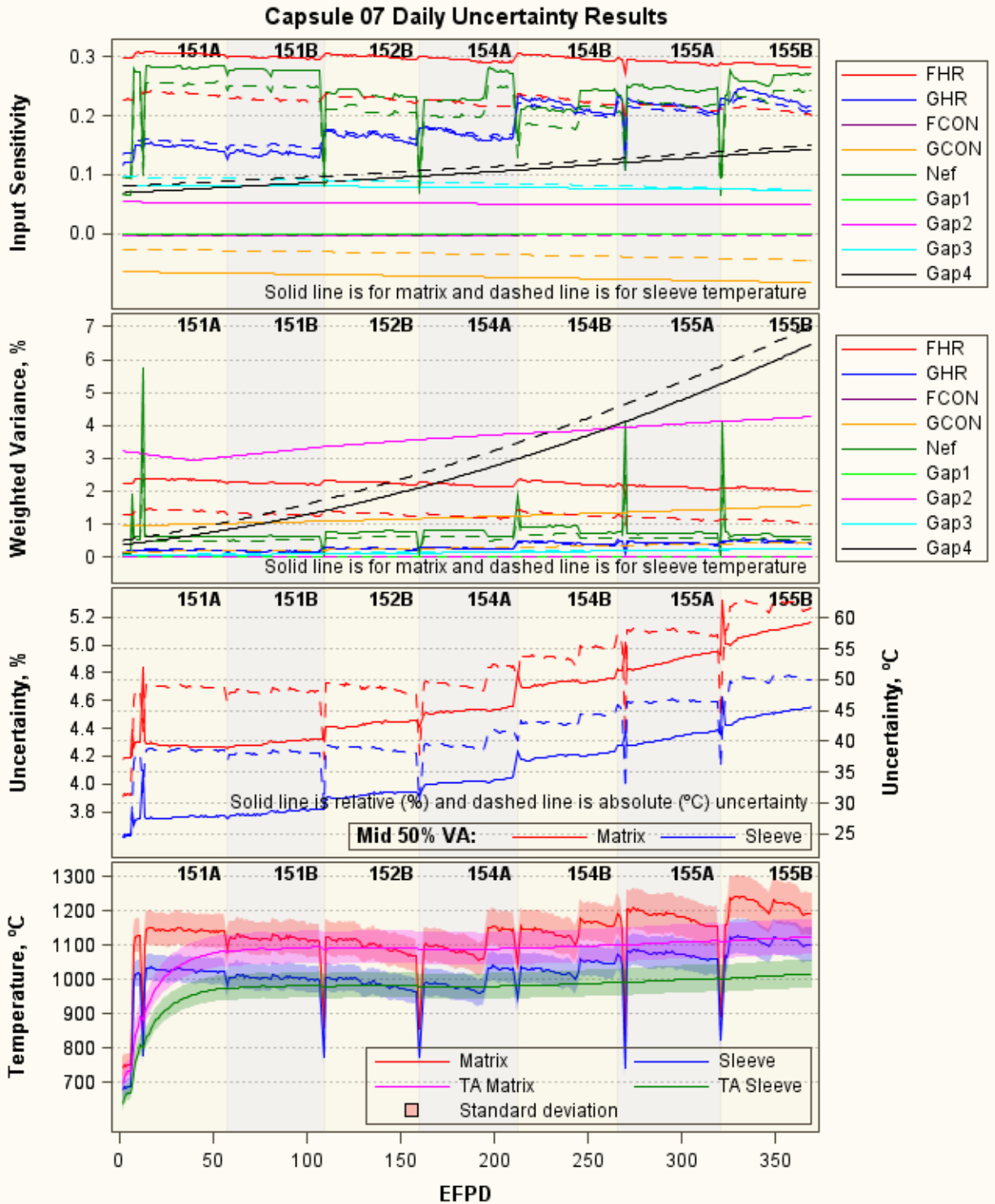


Figure 44. Daily uncertainty results for instantaneous and time-averaged mid-50%-VA matrix and sleeve temperatures in Capsule 7.

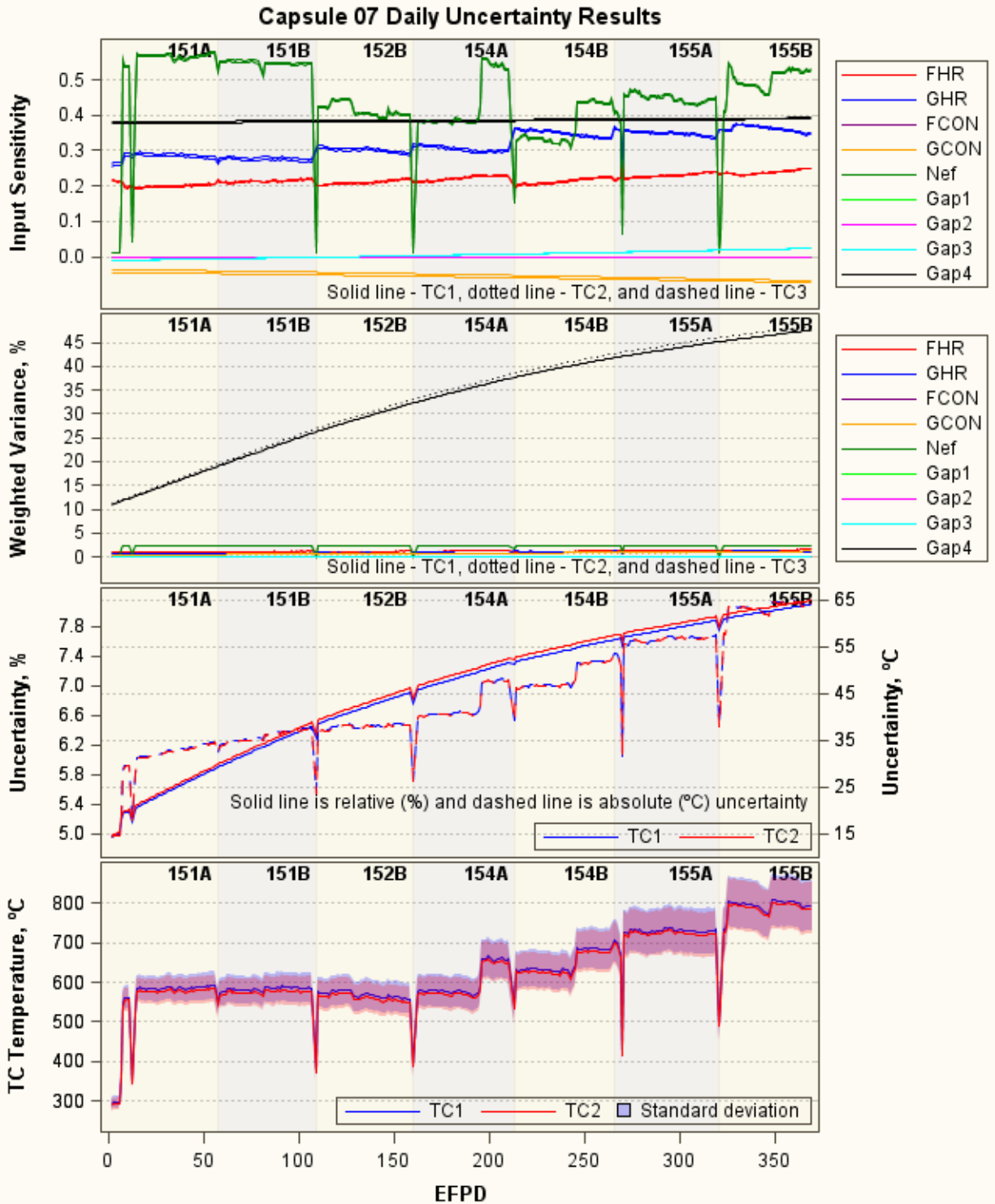


Figure 45. Daily uncertainty results for instantaneous TC temperatures in Capsule 7.

4.4 Temperature Uncertainty Results for Capsule 5

Table 11 summarizes the temperature uncertainty results for the Capsule 5. Figure 46 shows daily uncertainty for nine selected inputs. The daily uncertainty results for peak and VA fuel temperature are presented in Figure 47, mid-50%-VA matrix and sleeve temperatures are in Figure 48, and TC temperatures are in Figure 49. Note that only data for full days of power (EFPD = 1) are included in these plots because temperatures are much lower during start-up and power-down periods, making the plots look busy. The following results of calculated temperature uncertainty are observed:

- *Model bias*: 4.3% due to average of 25°C TC1 and TC2 residuals.
- *Input parameter uncertainty* (Figure 46): Gap 2 has highest input uncertainty (pink line), increasing from 42% for initial gap size up to 128% at the end of irradiation. This is because this gap has the smallest width among the four gaps and decreased gap size toward the end of irradiation. Gaps 2, 3, and 4 have lower uncertainty because they are significantly larger. The neon fraction uncertainties (green line) range between 3% and 10%, except a few higher values for time steps at the beginning of each cycle when the neon fraction was low. Uncertainties for remaining inputs are unchanged over time of irradiation.
- *Input parameter sensitivity* (top panels in Figure 47 through Figure 49): The fuel heat rate (red line) is the most sensitive for fuel and matrix temperatures (up to 0.42), and neon fraction is most sensitive for TC temperatures (up to 0.50). The graphite heat rate has about half of the fuel heat rate sensitivity. The four gaps and fuel and graphite conductivities have small sensitivity coefficients, which are generally less than 0.1.
- *Weighted variance* (second panels in Figure 47 through Figure 49): Gap 1 is a dominant factor for peak and VA fuel temperatures at the beginning and the end of irradiation; Gap 2 is a dominant factor for peak and VA fuel and mid-50%-VA matrix temperatures for most of irradiation period; Gap 3 is a dominant factor for mid-50%-VA sleeve temperature; And Gap 4 is a dominant factor for TC1 and TC2 temperatures. The 5% uncertainty in the fuel heat rate is only a third dominant factor for peak and VA fuel and mid-50%-VA matrix temperatures.
- *Overall calculated temperature uncertainty* (third panels in Figure 47 through Figure 49): The overall temperature uncertainties for this capsule are the largest among all capsules, ranging between 5.5 to 8.0% (corresponding to 17 to 78°C). This is because of 4.3% model bias and relatively large gap uncertainties due to smaller gap sizes. In terms of absolute standard deviation, the uncertainty is largest for peak fuel temperature (76°C on average) and smallest for peripheral TC1 and TC2 (40°C on average), located in the sink ring. The fourth panels show daily instantaneous and time-averaged temperatures plotted with one standard deviation.

Table 11. Summary of temperature uncertainty results for Capsule 5.

Peak Fuel	Volume-Averaged Fuel	Volume-Averaged Matrix	Volume-Averaged Sleeve	Peak Fuel	Volume-Averaged Fuel	Volume-Averaged Matrix	Volume-Averaged Sleeve	TC1/2	TC3
Dominant factors: Fuel heat rate and Gap 1 for all temperatures; neon fraction and Gap 4 for TC1/2.									
Relative Standard Deviation, %				Standard Deviation, °C					
Instantaneous Temperature – Minimum/Maximum									
6.7/7.0	6.3/6.8	6.0/8.3	5.5/7.4	45/79	39/72	30/69	24/62	17/52	31/71
Time-Averaged Temperature – at End of Irradiation									
6.8	6.6	7.5	6.7	75	68	62	49	N/A	N/A

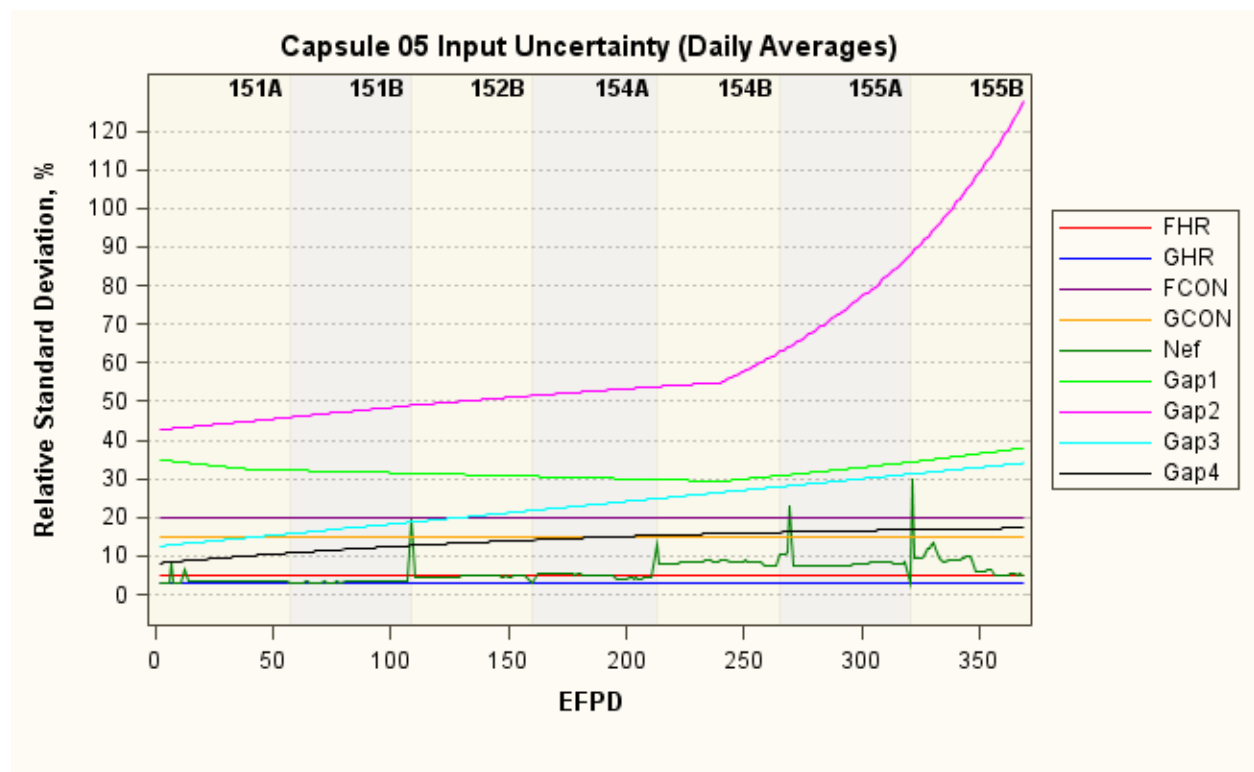


Figure 46. Daily relative standard deviations for nine inputs in Capsule 5.

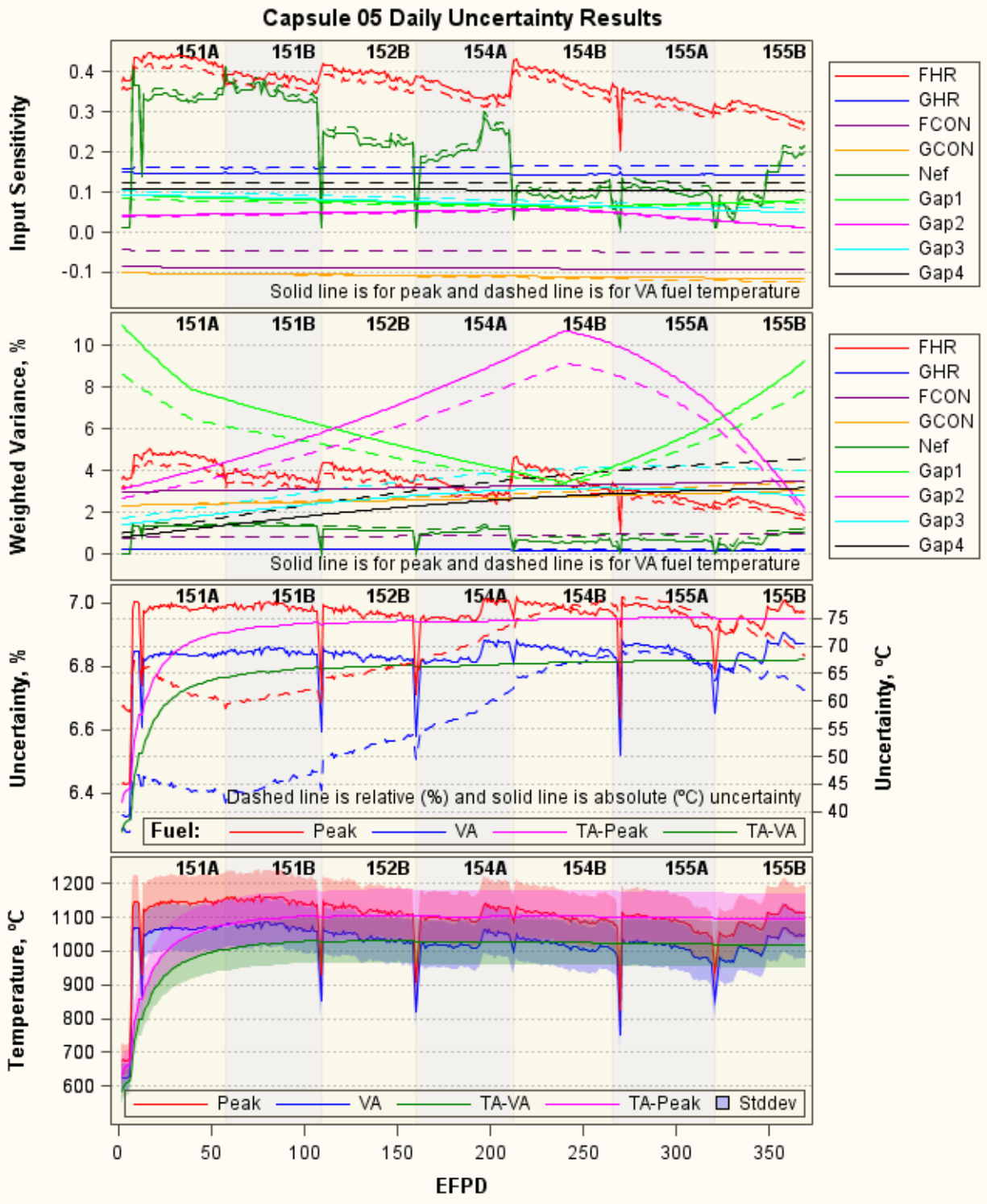


Figure 47. Daily uncertainty results for instantaneous and time-averaged peak and VA fuel temperatures in Capsule 5.

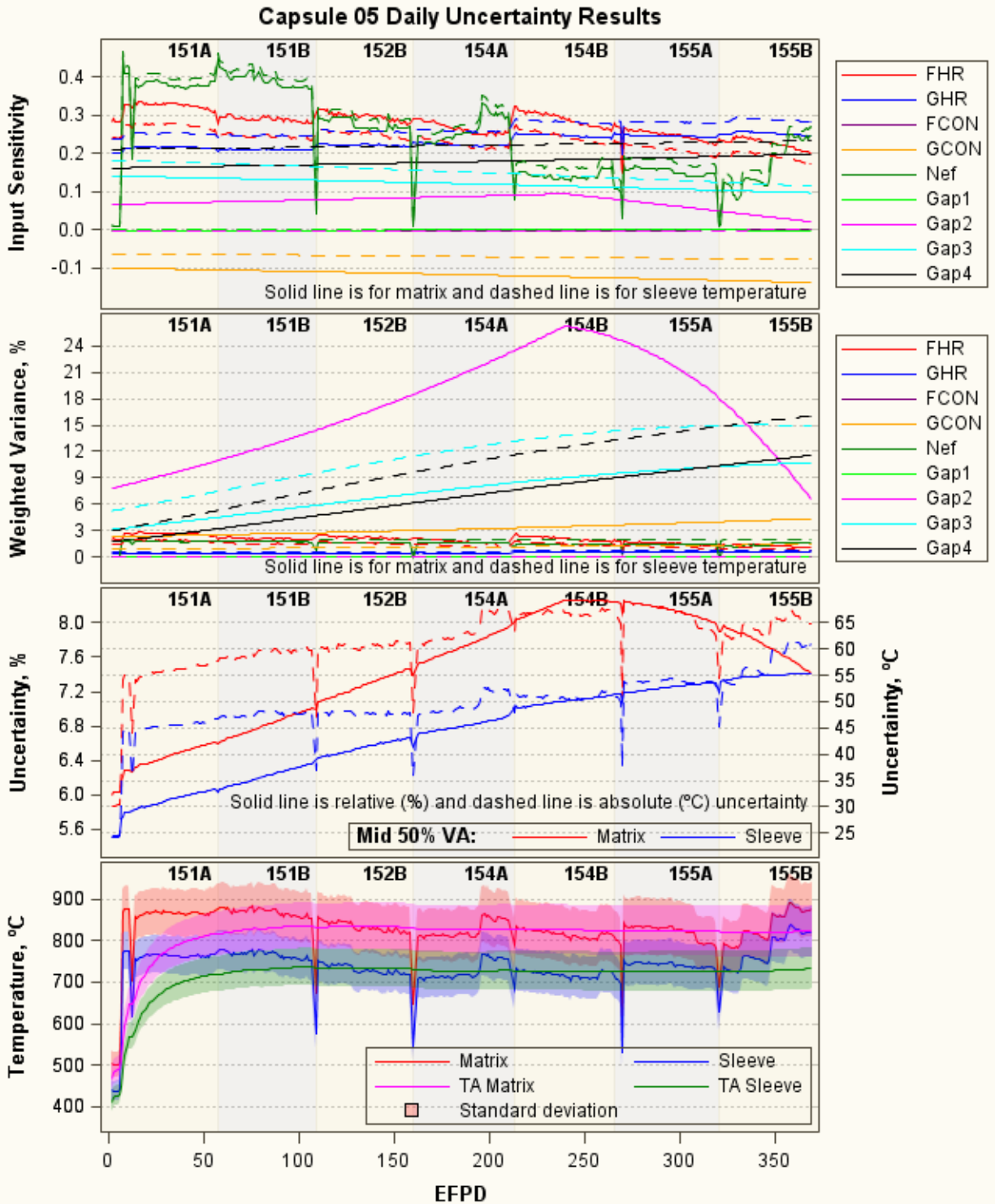


Figure 48. Daily uncertainty results for instantaneous and time-averaged mid-50%-VA matrix and sleeve temperatures in Capsule 5.

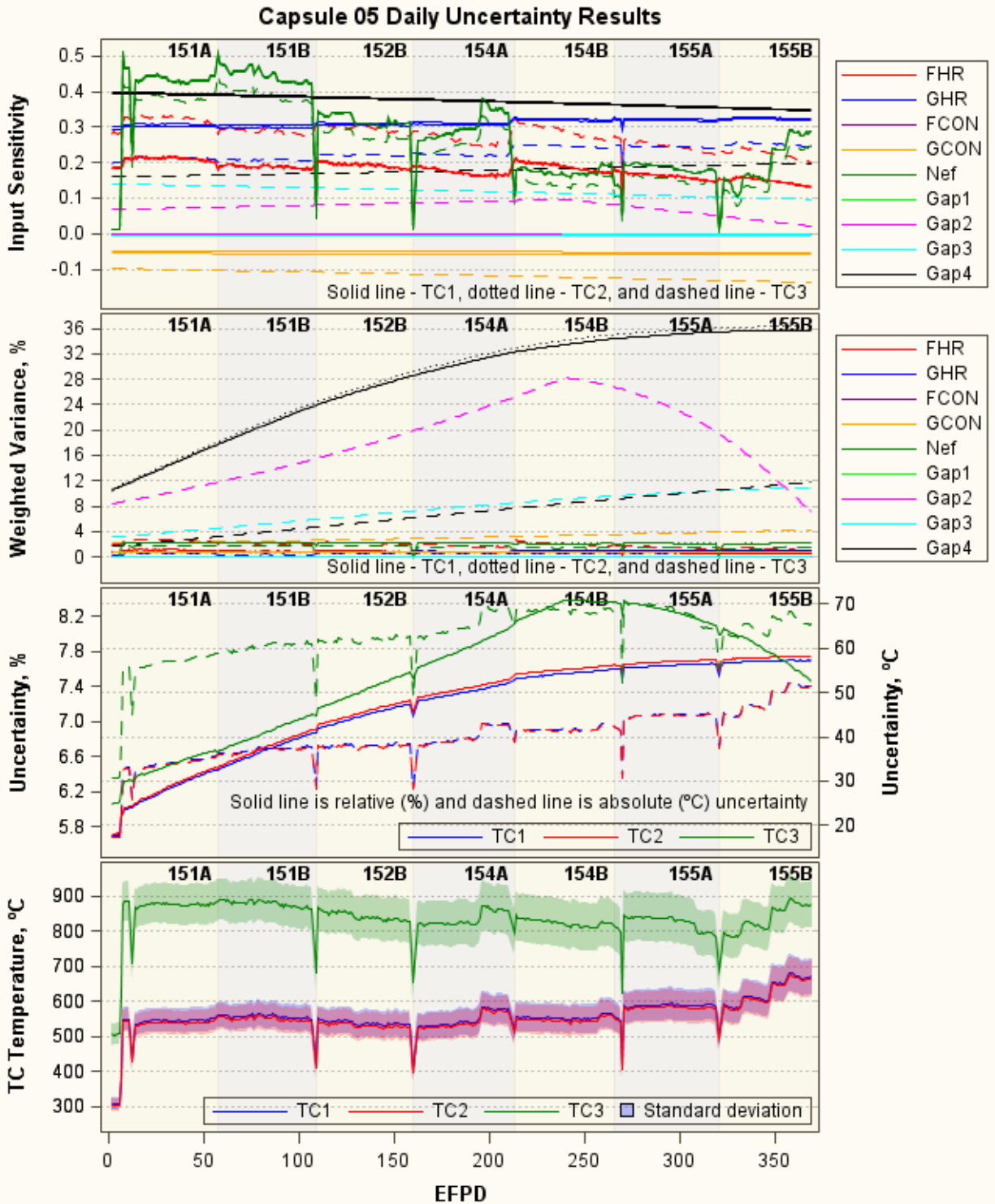


Figure 49. Daily uncertainty results for instantaneous TC temperatures in Capsule 5.

5. CONCLUSIONS

Knowledge of the thermal conditions and associated uncertainties of the nuclear fuel in a reactor experiment are central to the interpretation of the experiment results. It is necessary when using the experiment results for calibration and validation of nuclear fuel performance models and codes, ultimately in support of the design and licensing of the new nuclear fuel. The work documented in this report supports quantification of uncertainty in the computed thermal condition of nuclear fuels in the AGR-3/4 test, where it is not practical to obtain direct temperature measurements in the fuel compact domain.

The experiment was instrumented with TCs to provide temperature measurements in the graphite blocks surrounding the fuel compacts. In-depth analysis and qualification of the TC data for the AGR-1 experiment were performed in previous works using statistical methods (Pham and Einerson 2011, 2013). These analyses demonstrate that the AGR-1 TC data can be used to assess and calibrate thermal analysis models in the ABAQUS code (ECAR-2476). The AGR-3/4 TC temperatures also can be used to assess and calibrate thermal analysis models in the ABAQUS code (Hawkes 2015) for AGR-3/4 capsules. The calibrated code was then used to predict temperatures in the AGR-3/4 capsules.

This study uses thermal model parameters of potential importance to the AGR-3/4 predicted FTs based on the combination of input uncertainty and sensitivity. Expert judgment is used as a basis to specify the uncertainty range for a set of select parameters. This also takes into account all physics that occurred during AGR-3/4 irradiation which can impact input uncertainties (e.g., the gap size changes increased the uncertainty of the gaps). Propagation of model parameter uncertainty is then used to quantify the parameter uncertainty of AGR-3/4 calculated temperatures. The model-form uncertainties (or model bias) are also included in the overall uncertainty. This model bias is based on the average of TC residuals.

The parameter sensitivity defines how the predicted temperature would be influenced by changes in an input parameter. The uncertainty of the model output increases as the sensitivity coefficient of an input parameter increases. The sensitivity analysis performed in this work went beyond the traditional local sensitivity. Using experimental design, analysis of pairwise interactions of model parameters was performed to establish sufficiency of the first-order (linear) expansion terms in constructing the response surface. To achieve completeness, uncertainty propagation made use of pairwise noise correlations of model parameters. Further, using an interpolation scheme over the input parameter domain, the analysis obtains time-dependent sensitivity over the test campaign's duration. This allows computation of uncertainty for the instantaneous VA and peak FTs, VA graphite (matrix and sleeve) temperatures, and TC temperatures over the whole AGR-3/4 irradiation period. The following conclusions are drawn about the parameter sensitivity coefficients for AGR-3/4 temperature predictions:

- For heat rates and neon fraction, the sensitivity coefficients of fuel heat rate are highest for VA and peak fuel temperatures. The graphite heat rate is more sensitive to graphite rings' and TC temperatures. The neon fraction is sensitive to all temperatures of interest.
- For four gap sizes, the sensitivity coefficients range from about 0 to 0.4. Gap 1 is most sensitive to VA and peak fuel temperatures, but has very little impact on other temperatures. Gap 2 has small sensitivity on both fuel and matrix temperatures, but negligible impact on sleeve and TC1/2 temperatures. Gap 3 has relatively high sensitivity to all temperatures with highest value for sleeve ring temperature. Gap 4 had highest sensitivities to all temperatures of interest, especially for TC1/2 temperatures, which are located right next to this gap.
- The sensitivity coefficients of fuel compact thermal conductivity and graphite thermal conductivity are less than 0.1 for all temperatures of interest. The sensitivity coefficient of fuel thermal conductivity is near zero for sleeve and TC1/2 temperatures, leading to negligible impact on these temperatures, but graphite conductivity impacts all temperatures of interest.

The parameter uncertainty of calculated temperatures, in terms of one standard deviation, is obtained through propagation of model parameter uncertainty as the square root of the summation of the variances weighted by the squares of their sensitivity coefficients. Thus, the effect of a parameter uncertainty on the variation of temperature prediction is a product of input uncertainty and the sensitivity coefficient. The most significant factors contributing to overall uncertainty of the AGR-3/4 temperature predictions are:

- The fuel heat rate is most sensitive to temperature prediction; but its small input uncertainty (5%) makes it only the third influential factor on fuel temperature uncertainty. However, it is the most influential factor for matrix and graphite sleeve temperatures. The graphite heat rate and neon fraction are also sensitive to temperature, but their contribution to temperature uncertainty is very insignificant due to their relatively low input uncertainties (about 3%).
- Among the four gap sizes, Gaps 1 and 2 (about 3 mil width) have the highest relative input uncertainty (up to 128% by the end of irradiation for Gap 2 in Capsule 5). Even though these gap sensitivities are generally small (less than 0.1), they are the most significant factors contributing to the uncertainty of the FT predictions. On other hand, Gaps 3 and 4, having significantly lower relative uncertainty, have a minor impact on uncertainty of fuel and graphite temperatures. Gap 4 has the most impact on temperature uncertainty of TC1 and TC2, which are located near this gap.
- Finally, the fuel and graphite thermal conductivities have similar impact on FTs as the fuel heat rate. The fuel conductivity has a slight impact on matrix, sleeve, and TC temperatures.

In addition to parameter uncertainties, the model bias is also included in overall uncertainty in this analysis. The model biases are zero for Capsule 12, 2.8% for Capsule 11, 3.2% for Capsule 7, and 4.3% for Capsule 5. The overall uncertainty in the calculated temperatures for AGR-3/4 Capsule 5, 7, 11, and 12 ranged from 1.5% to 8.4%, depending on irradiation time (thermal conditions), capsule, and the temperature characteristic being predicted (peak, VA, fuel, matrix, sleeve, or TC). Result highlights are:

- Capsule 12 has lowest temperature uncertainty (up to 3.1%) because it has negligible model bias and lower input uncertainties of Gap 1 (32%) and Gap 2 (up to 48%).
- Capsule 11 has a slightly higher uncertainty (3.1 to 3.8%) than Capsule 12 due to 2.8% model bias.
- Capsule 7 uncertainty is in the range 3.6 to 8.1%, with the highest uncertainties up to 8.1% (or 65°C) for peripheral TC1/2 due to high Gap 4 uncertainty.
- Capsule 5 has highest temperature uncertainty (6.6 to 8.4%) with maximum of 8.4% for TC3, 8.3% relative standard deviation for mid-50%-VA matrix ring temperature, and 7.0% standard deviation for peak fuel temperature. This is caused by the highest model bias of 4.3% and high input uncertainties of Gap 1 (up to 40%) and Gap 2 (up to 128%).
- For AGR-1 and AGR-2, assuming negligible model bias the relative uncertainty ranged from 3 to 4% for instantaneous VA fuel temperature and from 3 to 5% for peak temperature. In addition, the AGR-1 Capsule 6 had 10% bias in fuel heat rate, causing the overall uncertainty to reach 5.8% for instantaneous temperature and 5.0% for time-averaged fuel temperature at the end of irradiation. Comparing to these experiments, the overall uncertainties of the AGR-3/4 Capsule 12 temperatures are lower for Capsule 12, which has negligible bias. Capsules 7 and 11 uncertainties including model bias (3.2% and 2.8% respectively) are comparable to those seen by AGR-1 and AGR-2 capsules. Conversely, Capsule 5 uncertainty including 4.3% model bias is clearly higher than the uncertainty in AGR-1 and AGR-2 capsules.

Besides uncertainties included in this study, other epistemic uncertainties still exist. These include modeling assumptions used to build the ABAQUS model for the AGR-3/4 capsules and uncertainty associated with numerical treatment (e.g., discretization errors) needed to implement and operate the ABAQUS simulations. Although the effect of these groups is generally very hard to evaluate, it is important to systematically delineate them, so not to over-state the confidence in predicted values (underestimating their uncertainties) stemming from a parameter uncertainty analysis alone.

6. REFERENCES

- Collin, B.P., 2015, *AGR-3/3 Irradiation Test Final As-Run Report*, INL/EXT-15-35550, Rev. 0, Idaho National Laboratory.
- Demkowicz, P., L. Cole, S. Ploger, and P. Winston, 2011, *AGR 1 Irradiated Test Train Preliminary Inspection and Disassembly First Look*, INL/EXT-10-20722, Idaho National Laboratory.
- Gontard, R., and H. Nabilek, 1990, "Performance Evaluation of Modern HTR TRISO Fuels," Forschungszentrum Julich GmbH., HTA IB 05/90.
- Harp, J.M., 2014, ECAR-1682, "Analysis of Individual Compact Fission Product Inventory and Burnup for the AGR-1 TRISO Experiment using Gamma Spectrometry," Rev. 3, Idaho National Laboratory.
- Hawkes, G., J. Sterbentz, and B. Pham, 2015, "Sensitivity Evaluation of the AGR 3/4 Experiment Thermal Model Irradiated in the Advanced Test Reactor," *Proceedings of the ASME IMECE2015, Paper No. 53544, International Mechanical Engineering Congress & Exposition Conference*, Houston, Texas, November 13-19, 2015. Accepted.
- Hawkes, G.L., 2015, ECAR-2807, "AGR-3/4 Daily As-Run Thermal Analysis," Idaho National Laboratory.
- Hawkes, G.L. et al., 2014, "Thermal Predictions of the AGR 3/4 Experiment with Time Varying Gas Gaps," *2014 ASME International Mechanical Engineering Congress & Exposition*, Paper IMECE2014 36943, November 2014, Montreal, Canada.
- Hawkes, Grant L., 2015a, e-mail to Binh T. Pham, May 13, 2015.
- Hrovat M.F., et. al., 2008, "Fabrication, Properties and Irradiation Performance of Molded Block Fuel Elements for HTGRs," paper No. HTR2008-58025, *Proceedings of the 4th International Topical Meeting on High Temperature Reactor Technology*, September 28 to October 1, 2008, Washington, DC, USA.
- INL, 2011, SPC-1345, "AGR-3/4 Irradiation Test Specification," Rev. 0, Idaho National Laboratory.
- INL, 2015, PLN-3636, "Technical Program Plan for INL Advanced Reactor Technologies Technology Development Office/Advanced Gas Reactor Fuel Development and Qualification Program," INL/MIS-10-20662, Rev. 4, Idaho National Laboratory.
- INL, 2015a, PLN-3867, "AGR-3/4 Irradiation Experiment Test Plan," Rev. 1, Idaho National Laboratory.
- Ostle, B., and R. Mensing, 1975, *Statistics in Research*, 3rd Edition, Ames, Iowa: Iowa State University Press.
- Petti, D., J. Maki, G. Hawkes, J. Sterbentz, Einerson, J., et al., 2015, "ART Program Meeting for AGR 3/4 Thermal Model Input Uncertainty Estimation," June 5, 2015.
- Pham, B.T., and J.J. Einerson, 2011, "Simulation Aided Qualification of Thermocouple Data for AGR Experiments," *Transactions-American Nuclear Society*, Volume 104, pp. 274–275.
- Pham, B.T., and J.J. Einerson, 2013, "The statistical analysis techniques to support the NGNP fuel performance experiments," *Journal of Nuclear Materials*, Volume. 441, Issues 1–3, October 2013, pp. 563–573.

- Pham, B.T., 2015, *AGR-3/4 Final Data Qualification Report for ATR Cycles 151A through 155B-1*, INL/EXT-14-33780, Idaho National Laboratory.
- Pham, B.T., G.L. Hawkes, and J.J. Einerson, 2014, Improving Thermal Model Prediction through Statistical Analysis of Irradiation and Post Irradiation Data from AGR Experiments, *Journal of Nuclear Engineering and Design*, Volume 271, pp. 209–216.
- Pham, B.T., J.J. Einerson, and G.L. Hawkes, 2013, *Uncertainty Quantification of Calculated Temperatures for the AGR 1 Experiment*, INL/EXT-12-25169, Rev. 1, Idaho National Laboratory.
- SAS, 2009, *JMP 8 Statistics and Graphics Guide*, Cary, NC: SAS Institute Inc., Second Edition.
- Snead, L.L., and T.D. Burchell, 1995, “Reduction in Thermal Conductivity Due to Neutron Irradiation,” *22nd Biennial Conference on Carbon*, pp. 774–775.
- Sterbentz, J., 2015, ECAR-2753, “JMOCUP As-Run Daily Physics Depletion Calculation for the AGR 3/4 TRISO Particle Experiment in ATR Northeast Flux Trap,” Idaho National Laboratory.
- Sterbentz, J., 2015a, email to Binh T Pham, July 7, 2015.
- Windes, W., 2012, *Data Report on Post-Irradiation Dimensional Change in AGC-1 Samples*, INL/EXT-12-26255, Idaho National Laboratory.